Bias-Adjustment of Satellite-Based Rainfall Estimates over the Central Himalayas of Nepal for Flood Prediction

By

Mandira Singh SHRESTHA

2011

Bias-Adjustment of Satellite-Based Rainfall Estimates over the Central Himalayas of Nepal for Flood Prediction

By

Mandira Singh SHRESTHA

A Dissertation

Submitted in partial fulfillment of the requirement for the

Degree of Doctor of Engineering

Department of Civil and Earth Resources Engineering

Kyoto University, Japan

2011

Acknowledgements

I would like to first and foremost express my heartfelt gratitude to my principal supervisor Prof Kaoru Takara. His guidance, support and continuous encouragement have enabled me to complete my research. He has shown great patience, kindness and provided excellent motivation throughout the course of my doctoral degree. Without his understanding and guidance the completion of my doctoral degree would have remained a farfetched dream.

I would also like to express my gratitude to Prof Yosuke Yamashiki who has provided support and guidance during my doctoral study. My gratitude also goes to Dr Kobayashi Kenichiro who I have consulted with during the preparation of this thesis as well as Prof Eiichi Nakakita, Prof Takashi Hosoda and Prof Yasuto Tachikawa for their reviewing the thesis and qualifying my PhD. I would also like to thank Ms Sono Innou and Ms Yuko Takii for their administrative support and Mr Fuiki Shigeo and Mr Tsuato Oizumi for their technical support while I was in Japan.

My gratitude also goes to Japan Society for the Promotion of Science (JSPS) for providing me the RONPAKU scholarship without which I would not have been able to complete this doctoral dissertation. I am grateful for the flexibility and the opportunity provided by such a program that enables people engaged in research like me to carry out a doctoral degree. It is indeed a very good opportunity and must thank the Government of Japan for providing such a scholarship.

I would like to thank Dr Andreas Schild, Director General of the International Centre for Integrated Mountain Development (ICIMOD) for his continuous support and encouragement in enabling me to complete my PhD degree. His understanding and support towards staff's wellbeing and professional development is much appreciated. Without this understanding and support I would not have been able to participate in such a doctoral dissertation program. Prof Hua Ouyang, Programme Manager of the Integrated Water and Hazard Management (IWHM) program of ICIMOD is another person I would like to thank. He kept encouraging me and motivating me to complete this dissertation on time despite a number of activities that had to remain on hold. I would also like to thank Dr Arun Bhakta Shrestha, and Mr Pradeep Mool, Teamleaders for their patience, understanding and encouragement and all my colleagues at IWHM. I would also like to thank my colleague Dr Beatrice Murray who is a good friend and

colleague and provided the much needed advice and encouragement during hard times. My appreciation and deep sense of gratitude is also for Prof Suresh Raj Chalise who are amongst those that inspired me to pursue a doctoral degree.

This doctoral research is part of a project "Application of Satellite Rainfall Estimation in the Hindu-Kush Himalayan region" funded by USAID/OFDA under the Asia Flood Network Program. I would like to take this opportunity to express my gratitude to United States Agency for International Development Office of US Foreign Disaster Assistance (USAID/OFDA) for the funding and Dr Sezin Tokar, hydrometeorological advisor of USAID/OFDA for her continuous support and encouragement. Her guidance, encouragement and kind words have provided me the energy and motivation to complete my thesis. I would like to thank Dr Guleid Artan from USGS who is my mentor and "Guru" particularly on the hydrological modelling and analysis part. His patience in answering my simple and at times difficult questions through long distance communication was very helpful. I would also like to thank Dr Tim Love and Mr Eric Wolvovsky from National Oceanic and Atmospheric Administration (NOAA) for familiarizing me with the NOAA CPC_RFE2.0 satellite-based rainfall product. The kind advise and support of Dr Takuji Kubota from Japan Aerospace Exploration Agency (JAXA) is also much appreciated. I would like to thank my colleague Mr. Sagar Ratna Bajracharya who has been with me through this whole research period and has worked very closely with me in different aspects of this research. His pleasant attitude and willingness to help at all times of need has provided me the support to learn from him some of the tedious ArcGIS modules much needed for the analysis. I would also like to thank Mr. Rupak Rajbhandari for all the professional support and contributions he has made to the project as well as all the regional partners from the Hindu Kush-Himalayan region.

I would like to thank the Department of Hydrology and Meteorology (DHM) for providing the data for the research and to Dr Dilip Gautam and Mr Rishi Ram Sharma from DHM in particular, for their constructive engagement in the project.

Last but not the least there are a whole group of people close to my heart I would like to thank. My mother Mrs Indira Shrestha has been my principal motivator. "Yes you can do it" is what she told me at all stages of this doctoral dissertation – "without pain there is no gain" is what she reminded me of every time I felt a little distracted. My mother in law Mrs Yanchu Singh always provided me that feeling of security and confidence. While I was away for the doctoral study she took care of the family despite her occasional ill health and gave me that

freedom to do what I always wanted to do. My sister Bandana Shrestha and brother Jay Pal Shrestha have pushed me towards completing my dissertation with encouraging words at all times. My children Juni, Manzari and Ravi have also been very supportive and understanding. “Go do it Mamu – we will take care of ourselves while you are away” was what they use to tell me providing me that much needed support and understanding despite their mother being away. Finally, my gratitude goes to my beloved husband Mr. B.K. Man Singh who has been the man holding the candle for me in the darkness at all times. His love, sincerity and constant encouragement has made me complete this dissertation.

Thank you all very much.

Mandira Singh Shrestha

Abstract

This research is a part of a long term regional project on "Application of Satellite Rainfall Estimation in the Hindu Kush-Himalayan Region" implemented by the International Centre for Integrated Mountain Development (ICIMOD) and the regional partners.

Flood disasters are recurrent in Nepal leading to huge loss of lives, infrastructure damage and adverse impacts on socioeconomic development. An important approach to non-structural flood management lies in the provision of an end-to-end flood forecasting and warning services. Due to the limited spatial coverage of ground based gauges, unavailability of real-time rainfall data, and constraint in technical and financial resources, the Department of Hydrology and Meteorology (DHM) of Nepal is yet to initiate an operational flood forecasting. The availability of global coverage of satellite data offer effective and economical means of calculating areal rainfall estimates in sparsely gauged areas. Thus, satellite-based rainfall estimates (SRE) may be one of the best and appropriate approaches for Nepal to predict and forecast rainfall-induced runoff that may produce flooding.

Satellite-based rainfall estimation technology has rapidly developed in the last few decades but this technology is still in its infancy in most of the Hindu Kush Himalayan (HKH) countries including Nepal. A clear understanding of the satellite rainfall estimation methods and products are a prerequisite to apply SRE for flood prediction. The research focussed on three broad objectives (i) to evaluate the accuracy of SRE over the central himalayas of Nepal (ii) to improve the SRE with bias-adjustment (iii) to improve the flood prediction by applying bias-adjustment. This research carried out review of the various satellite-based rainfall estimation methods and products. Quantitative validation of the National Oceanic and Atmospheric Administration (NOAA) CPC-RFE2.0 (RFE) and Japan Aerospace Exploration Agency (JAXA) GSMaP_MVK+ (GSMaP) products based on independent ground station observed data were carried out. The verifications were conducted at three levels. The first set of verification was conducted considering the whole country as one homogeneous region. The second level verification was conducted partitioning the county into various physiographic regions and the third was at river basin level. At a regional level the analysis data from 422 rainfall stations were available for the verification out of which 176 are within Nepal for the period 2002 to 2006. The accuracy of the SRE was evaluated using the standard verification technique which included visual analysis as well as continuous verification statistics and categorical verification statistics.

Visual verification was subjective and compared maps of satellite estimates with observations. The continuous verification statistics included correlation coefficient, root mean square error (RMSE), bias, and percentage error, to provide a quantitative assessment for each set of verification data. The categorical verification statistics were qualitative and included probability of detection (i.e., events diagnosed correctly) and false-alarm ratio (which detects non-events).

The results in general show underestimation of rainfall in intense rainfall periods and heavy rainfall regions and overestimation of rainfall in rainshadow and arid areas with both the SRE products. In general the rainfall events matched qualitatively when spotting extreme rainfall, but quantitatively there were some differences. The GSMaP estimates were found to underestimate the whole Nepal averaged annual rainfall by 48 % and RFE by 30%. The daily bias averaged over whole of Nepal was -1.1 mm/day with RFE and -2.0 mm/day with GSMaP for the period 2003 to 2006. The RMSE over whole of Nepal was -4.0 mm/day with RFE and -4.9 mm/day with GSMaP for the same period. The bias and the RMSE were higher for the June July, August and September (JJAS) period compared to the annual. The GSMaP however showed better correlation with the observed data as compared to RFE.

The second level of verification was conducted for various physiographic regions to assess the performance of RFE and GSMaP. Both SREs performed better in the flatter regions in the Terai and Siwalik regions. The performance deteriorated with higher elevations with the minimum performance in the High Mountains. The Middle Mountain regions despite denser network of stations compared to other regions showed poorer performance of SREs. At the basin level the bias was smaller in the Bagmati than the Narayani. These results indicate that overall the SREs provides reasonable rainfall estimates but needs to be improved before it can be implemented for operational flood forecasting.

The United States Geological Survey (USGS) GeoSpatial Streamflow Model (GeoSFM) model was applied in two basins, the Bagmati and Narayani. In both basins there was a good correlation between the simulated and observed discharge at Pandheradovan and Devghat using gauge observed rainfall, for the period 2002-2004, with correlation values of 0.95 for Bagmati and 0.94 for Narayani. With the RFE estimates the simulated discharges followed the trend of the observed values quite well, although there was a significant difference in the magnitude of the flows indicating a need for bias correction prior to application into operational flood prediction.

With five years of data from 2002 to 2006; the seasonal, monthly and 7-day moving average bias-adjustments were derived comparing the RFE rainfall estimates and gridded gauge observed rainfall data at grids with one or more gauges. These bias-adjustments were applied to the RFE to obtain a new set of rainfall estimates. These bias-adjusted rainfalls when applied to the GeoSFM model resulted in improvement in flood prediction. The second approach of improving the SREs was by ingesting additional local rain gauge data into the RFE algorithm (referred to as "improved RFE") by expanding the Global Telecommunication Satellite (GTS) data input. The GeoSFM model calibrated with the gauge observation and the "improved RFE" provided considerable improvement in flood prediction. However, there seemed to be some discrepancy in the medium flow estimation. Therefore, keeping in mind the inherent errors in the SREs the model was recalibrated with improved RFE. The recalibrated model with new gauge-satellite merged rainfall estimates showed further improvement in the simulation of flows.

Overall, findings from this study indicate that the SRE underestimates rainfall significantly over Nepal but with correlation higher than 0.70. The performance of the SRE is better in the flatter terrain than in the mountainous areas. The accuracy of SREs can be improved by applying a bias-adjustment. Prediction of discharge using bias-adjusted rainfall estimates can improve the accuracy of discharge prediction with considerable increase in the predictive capability of flood prediction for which the hydrological model needs to be recalibrated.

Acronym

AFN	Asia Flood Network
AMSU	Advanced Microwave Sounding Unit
AVHRR	Advanced Very High Resolution Radiometer
CN	Curve Number
CPC	Climate Prediction Center
DEM	Digital Elevation Model
DHM	Department of Hydrology and Meteorology, Nepal
DMSP	Defense Meteorological Satellite Program
DMSW	Digital Soil Map of the World
EROS	Earth Research Observation and Science
ESRI	Environmental Systems Research Institute
FAO	Food and Agricultural Organization
FAR	False Alarm Ratio
FEWS	Famine Early Warning System
GCM	Global Climate Model
GDAS	Global Data Assimilation System
GeoSFM	Geospatial Streamflow Model
GIS	Geographic Information System
GLCC	Global Land Cover Characteristics
GLOF	Glacial Lake Outburst Flood
GOES	Geostationary Operational Environmental Satellite
GPCP	Global Precipitation Climatology Project
GPI	GOES Precipitation Index
GSMaP	Global Satellite Mapping Project

GTS	Global Telecommunication System
GUI	Graphical User Interface
HKH	Hindu Kush-Himalayan
ICIMOD	International Centre for Integrated Mountain Development
IDW	Inverse Distance Weighted
INSAT	Indian Satellite
IR	Infra red
JAXA	Japan Aerospace Exploration Agency
MAE	Mean Absolute Error
MOSCEM	Multiobjective Shuffled Complex Evolution Metropolis
MW	Microwave
NOAA	National Oceanic and Atmospheric Administration
NRL	Naval Research Laboratory
OFDA	Office of US Foreign Disaster Assistance
PET	Potential Evapotranspiration
PERSIANN	Precipitation Estimate from Remotely Sensed Information using Artificial Neural Network
PMW	Passive Microwave
POD	Probability Of Detection
PR	Precipitation Radar
RCM	Regional Climate Model
RFE	Rainfall Estimation
RMSE	Root Mean Square Error
SA	Sensitivity Analysis
SRE	Satellite-based Rainfall Estimate
SSM/I	Special Sensor Microwave / Imager

SWHC	Soil Water Holding Capacity
TMI	TRMM Microwave Imager
TMPA	TRMM Multisensor Precipitation Analysis
TRMM	Tropical Rainfall Measuring Mission
UNDP	United Nations Development Programme
USAID	The United States Agency for International Development
USGS	United States Geological Survey
VIRS	Visual Infra Red Scanner
VIS	Visible
WMO	World Meteorological Organization

Table of Contents

Abstract ……v

Acronyms ……ix

List of Figures ……..…..xvii

List of Tables …….…....xxi

1 INTRODUCTION 1

1.1 Background 1

1.2 Identification of Problem 2

1.3 Background of the Research 5

1.4 Study Area 5

1.5 Objectives 7

1.6 Outline of the Thesis 8

2 REVIEW OF GLOBAL SATELLITE-BASED RAINFALL ESTIMATION METHODS, PRODUCTS AND VERIFICATION 13

2.1 Satellite-Based Rainfall Estimation Methods 13

2.1.1 VIS/IR Method 14

2.1.2 Passive Microwave method 15

2.1.3 Mutli-Sensor Technique 16

2.2 Satellite Rainfall Estimate Products 16

2.2.1 The NOAA CPC_RFE2.0 Satellite Rainfall Estimates 16

2.2.2 The NOAA CMORPH Rainfall Estimates 19

2.2.3 Tropical Rainfall Measuring Mission (TRMM) 19

2.2.4 Global Satellite Mapping Project (GSMaP) 22

2.2.5 Precipitation Estimation from Remote Sensing Information using Artificial Neural Network (PERSIANN) 23

2.3 Review of Verification of Satellite-Based Rainfall Estimates 25

2.4 Summary 31

3 VERIFICATION OF SATELLITE-BASED RAINFALL ESTIMATES OVER CENTRAL HIMALAYAS OF NEPAL 35

3.1 Methodology for Verification of Satellite-Based Rainfall Estimates 35

3.1.1 Visual Verification 36

3.1.2 Continuous Verification Technique 36

3.1.3 Categorical Verification Technique 38

3.2 Interpolation of the Observed Rainfall - Kriging 40

3.3 Verification of Satellite-Based Rainfall Estimates over Nepal 42

3.3.1 Data Preparation 43

3.3.2 Country Level Verification - Assessment of the Accuracy of the Satellite-Based Rainfall Estimates over the Whole of Nepal 45

3.3.3 Physiographic Level Verification - Assessment of the Accuracy of the Satellite-Based Rainfall Estimates for Various Physiographic Regions 60

3.3.4 Basin Level Verification in the Bagmati and Narayani Basins 65

3.4 Summary 75

4 RAINFALL-RUNOFF MODELLING USING SATELLITE-BASED RAINFALL ESTIMATES 79

4.1 Introduction 79

4.2 The GeoSFM Model 80

4.2.1 Introduction 80

4.2.2 Model Formulation 82

4.3 Data Inputs 83

4.3.1 Digital Elevation Model 83

4.3.2 Soil Data 83

4.3.3 Land Cover Data 84

4.3.4 Evaporation Data 84

4.3.5 Rainfall Data 84

4.4 Methodology - Geospatial Processing and Hydrologic Computations 85

4.4.1 Preprocessing Modules 85
4.4.2 Hydrologic Simulation Modules 86
4.4.3 Post Processing Modules 88
4.5 Model Performance Indicators used for the Study 90
4.5.1 Correlation Coefficient 90
4.5.2 Nash Sutcliff Coefficient of Efficiency (NSCE) 91
4.5.3 Bias 91
4.5.4 Root Mean Square Error (RMSE) 91
4.5.5 Peak Flow Error 91
4.6 GeoSFM Model of the Bagmati Basin 92
4.6.1 Data Parameterization and Analysis 93
4.6.2 Results and Discussion 94
4.7 GeoSFM Model of the Narayani Basin 99
4.7.1 Data Parameterization and Analysis 99
4.7.2 Results and Discussion 100
4.8 Summary 103
5 BIAS-ADJUSTMENT OF SATELLITE-BASED RAINFALL ESTIMATES 108
5.1 Introduction 108
5.2 Bias-Adjustment 109
5.2.1 Gamma Transform for Bias-Adjustment 110
5.2.2 Power Transform for Bias-Adjustment 110
5.2.3 Ratio Based Bias-Adjustment 111
5.2.4 Improved Gauge-Satellite Merged Rainfall Estimates for Bias-Adjustment 112
5.3 Rainfall-Runoff Simulation Using Bias-Adjusted Satellite-Based Rainfall Estimates 113
5.3.1 Satellite-Based Rainfall Estimates with Bias-Adjustment 113
5.3.2 Rainfall Simulation with Bias-Adjusted Satellite-Based Rainfall Estimates 115

5.4 Summary 122

6 CONCLUSIONS AND RECOMMENDATIONS 125

6.1 Satellite-Based Rainfall Estimate Validation..... 127

6.2 Hydrological Modelling Using Satellite-Based Rainfall Estimates..... 128

6.3 Recommendations and Future Perspectives..... 129

ANNEX 1 Loss from Floods, Landslides and Avalanches in Nepal from 1983 – 2005…….132

ANNEX 2 List of Rainfall Stations used for the research ……..133

List of Figures

Figure 1.1 Location and drainage network of Nepal 7

Figure 1.2 Physiographic regions of Nepal..... 7

Figure 1.3 Conceptual framework of research..... 8

Figure 2.1 The Global Observing System of Meteorological Satellites (source: Kidd *et al*., 2009). 14

Figure 2.2 CPC_RFE2.0 rainfall estimates over South Asia domain 18

Figure 2.3 Domain of the CPC RFE-2.0 (Source: Love, T., 2006) 18

Figure 2.4 Daily TRMM 3B42_V6 rainfall estimates in the South Asia domain 21

Figure 2.5 Global TRMM Multisatellite Precipitation Analysis (TMPA) rainfall estimates . 21

Figure 2.6 GSMaP_NRT rainfall estimates over South Asia 22

Figure 3.1 Flowchart of satellite rainfall verification 42

Figure 3.2 Distribution of rain gauge stations in Nepal..... 45

Figure 3.3 Time series comparison of GSMaP and gauge observed daily rainfall for 2003-2006 over whole of Nepal. 46

Figure 3.4 Spatial distribution of average annual precipitation from 2003 to 2006, a) gauge observed, b) GSMaP and c) RFE..... 49

Figure 3.5 Bias Map of average annual precipitation for 2003-2006, a) GSMaP and b) RFE50

Figure 3.6 Spatial distribution of annual precipitation with GSMaP, RFE and gauge observed rainfall for 2003 to 2006 51

Figure 3.7 Annual bias map for each year from 2003 to 2006 with GSMaP and RFE 52

Figure 3.8 Spatial distribution of June, July, August and September (JJAS) average rainfall map for 2003-2006 a) gauge observed, b) GSMaP and c) CPC_RFE2.0. 54

Figure 3.9 Bias Map of average JJAS precipitation for 2003-2006, a) GSMaP and b) RFE . 55

Figure 3.10 Spatial distribution of year wise average JJAS rainfall using GSMaP, CPC_RFE2.0 and gauge observation over Nepal for 2003 to 2006. 56

Figure 3.11 Bias Map of JJAS precipitation for 2003-2006, a) GSMaP and b) RFE..... 57

Figure 3.12 Scatter plot of area averaged daily rainfall for monsoon (JJAS) of 2003-2006 from a) observed and GSMaP, (b) observed and RFE..... 58

Figure 3.13 Scatter plot of accumulated average rainfall for JJAS of 2003-2006 from a) GSMaP and b) CPC_RFE2.0for each 0.1^{o}x0.1^{o} grid cell. 59

Figure 3.14 Location of rainfall stations in various physiographic regions of Nepal..... 61

Figure 3.15 Scatter plot of accumulated rainfall for JJAS of 2003 from observed and GSMaP for each 0.1^{o}x0.1^{o} grid cell..... 64

Figure 3.16 Scatter plots of area averaged rainfall for various physiographic regions of Nepal 65

Figure 3.17 Major river basins of Nepal 66

Figure 3.18 Location of rainfall station in the Bagmati Basin and its vicinity 67

Figure 3.19 Comparison of rain gauge observed and RFE for the Bagmati Basin on July 23, 2002 68

Figure 3.20 Basin average rainfall of Bagmati Basin for 2002 69

Figure 3.21Time series comparison of gauge observed and RFE daily basin average rainfall for monsoon (JJAS) from 2002 to 2006 in the Bagmati Basin 70

Figure 3.22 Daily basin averaged gauge observed rainfall with RFE for JJAS of 2003 in the Bagmati Basin 70

Figure 3.23 Comparison of gauge observed and RFE for 9 July, 2003 in the Narayani Basin 73

Figure 3.24 Time series comparison of gauge observed and RFE daily basin average rainfall for monsoon (JJAS) from 2002 to 2006 in the Narayani Basin 75

Figure 3.25 Daily basin averaged gauge observed rainfall with RFE for JJAS of 2003 in the Narayani Basin 75

Figure 4.1 General framework of the GeoSFM model 81

Figure 4.2 Process Map and System Diagram for the GeoSpatial Streamflow Model (Source: Asante *et al*. 2001) 83

Figure 4.3 River system of the Bagmati Basin 92

Figure 4.4 Location of rainfall and discharge gauging stations in the Bagmati Basin and its vicinity 93

Figure 4.5 Observed and simulated daily flows at Panheradovan, the daily flows were simulated using gauge observed rainfall data (July 1 – August 7, 2002) 94

Figure 4.6 Scatter Plot of daily Observed and Simulated Discharge (July 1 – August 7, 2002) 95

Figure 4.7 Comparison of observed and simulated daily flows at Pandheradovan using gauge observed rainfall and RFE data as an input rainfall (July 1 – August 7, 2002) 96

Figure 4.8 Scatter plot of observed and simulated discharge when the GeoSFM was driven with RFE (July 1 – August 7, 2002) 96

Figure 4.9 Observed and simulated streamflows using RFE from 2002 to 2004 (calibration) 97

Figure 4.10 Observed and simulated flows for 2002-2005 98

Figure 4.11 Average soil water holding capacity of the 21 sub-basins modelling units when the GeoSFM (a) is calibrated with satellite-based rainfall fields, and (b) when the model is calibrated with rain 98

Figure 4.12. Location of the rainfall stations within and in the vicinity of the Narayani Basin 99

Figure 4.13 Comparison and scatter plot of observed and simulated discharge at Devghat using 2003 monsoon gauge observed rainfall (June to September) 101

Figure 4.14 Comparison and scatter plot of daily observed and simulated discharge at Devghat using 2004 monsoon gauge observed rainfall (June to September) 101

Figure 4.15 Comparison and scatter plot of daily observed and simulated discharge at Devghat using gauge observed rainfall and RFE data as input rainfall (June to September 2003) 102

Figure 4.16 Hydrograph and scatter plot of daily observed and simulated discharge at Devghat with RFE calibrated model from June to September 2003 103

Figure 5.1 Methodology for bias correction 112

Figure 5.2 Scatter plot of daily area averaged gauge observed rainfall and SRE with and without bias-adjustment for monsoon of 2003. 115

Figure 5.3 Daily observed and simulated flows using bias-adjusted CPC_RFE2.0 rainfall fields..... 117

Figure 5.4. Comparison of new gauge-satellite merged and gauge observed rainfall over grid boxes where there is at least one reporting station for 9 July 2003 118

Figure 5.5. Comparison of daily basin averaged gauge observed rainfall with CPC_RFE2.0 and adjusted CPC_RFE2.0 for JJAS of 2003 in the Narayani Basin..... 120

Figure 5.6. Scatter plots of observed and CPC_RFE2.0 rainfall estimates a) without adjustment and b)with ingestion of local rain gauge averaged over the Narayani Basin 120

Figure 5.7 Observed and simulated hydrographs obtained when the model was calibrated with a) gauge observed rainfall and b) new gauge-satellite rainfall estimates. 122

List of Tables

Table 2.1 A list of selected high resolution satellite-based products 24

Table 2.2 Verification of satellite based rainfall estimates in selected regions 29

Table 3.1 2 x 2 contingency table 39

Table 3.2 Comparison of area averaged annual rainfall estimates over whole of Nepal using GSMaP and RFE 47

Table 3.3 Time series comparison of daily area averaged rainfall from 2003 to 2006 47

Table 3.4 Statistical error of daily area average rainfall from 2003-2006 for JJAS 58

Table 3.5 Statistical error of accumulated rainfall for monsoon (JJAS) from 2003-2006 at each grid cell 59

Table 3.6 Comparison of GSMaP and gauge observed rainfall for 2003 60

Table 3.7 Error statistics of area averaged annual GSMaP and gauge observed rainfall in various physiographic regions for 2003. 62

Table 3.8 Error statistics of monsoon (JJAS) GSMaP and gauge observed rainfall in physiographic regions for 2003. 62

Table 3.9 Error statistics of daily GSMaP and gauge observed rainfall during JJAS in various physiographic regions for 2003. 63

Table 3.10 Characteristics of Bagmati and Narayani Basins 66

Table 3.11Statistics of performance of daily RFE compared to gauge observed data for JJAS from 2002 to 2006 70

Table 3.12 Statistics of performance of daily RFE compared to gauge observed data for JJAS from 2002 to 2006. 74

Table 5.1 Error statistics of discharge with bias-adjusted CPC_RFE rainfall estimates 117

Table 5.2 Statistical summary of the comparison between simulated and observed streamflow for JJAS of 2003with RFE, gauge-satellite merged model calibrated with gauge observed data and gauge satellite merged calibrated model. 121

CHAPTER 1

1 INTRODUCTION

1.1 Background

Water induced disasters are very prevalent in Nepal and annually many lives and properties worth millions of dollars are destroyed. Due to the diverse geological settings rugged terrain and monsoon precipitation Nepal is prone to floods, landslides, and glacial lake outburst floods similar to other mountainous countries in the Hindu Kush-Himalayan (HKH) region (Shrestha and Choppel, 2010). Nepal is primarily under the influence of the southwest monsoon from the Bay of Bengal. The monsoon season in Nepal occurs between June and September; the monsoon is the dominant rainfall season with almost 80% of the annual rainfall occurring in that period. Based on twenty years of data (1980-2000) Nepal is found to have high vulnerability for flood disasters as reported in the UNDP global report on Reducing Disaster Risk (UNDP, 2004). Between 1983 and 2005 on average 309 people lost their lives in Nepal due to floods and landslides (Annex A) accounting for over 60% of those dead due to different types of disasters in the country (Khanal *et al*., 2007). Recent flood disasters in Nepal include the 1981 flood in Lele, the 1993 flood of the Bagmati and Narayani, the 1998 Andhi Khola flood (Chalise and Khanal, 2002), the 2002 flood in the Narayani and Bagmati and the 2008 flood in the Koshi. The high level of poverty and rate of population growth has further increased the vulnerability to flood disasters. Floods are posing severe constraints for socio-economic development, investment in agriculture, physical infrastructure and industrial production where they are most needed. Thus, flood mitigation in Nepal is more than a hydrological priority; it is a socio-economic necessity.

Flood early warning systems are one of the most effective ways to minimize the loss of life and property. A reliable flood forecasting system is very important to enable establishment of a reliable early warning system that transmits down to the community for minimizing the impacts of disasters. Accurate rainfall estimations are essential for timely flood forecasting and warning. In many regions operational flood forecasting has traditionally been relied upon by a dense network of rain gauges or ground-based rainfall measuring radars that report in real time. In Nepal, like many other developing countries, the hydrometeorological station networks are sparse and rainfall data are available only after a significant delay. According to the Department

of Hydrology and Meteorology (DHM) of Nepal the country average density is one gauge for about 331 km^2 and is especially very sparse in mountainous areas. Due to the limited spatial coverage and uneven distribution of ground based gauges, unavailability of real-time rainfall data, and constraint in technical and financial resources, operational flood forecasting is yet to be initiated (Shrestha *et al*., 2008a). In mountainous terrain where lag times may be as measured in terms of minutes or hours, rainfall estimation and forecasting is especially difficult.

Through the use of hydrologic modelling techniques it is possible to better prepare for and respond to flood events. There are many rainfall-runoff models available in the world today. For example the lumped and conceptual models are applicable for prediction of runoff for un-gauged catchments and also water balance studies. Semi-distributed models are suitable for streamflow records and real-time runoff simulations. Use of appropriate hydrologic models to predict floods can mitigate flood damage, provide support to contingency planning, and warning to people threatened by floods. However, flood forecasting model predictions are subject to uncertainty due to model simplifying assumptions in terms of model structure and uncertainties in model parameters and input. Precipitation is an important input in rainfall-runoff modelling and is highly variable in both space and time. Flood forecasting in basins with sparse rain gauges pose an additional challenge. The availability of global coverage of satellite data offer effective and economical means of calculating areal rainfall estimates in sparsely gauged areas (Artan *et al*., 2007; Shrestha *et al*., 2008a). Thus, satellite-based rainfall estimates (SRE) may be one of the best and appropriate approaches for Nepal to predict and forecast rainfall-induced runoff that may produce flooding.

1.2 Identification of Problem

Precipitation is an essential component of the hydrological cycle. Accurate global rainfall coverage is necessary to improve short term, medium and long term weather forecasts, and climate monitoring and prediction. A longstanding promise of meteorological satellites is the improved identification and quantification of rainfall at different temporal and spatial scales consistent with the nature and development of cloud rain. Meteorological satellite data strengthens the geographical (spatial) coverage and time-base of conventional ground-based rainfall data observation for a number of applications, including hydrology analysis and weather monitoring and forecasting. The primary scope of satellite rainfall monitoring is to provide information on rainfall occurrence, amount and distribution over the globe for climatology, hydrology, and environmental analysis. SRE is a significant method for rainfall measurements

compared with conventional gauge data and supplements gauge stations. Conversely, conventional gauge data are needed to calibrate the SREs, so together they can provide improved real-time rainfall information.

Because there is a lag time between the onset of rainfall and the occurrence of flooding, accurate rainfall estimation is very essential to reduce the impact of floods. This is done through early warnings issued by government systems that monitor and forecast floods. Modernization of data sources and programming techniques has increased the accuracy of the rainfall estimation with near real-time availability.

The global coverage of space-based precipitation estimates provides information on rainfall frequency and intensity in regions that are inaccessible to other observing systems such as rain gauges and radar. Several high resolution SREs are now available from various operational agencies and academic institutions for example CMORPH (Joyce *et al*., 2004), TRMM Multisensor Precipitation Analysis (TMPA) (Huffman *et al*., 2007), CPC_RFE2.0 (Xie *et al*., 2003) and GSMaP (Ushio *et al*., 2009). The verification of accuracy of SREs have been studied in various regions of the world at varying temporal and spatial scales (Kubota *et al*., 2009; Ebert *et al*., 2007; Kidd *et al*., 2009; Hughes, 2006; Dinku *et al*., 2008). However, there has been no rigorous verification of the SREs over the Himalayan region for application into flood forecasting purposes.

Often in developing countries like Nepal the availability of ground measuring stations is very limited with scarce density of hydrometeorological network and uneven distribution making it challenging for accurate flood prediction. Accurate quantitative documentation of regional rainfall analysis (gridded data) remains a challenging task because of the large spatial and temporal variability of rainfall and lack of a comprehensive observing system. As the SRE technique provides information on rainfall occurrence, amount, and distribution over a region it is an important technology for rainfall measurement that provides near real-time data. It can be used alongside conventional gauge data. Satellite-enhanced rainfall estimation appears to offer an effective and viable alternative means for estimating precipitation. The use of SREs will enable a more thorough, accurate, and timely analysis of the rainfall estimates. Satellite-improved rainfall estimates delivered in a timely fashion can facilitate the use of flood-information systems. These estimates, enhanced by gauge data, can improve rainfall analyses that are currently interpolated solely from sparse rain-gauge data, and will lead to value-added agricultural and hydrological applications such as crop monitoring and flood

forecasting. Mitigation measures for weather-related disasters will thus be able to use more accurate and timely information in the decision-making process.

The satellite derived rainfall estimates can be applied to various rainfall-runoff models to simulate the floods downstream well in advance depending upon the size of the basin. However, the accuracy in predicting flood parameters such as peak runoff and time to peak is dependent on the ability to monitor the spaciotemporal variability of rainfall (Hossain and Katiyar, 2006). Given the uncertainty of space based rainfall observation the accuracy of the estimates needs to be assessed by validating the space-based observations with that from gauged stations. Hossain (2005) cautions that the uncertainty that rise from the space based rainfall estimates propagates in the rainfall run-off models thereby increasing the prediction uncertainty of floods. Hossain and Katiyar (2006) stresses on the need to use the existing streamflow measuring systems for validation and calibration of the space based forecasting systems. Literature review indicates that there are many rainfall-runoff models like the HEC-HMS, TOPMODEL, OHYMOS, GeoSFM, and others that have been applied in for runoff prediction.

Some work has also been attempted to look into the application of satellite based rainfall estimates into flood forecasting. Artan *et al.* (2007) investigated the utility of SRE for flood forecasting purposes. Harris *et al.* (2007) tried to assess the hydrologic implications of uncertainty of satellite rainfall data at the coarse scale using TRMM data. Yilmaz *et al*., (2005) evaluated the utility of SRE for hydrologic forecasting. Hughes (2006) evaluated SRE with gauge observed data at a monthly time step for application in hydrological modelling. Hong et al. (2007) proposed the application of satellite rainfall data in near real time using Tropical Rainfall Measuring Mission (TRMM) in global monitoring system for early warning of floods and landslides.

However, there has been no verification over the Himalayan region for flood prediction. The SREs could provide information on spatiotemporal variation of precipitation in data sparse regions of Nepal and can be used as input to streamflow modelling system in basins for flood forecasting. Therefore, it is necessary to assess the quality of the SRE over the Himalayan region for improved rainfall monitoring. The intent is to evaluate the SREs, make bias-adjustments so they can be used with confidence in providing rainfall input to improved flood forecasting systems**.**

1.3 Background of the Research

This research is a part of a longer term regional project "Application of Satellite Rainfall Estimation in the Hindu Kush Himalayan Region" implemented by ICIMOD and its regional partners under the Asia Flood Network (AFN) Programme of USAID/OFDA. The first phase of the project was initiated in June 2006 to June 2008. A follow on second phase project was from December 2008 to June 2010. As this was a regional project the partners were from the regional member countries primarily the hydromet services.

The project aimed to minimise the loss of lives and property by reducing the region's vulnerability to floods and droughts – in particular in the Indus, and Ganges-Brahmaputra-Meghna basins (Shrestha *et al*., 2008b). The project sought to strengthen regional cooperation in flood forecasting and information exchange, and build capacity among the partner institutions.

The main objective was to validate the National Oceanic and Atmospheric Administration (NOAA) Climate Prediction Centre's (CPC) rainfall estimate CPC_RFE2.0 (hereafter referred to as RFE) for the HKH region to determine their operational viability and improve the algorithm, and to apply rainfall estimates to the United States Geological Survey (USGS) Geospatial Streamflow Model (GeoSFM).

The specific objectives included

- to validate NOAA RFE and improve river forecast products
- determining the relationship between RFE and the corresponding observed rainfall, and assessing whether the satellite data can be used in conjunction with gauge data as inputs to a hydrological model.
- to test the GeoSFM model for selected basins and explore its applications.

In August 2010 a new phase of this project was initiated to build on the application of satellite rainfall estimation in the HKH region. This phase will focus on carrying out intercomparison of SREs and adding the snow and glacier melt component into the GeoSFM model for better discharge prediction particularly for estimating flow availability.

1.4 Study Area

The study area is the central himalayas in Nepal. Geographically Nepal is located between 80^o 4' to 88^o 12' east longitudes and 26^o 22' to 30^o 27' north latitudes with a total area of 147,100 km^2 (Fig1.1). The topography is highly rugged with elevation ranging from 60 m in the south to 8848

m in the north within a short distance of about 160 km. Physiographically, the country is divided into five regions, the Terai in the south, the Siwalik, the Middle Mountains, the High Mountains and the High Himal in the north (Fig.1.2).

The Terai in the south is the northern extension of Indo-Gangetic plain (13 % of the country's area) with altitude ranging from 60-300 m. Flooding is common during monsoon inundating large areas. The Siwaliks is 10-30 km wide foothill belt (12 % of the total area of Nepal) and have relative relief less than 1000 m; the slope are generally steep with shallow soils. The Middle Mountains covers 30% of the total area of Nepal, with a total width range from 60-80 km and rises fairly abruptly from the Siwaliks to elevations between 1500 and 3000 m above mean sea level. The High Mountain ranges from 2000 to 4000 m and occupies 21 % of the total area. Topographically, this mountain range shows extremely rugged terrain with very steep slopes and deeply cut valleys. The High Himal in the north occupies nearly 24% of the total area.

The climate at macro-level is dominated by the summer monsoon and topography plays an important role in creating meso and micro level differences. Hence, there are pronounced temporal and spatial variations in precipitation. The average area-weighted annual precipitation for Nepal is about 1,630 mm. More than 80% of the total annual precipitation occurs during the monsoon from June through September. Kansakar *et al*. (2004) derived climatological patterns of monthly precipitation, and classified regimes by the shape and magnitude of monthly precipitation using rainfall data from 222 stations over Nepal. They found that precipitation patterns were controlled by the summer monsoon and by orographic effects induced by the mountain ranges. Ichiyanagi *et al*. (2007) investigated the spatial and temporal variability in monthly precipitation and annual and seasonal precipitation patterns over Nepal. The maximum annual precipitation is found to increase with altitude for elevations below 2000 m but decreased for elevations of 2000–3500 m. In extreme cases up to 37% of the mean annual precipitation has been reported to occur within 24 hours for example the 540 mm of rainfall that occurred in July 1993 in central Nepal caused a large flood disaster killing more than 1100 people. Spatially, mean annual precipitation ranges from less than 160 mm in Lomangthang (Mustang) located in the trans-himalayan zone north of the Higher Himalayan ranges, to more than 5000 mm in Lumle (near Pokhara) located in the southern part of the Higher Himalayan ranges (Sharma, 1977; Chalise *et al*., 1996). A few isolated pockets of dense precipitation are located in different parts of the country.

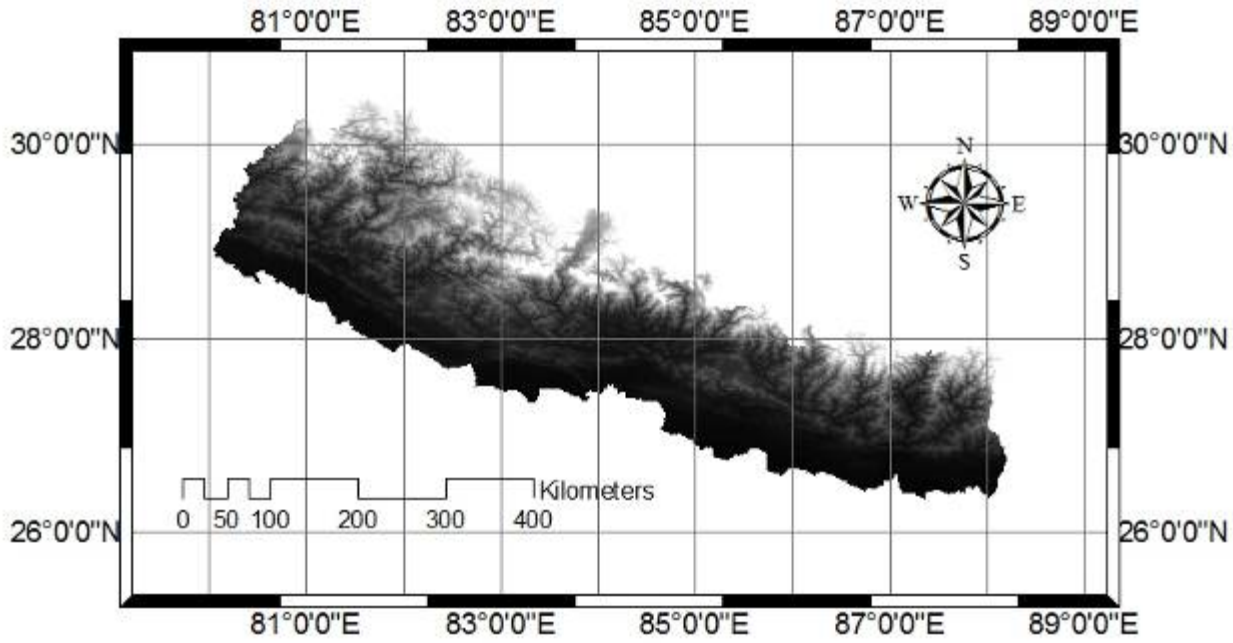

Figure 1.1 Location and drainage network of Nepal

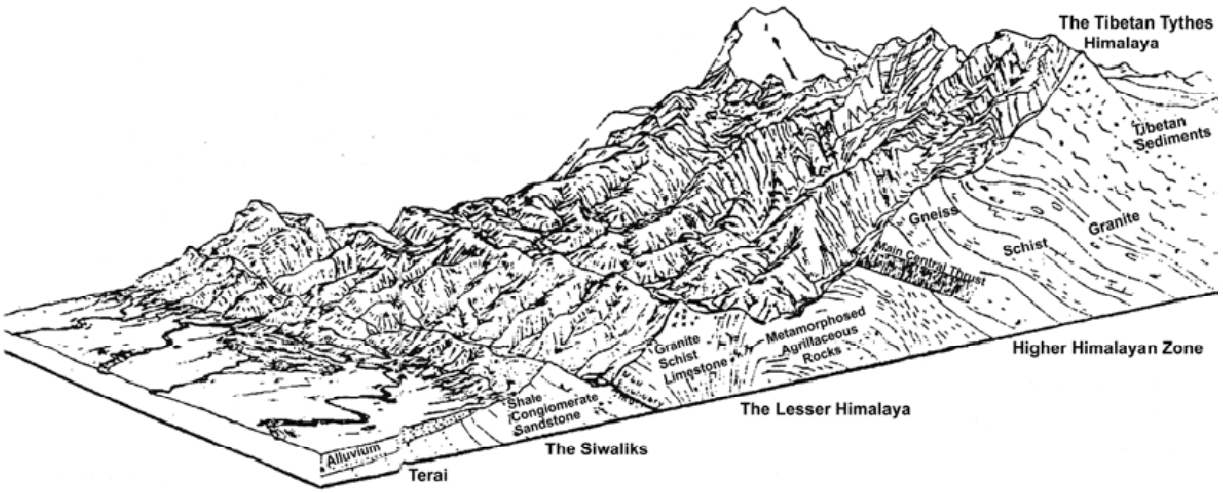

Figure 1.2 Physiographic regions of Nepal

1.5 Objectives

This study focuses on the application of SREs for flood prediction in the central himalayan region of Nepal. The conceptual framework is provided in Figure1.3. The main objectives of the Thesis are as follows.

[1] To review and understand the global SRE products that can be applied to flood forecasting in the Himalayan region

[2] To assess the accuracy of the SRE over Nepal and understand the knowledge gaps for satellite-based flood prediction

[3] To assess the performance of SREs in flood prediction using rainfall-runoff model in various basins

[4] To assess how SRE can be improved for better flood prediction using bias-adjustment – the relationship between gauge observed and satellite data needs to be established and calibrated for correcting the satellite-based data

[5] To use rainfall-runoff modelling framework with SRE for improved flood prediction.

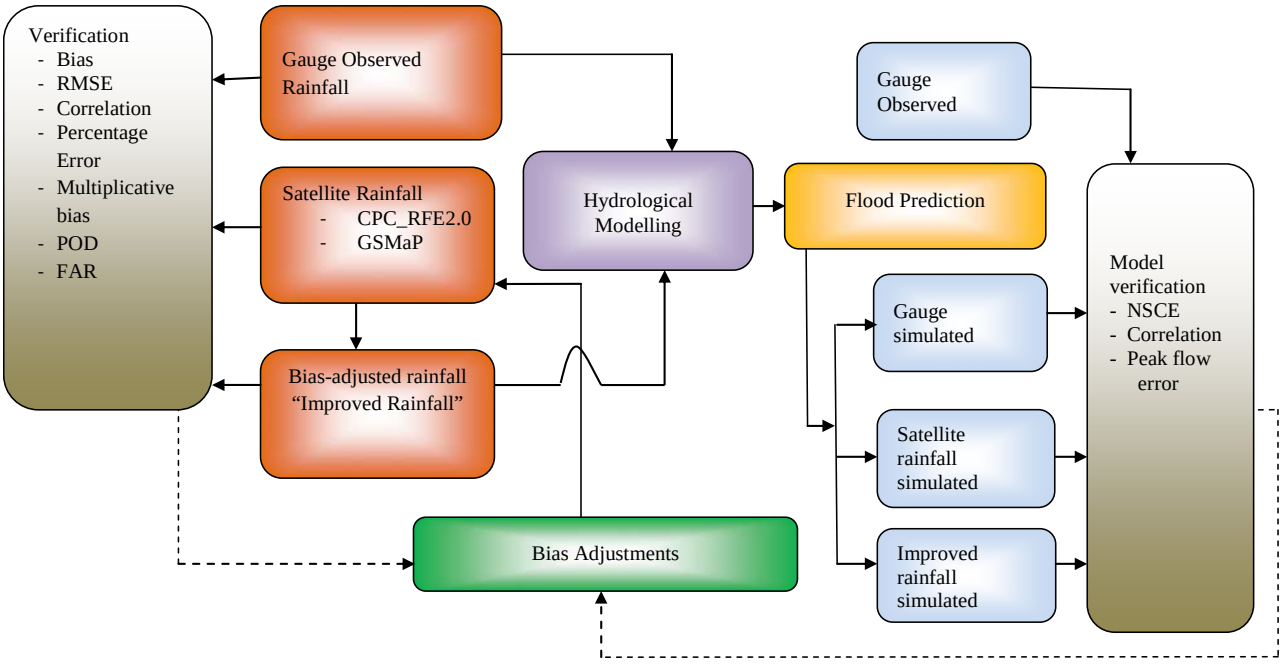

Figure 1.3 Conceptual framework of research

1.6 Outline of the Thesis

This thesis has six chapters. Chapter one is the introduction. Chapter two provides a review of the satellite-based rainfall estimation methods and products. The SRE products that have been reviewed mainly include the high resolution satellite-based products that have been in operation since 2001.The purpose of this chapter is to have a thorough knowledge of the SRE products and

understand the spatial and temporal scales at which they are produced at. The SRE products that are now available are usually a combination of inputs from various satellites rather than using a sole satellite input as it has been demonstrated the accuracy of estimates increase with a combination of products to weigh the strengths and weakness. This chapter also provides a review of the verification of SREs in other regions of the world. The purpose of this section is to understand the types of verification and the general trend in performance of SREs in various regions to draw on lessons for the himalayan region of Nepal.

Chapter three provides a thorough verification of SREs over Nepal using two products RFE and Japan Aerospace Exploration Agency (JAXA) GSMaP_MVK+ (hereafter referred to as GSMaP). The second section of this chapter provides the methodology of verification of SREs. The standard statistical verification technique has been described including the various performance indicator for assessing the accuracy of the SREs. The third section of this chapter provides an exhaustive verification of satellite based rainfall estimates over Nepal using three approaches. The first approach is assessment of the accuracy over whole of Nepal considering it as one homogeneous region. The second approach of verification is assessing the accuracy of SREs in various physiographic regions of Nepal to better understand the variation of performance of the estimates with elevation. The third approach of verification is at a basin level.

Chapter four presents the rainfall-runoff analysis using the GeoSFM streamflow model forced with SREs for flood prediction. This chapter provides a description of the model, the input parameters and flood prediction for two basins, Bagmati and Narayani. The purpose of this chapter is to demonstrate the applicability of SREs in flood prediction. The chapter provides an assessment of the accuracy of the rainfall estimates by comparing the simulated and observed discharge and provides as opportunity to understand the uncertainty in prediction of the rainfall-runoff model with observed rainfall as well as SREs.

Chapter five presents the rainfall-runoff analysis using GeoSFM streamflow model forced with bias-adjusted rainfall estimates for flood prediction. The first section of this chapter provides bias-adjustment method for flood prediction. It also describes the three ratio-based bias adjustments derived in this research. The next section presents the application of these bias-adjustments for improved flood prediction. The improvement in the SRE by ingesting the local rain gauge data into the RFE algorithm and application in improved flood prediction is also presented. This section also provides a comparative analysis of flood prediction with and without bias-adjustment.

Finally, the conclusions and recommendations from the study are presented in Chapter six.

References

Artan, G.A., Gadain, H., Smith, J., Asante, K., Bandaragoda, C.J., Verdin. J. (2007) Adequacy of satellite derived rainfall data for streamflow modeling. *Natural Hazards*, 43(2), pp.167-185

Chalise, S.R., Khanal, N.R. (2002) Recent extreme weather events in the Nepal himalayas. In, Snorrason, A.; Finnsdottir, H.P.; and Moss, M.E. (eds) The Extreme of the Extremes: Extraordinary Floods. Proceedings of a Symposium Held in Reykjavik, July 2000, pp. 141-146. Publ. No. 271. Wallingford: IAHS

Chalise, S.R., Shrestha, M.L., Thapa, K.B., Shrestha, K.B., Bajracharya, B. (1996) *Climatic and hydrological Atlas of Nepal*. Kathmandu: ICIMOD

Dinku, T., Ceccato, P., Grover-Kopec, E., Lemma, M., Connor, S.J., Roplewski, C.F. (2008) Validation of high-resolution satellite rainfall products over complex terrain. *International Journal of Remote Sensing*. Vol 29, No. 14, pp. 4097-4110.

Ebert, E.E. (2007) Methods for verifying satellite-based precipitation estimates. *Measuring Precipitation from Space*, V. Levizzani et al. (eds) Eurainsat and the Future, pp. 345-356.

Ebert, E.E.; Janowiak, J.E.; Kidd, C. (2007) Comparison of near-real-time precipitation estimates from satellite observations and numerical models. *Bull. Amer. Meteorol. Soc*. 88(1), 47–64.

Harris, A., Rahman, S., Hossain, F., Yarborough, L., Bagtzoglou, A.C., Easson, G. (2007) Satellite-based flood modelling using TRMM-based rainfall products. *Sensors*, 7, 3416–3427.

Hong, Y.; Adler, R.F.; Negri, A.; Huffman, G.J. (2007) Flood and landslide applications of near real-time satellite rainfall estimation. *Nat. Hazards*, 43, 285–294.

Hossain, F. (2005) Towards Formulation of a Space-borne System for Early Warning of Floods: Can Cost-Effectiveness outweigh Prediction Uncertainty? *Natural Hazards* (2005) 00: 1-15

Hossain, F., Katiyar, N. (2006) Improving Flood Forecasting in International River Basins. EOS, Vol. 87, No. 5, Transactions American Geophysical Union

Huffman, G.J., Adler, R.F., Bolvin, D.T., Gu, G., Nelkin, E.J., Bowman, K.P., Hong, Y., Stocker, E.F., Wolff, D.B. (2007) The TRMM Multisatellite precipitation analysis (TMPA):

quasi-global, multiyear, combined sensor precipitation estimates at fine scales. *Journal of hydrometeorology*. Vol.8 pp. 38 – 55.

Hughes, D.A. (2006) Comparison of satellite rainfall data with observation from gauging station networks. *J. Hydrol*. 327, pp. 399-410.

Ichiyanagi, K., Yamanaka, M.D., Muraji, Y., Vaidya, B.K. (2007) Precipitation in Nepal between 1987 and 1996. *International Journal of Climatology*. 27, pp. 1753-1762

Janowiak, J. E., Xie, P. (1999) CAMS–OPI: A global satellite– rain gauge merged product for real-time precipitation monitoring applications. *J. Climate,* 12, pp. 3335–3342.

Joyce, J.J., Janowiak, J.E., Arkin, P.A., Xie, P. (2004) CMORPH: A method that produces global precipitation estimates from passive microwave and infrared data at high spatial and temporal resolution. J. Hydrometeorol. 5, 487–503.

Kansakar, S.R.; Hannah, D.M.; Gerraed, J.; Rees, G. (2004) Spatial pattern in the precipitation regime of Nepal. *International Journal of Climatology* **24**, 1645–1659.

Khanal, N., Shrestha, M., Ghimire, M. (2007) *Preparing for Flood Disaster: Mapping and Assessing Hazard in the Ratu Watershed*. Kathmandu: International Centre for Integrated Mountain Development (ICIMOD)

Kidd, C., Levizzani, V., Turk, J., Ferraro, R. (2009) Satellite precipitation measurements for water resources monitoring. *Journal of the American Water Resources Association*. Vol. 45, No.3 pp. 567-579.

Kubota, T., Ushio, T., Shige, S., Kachi, M., Okamoto, K. (2009) Verification of high resolution SREs around Japan using a gauge-calibrated ground-radar dataset. *J. Meteorol. Soc.* Japan 87A, 203–222.

Sharma, C.K. *River systems of Nepal*. Sangeeta Sharma, p. 214. Kathmandu, 1977.

Shrestha, M.S., Bajracharya, S., Mool, P. (2008b) *Satellite Rainfall Estimation in the Hindu Kush-Himalayan Region*. Kathmandu: ICIMOD

Shrestha, M.S., Choppel, K. (2010) Disasters in the Himalayan Region: A case study of Tsatichu Lake in Bhutan. *Integrated Watershed Management: Perspective and Problems*, Einar Beheim et al. (eds) Springer, pp. 211- 222

Shrestha, M.S.; Artan, G.A.; Bajracharya, S.R.; Sharma, R.R. (2008a) Applying satellite based rainfall estimates for streamflow modelling in the Bagmati Basin, Nepal. *J. Flood Risk Management*, 1, 89–99.

UNDP (United Nations Development Program) (2004) *Reducing Disaster Risk: A Challenge for Development*. New York: UNDP Bureau for Crisis Prevention and Recovery. Available at www.undp.org/bcpr

Ushio, T., Sasashige, K., Kubota, T., Shige, S., Okamota, K., Aonashi, K., Inoue, N., Takahashi, T.; Iguchi, T., Kachi, M., Oki, R., Morimoto, T., Kawasaki, Z.I. (2009) A Kalman Filter approach to the global satellite mapping of precipitation (GSMaP) from combined passive microwave and infrared radiometric data, *J. Meteorol. Soc*. , Japan, Vol.87A, pp. 137-151.

Xie, P., Yarosh, Y., Love, T., Janowiak, J E., Arkin, P.A. (2002) A Real-Time Daily Precipitation Analysis Over South Asia. Preprints, 16th Conference of Hydrology, Orlando, FL, American Meteorological Society 12-17 January 2002.

CHAPTER 2

2 REVIEW OF GLOBAL SATELLITE-BASED RAINFALL ESTIMATION METHODS, PRODUCTS AND VERIFICATION

Since the launch of a meteorological satellite Television Infra-Red Observation Satellite (TIROS-1) in 1960 the study of the earth's atmosphere and oceans using data obtained from these remote sensing devices has advanced rapidly. Particularly, since the last two decades, there has been a lot of advancement in the estimation of rainfall from space. In the 1970s rainfall estimation using Infra-Red (IR) sensors on geostationary platforms to track cloud movement and advance climate and weather prediction was developed (Janowiak *et al.*, 2001). Since then, this technology for monitoring precipitation from space obtained from satellites orbiting the earth has rapidly advanced. The primary scope of satellite rainfall monitoring is to provide information on rainfall occurrence, amount and distribution over the globe on a continuous basis from all areas including those inaccessible to gauges and radar for various applications in meteorology, climatology, hydrology, and environmental sciences. This chapter reviews the satellite-based rainfall estimation methods and provides a summary of the satellite-based rainfall estimate (SRE) products available at high resolution from operational and academic institutions and suitable for water resources monitoring particularly for flood prediction. In this chapter a review of verification of high resolution SREs available in the literature is also presented.

2.1 Satellite-Based Rainfall Estimation Methods

SRE are primarily from two types of meteorological satellites, geostationary satellites and polar orbiting satellites. Figure 2.1 shows the global observing system of meteorological satellites. Geostationary Operational Environmental Satellites (GOES) are located over the equator and are at about 35,800 km away from the earth surface stationary relative to the earth and uses infrared channels. The orbits of these satellites are such that they rotate at the same speed as the earth and hence appear to be stationary relative to the earth. Geostationary satellites provide continuous observation of the earth’s surface and provide data on a half hourly basis. Imagery obtained from these satellites is mainly visible (VIS) and IR at resolution of about 4 km, with information on clouds collected once every 30 minutes (Kidd *et al*., 2009). Though a continuous coverage is provided by these satellites they are said to be limited by their range and resolution of the

imagery. There are several operational geostationary meteorological satellites in orbit such as the MTSAT, GOES, Meteosat, FY series, and INSAT.

The second type of satellites is the polar orbiting satellites. Polar-orbiting satellites travel in a circular orbit from pole to pole orbiting at an altitude of about 800 km and use microwave (MW) channels. The orbits of these satellites are such that they pass the equator at the same local time on each orbit, providing about two overpasses each day. These satellites carry a range of instruments such as MW sounders and imagers that are capable of more direct measurement of precipitation. The polar orbiting satellites include the NOAA-17 and 18, DMSP-F13,16,17, FY-1D, and METOP-A operated by various operational agencies.

Broadly there are three methods for estimating rainfall, the VIS/IR method, passive microwave (PMW) method and multi sensor technique which are briefly described below.

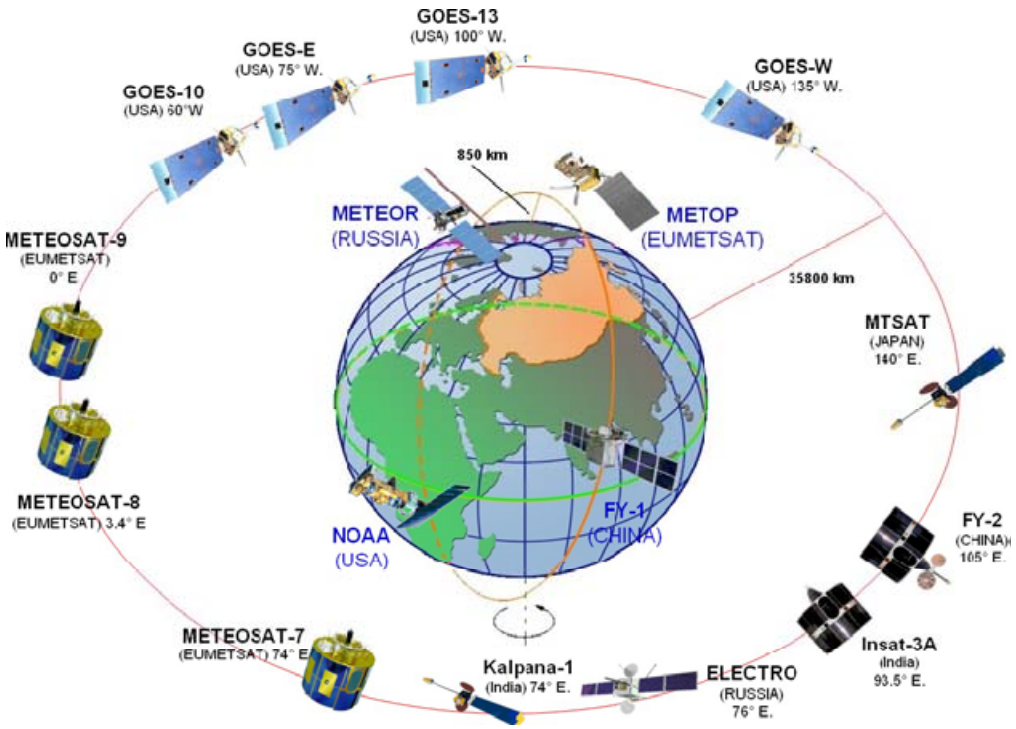

Figure 2.1 The Global Observing System of Meteorological Satellites (source: Kidd *et al.*, 2009).

2.1.1 VIS/IR Method

The visible (VIS) and infrared (IR) imagers uses cloud top temperatures which are indirect measurements but provides rapid temporal update cycle with a continuous temporal coverage every half an hour needed to capture the growth and decay of precipitating clouds (Levizzani and Amorati, 2002). Due to the indirect measurement of precipitation using cloud top temperatures

the precipitation estimates has a lower degree of accuracy. There are many IR rainfall estimation techniques that have been described in literature for example GOES precipitation technique, Negri-Adler-Wetzel technique, Infrared power law rain-rate technique, RAINSAT technique, Griffith-Woodley technique (Ebert *et al*., 1995; Levizzani and Amorati, 2002). The GPI technique is briefly described below.

The GOES precipitation index (GPI) is one of earliest satellite rainfall estimation technique developed by Arkin and Meisner (1987). This technique utilizes the correlation between the frequency of cold tropical cloud-top temperatures and rainfall rates observed at the surface on a time-scale of one month at spatial scales of 2.5^{o} latitude and longitude (Ebert *et al*., 1995; Kidd *et al*., 2009). A threshold temperature of 235 K is set to determine a constant rain rate. For each pixel, the rain rate, RR, is estimated as

$$RR = 3\ mm\ h^{-1} \quad T_b < 235\ K$$

$$RR = 0\ mm\ h^{-1}\ T_b \geq 235\ K$$

where T_b is the brightness temperature.

2.1.2 Passive Microwave method

As the IR method is an indirect measurement of rainfall using only cloud top temperatures in the late 1980 the Passive Microwave (PMW) evolved. Passive Microwave are considered more accurate estimate as it provides the direct interaction between the hydrometeors and the radiation field and more physically based rain estimates by monitoring rainfall structure inside the clouds. Precipitation drops strongly interact with MW radiation and are detected by radiometers. The major instruments used for MW-based rainfall estimations are the Special Sensor Microwave/Imager (SSM/I), a scanning-type instrument. The biggest disadvantage of this technique is the poor spatial and temporal resolution, the first due to diffraction, which limits the ground resolution for a given satellite MW antenna, and the latter to the fact that MW sensors are consequently only mounted on polar orbiting satellites with infrequent passes (twice per day per satellite) resulting in gaps in time series data (Levizzani and Amorati, 2002; Kidd *et al*., 2009). The rainfall estimation techniques based upon PMW observations is broadly categorized into two groups; the empirical and physical techniques the details of which are provided by Kidd *et al.* (1998).

2.1.3 Mutli-Sensor Technique

Techniques to generate merged products of high resolution precipitation estimates are relatively new and evolved rapidly in recent years (Xie *et al*., 2007). As each of the techniques based on IR and MW sensors described above have their strengths and limitations, techniques in combining these satellite data have been developed to improve accuracy, coverage and resolution for better rainfall estimates (Huffman *et al*., 2007). There are several algorithms that have been developed to combine the various satellite data the details of which can be referred in Levizzani and Amorati, 2002). Combining information from multiple satellite sensors as well as gauge observations and numerical model outputs yielded analyses of global precipitation with stable and improved quality (Huffman *et al*., 1997; Xie and Arkin, 1996; Hsu *et al*., 1997; Janowiak and Xie, 1999; Huffman *et al*., 2001; Adler *et al.*, 2003; Xie *et al*., 2003; Huffman *et al*., 2004; Joyce *et al*., 2004; Xie *et al*., 2007).

2.2 Satellite Rainfall Estimate Products

As we have seen from the previous section the last two decades have produced a great deal of research on estimating rainfall from IR radiometers and microwave satellite observations. As a result, there are now several operational and semi-operational algorithms available from national centres and universities to produce rainfall estimates for time periods ranging from half-hourly to monthly. There are now many global SREs that blends various sources of satellite data such as, TRMM Multi Satellite Precipitation Algorithm (TAMPA) (Huffman *et al*., 2007), Global Satellite Mapping Project (GSMaP) (Ushio *et al*., 2009), CMORPH (Joyce *et al.*, 2004), Climate Prediction Centres CPC_RFE2.0 (Xie and Arkin, 1996), PERSIANN which are described briefly in the following section.

2.2.1 The NOAA CPC_RFE2.0 Satellite Rainfall Estimates

The National Oceanic and Atmospheric Administration (NOAA) has developed several satellite-based techniques and algorithms for estimating rainfall to support the weather and flood monitoring activities of the USAID and USGS. Among them is the system developed at the Climate Prediction Center (CPC) of NOAA known as the CPC_RFE2.0 (RFE). The RFE estimates precipitation for the whole globe on a 0.1° x 0.1° grid and was produced for USAID Famine Early Warning System (FEWS) to assist in drought monitoring activities over Africa. The system merges various satellite estimates, which increases accuracy by reducing bias and

random error compared to individual data sources (Xie and Arkin ,1996), thereby adding value to rain-gauge interpolations.

The initial version RFE1.0 was operational from 1996 to 2000 over Africa. Since January 2001 the new version RFE2.0 has been operational. Input data used for operational rainfall estimates are from 4 sources; 1) Daily World Meteorological Organization's (WMO) Global Telecommunication Satellite (GTS) rain gauge data 2) Advanced Microwave Sounding Unit (AMSU) microwave satellite precipitation estimates up to 4 times per day 3) SSM /I satellite rainfall estimates up to 4 times per day 4) GPI cloud-top IR temperature precipitation estimates on a half-hour basis. The three satellite estimates are first combined linearly using predetermined weighting coefficients, then are merged with station data to determine the final rainfall. The shape of the precipitation is given by the combined satellite estimates, while the magnitude is inferred from GTS station data (NOAA 2009). This RFE has been put into operation at the CPC on a semi real time basis for South Asia since June 2001 (Xie *et al*., 2002). Figures 2.2 and 2.3 shows the domain for which the RFE are available over South Asia. The initial domain was expanded to $60^{o} – 110^{o}$ E longitude and $5^{o} – 40^{o}$ N latitude at 0.1^{o} spatial resolution and provides daily rainfall estimates over South Asia (http://www.cpc.ncep.noaa.gov/products/fews/SASIA/rfe.shtml).

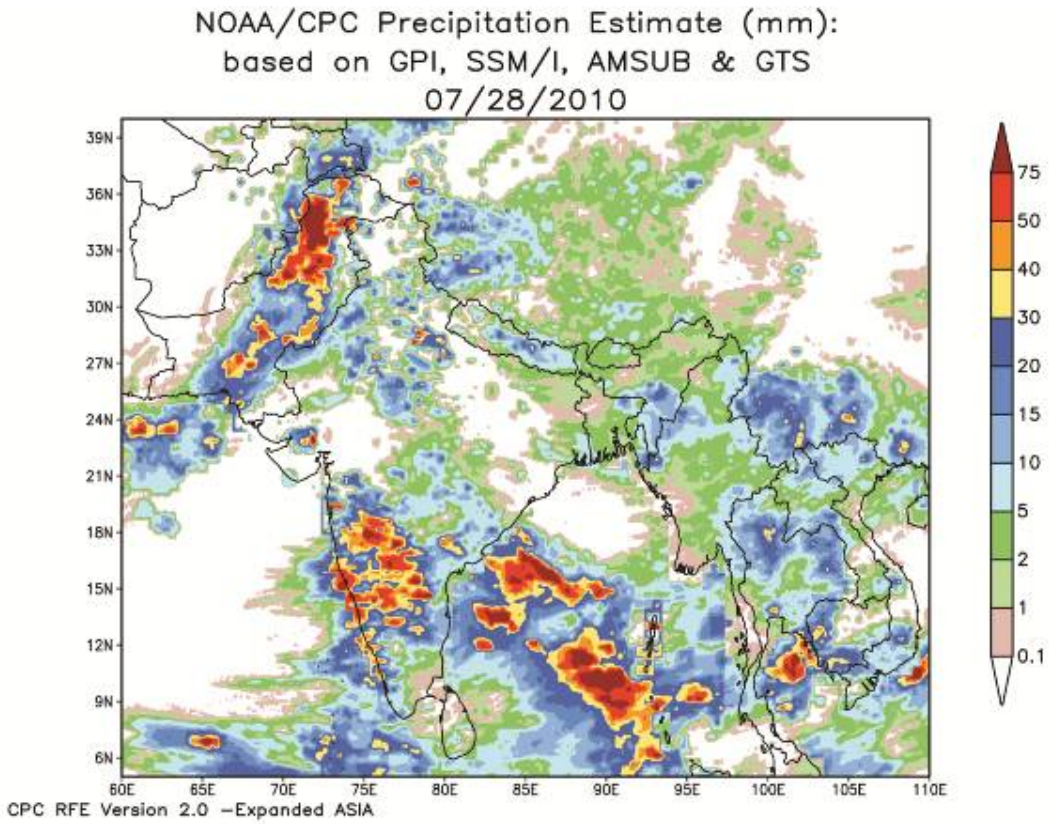

Figure 2.2 CPC_RFE2.0 rainfall estimates over South Asia domain

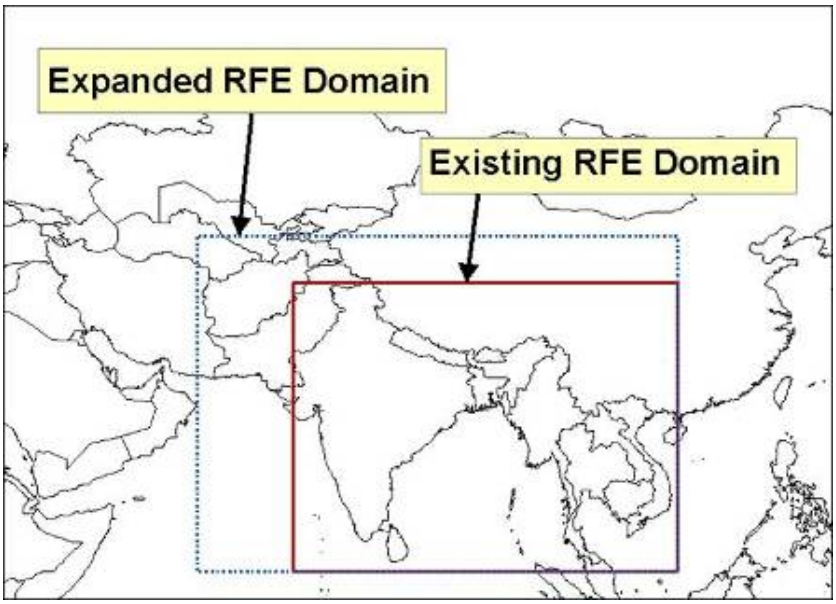

Figure 2.3 Domain of the CPC RFE-2.0 (Source: Love, T., 2006)

2.2.2 The NOAA CMORPH Rainfall Estimates

CPC MORPHing technique (CMORPH) is a method that produces global precipitation estimates from passive microwave and infrared data at high spatial and temporal resolution. This technique uses precipitation estimates that have been derived from microwave observations, and whose features are transported via spatial propagation information that is obtained entirely from geostationary satellite IR data (NOAA-CP website). First, the time sequence of feature motions are determined from the IR data, and then this information is used to provide the displacement vector for morphing from one instantaneous microwave estimate to the next. In this way, CMORPH combines the superior retrieval accuracy of PM estimates and the higher temporal and special resolution of IR data. The final product is PM only, with the IR data used indirectly. This technique is not a precipitation estimation algorithm but a means by which estimates from existing microwave rainfall algorithms are combined. Therefore, this method is extremely flexible such that any precipitation estimates from any microwave satellite source can be incorporated. CMORPH produces global precipitation analyses at very high spatial (8 km) and temporal (30 min) resolution starting from December 2002 and is available 60N-60S. The rainfall estimates are also available 3 hrly at 0.25^{o} x 0.25^{o} spatial resolution and can be accessed from http://www.cpc.noaa.gov/products/janowiak/cmorph_description.html/.

2.2.3 Tropical Rainfall Measuring Mission (TRMM)

The Tropical Rainfall Measuring Mission (TRMM) satellite was launched in 1997 to provide accurate measurement of the spatial and temporal variation of tropical rainfall around the globe. Three instruments form the original TRMM rainfall estimates, the Precipitation Radar (PR), the TRMM Microwave Imager (TMI), a multi-channel passive microwave radiometer, and the Visible Infrared Scanner (VIRS). The PR provides three-dimensional structure of rainfall, particularly the vertical distribution and 2) obtains high quality, quantitative rainfall measurements over land as well as over ocean. The TMI complements the PR by providing total hydrometeor (liquid and ice) content within precipitating systems. The VIRS is used to provide the cloud context of the precipitation structures and is used as part of a transfer strategy to connect microwave precipitation information to infrared-based precipitation estimates from geosynchronous satellites.

The Tropical Rainfall Measuring Mission (TRMM) Multisatellite Precipitation Analysis (TMPA) provides global precipitation estimates from a wide variety of meteorological satellites. Rainfall estimates are provided at fine resolution (0.25°x0.25°, 3-hourly) in both real and post-real time basis. Products from TMPA include the 'TRMM and Other Satellites' (3B42) and 'TRMM and Other Sources' (3B43) described in Huffman *et al.* (2003). The major inputs into the 3B42 algorithm are IR data from geostationary satellites, PM data from the TMI, SSM/I, AMSU and Advanced Microwave Sounding Radiometer-Earth Observing System (AMSR-E). The 3B42 estimates are produced in four steps: (1) the PM estimates are calibrated and combined, (2) IR precipitation estimates are created using the PM estimates for calibration, (3) PM and IR estimates are combined, and (4) the data are rescaled to monthly totals whereby gauge observations are also used indirectly (Huffman *et al.*, 2007). This product is however not real time but available about 10 to 15 days after the end of each month. There is a near-real-time version, 3B42-real-time (3B42RT), that is available with a time lag of about 9 hours. This version is just a product at the third step above, and does not include gauge information. It starts from 2002 and is still an experimental product. Finally, 3B42 estimates are accumulated and merged with gauge data to produce the monthly product (3B43) at 0.25° spatial resolution. The data covers the domain from 50° N- 50° S. The 3B42 and 3B43 products have been available since 1998. An easy web-based interface TRMM Online Visualization and Analysis System (TOVAS) has been designed for visualization and analysis of the daily TRMM and other rainfall estimates (3B42_V6 derived). The details of the algorithm can be obtained from http://trmm.gsfc.nasa.gov/3b42.html and easy visualization of data from http://disc2.nascom.nasa.gov/Giovanni/tovas/TRMM_V6.3B42_daily.shtml. Figure 2.4 provides the daily TRMM 3B42_V6 rainfall map for 28th July 2010 during the recent Pakistan floods and Figure 2.5 shows the global near real-time 3 hrly TMPA rainfall estimates.

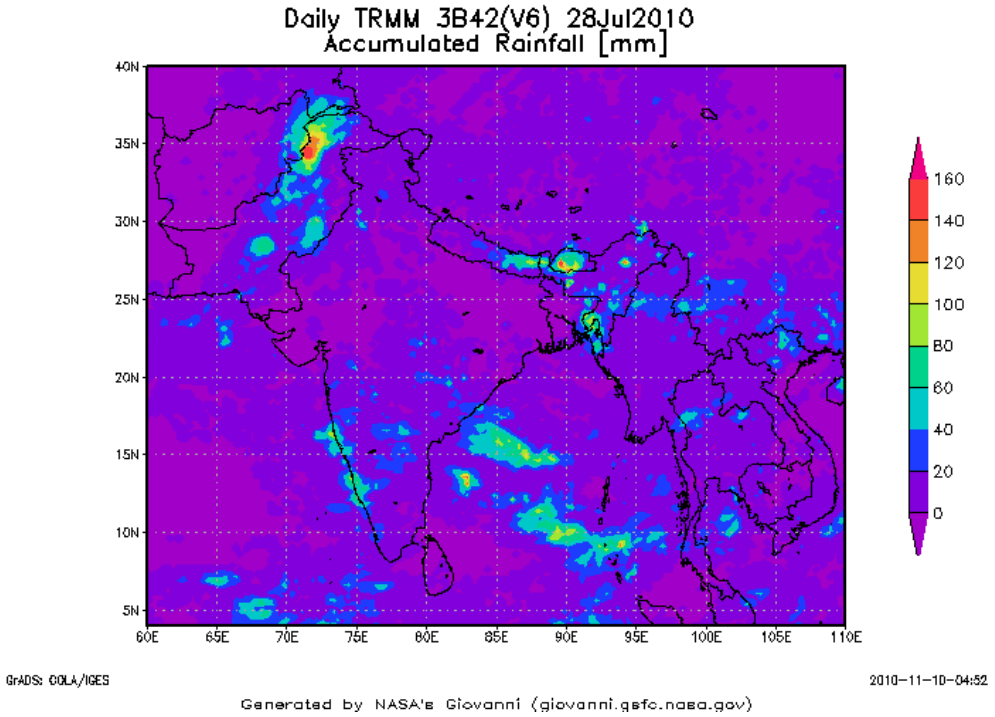

Figure 2.4 Daily TRMM 3B42_V6 rainfall estimates in the South Asia domain

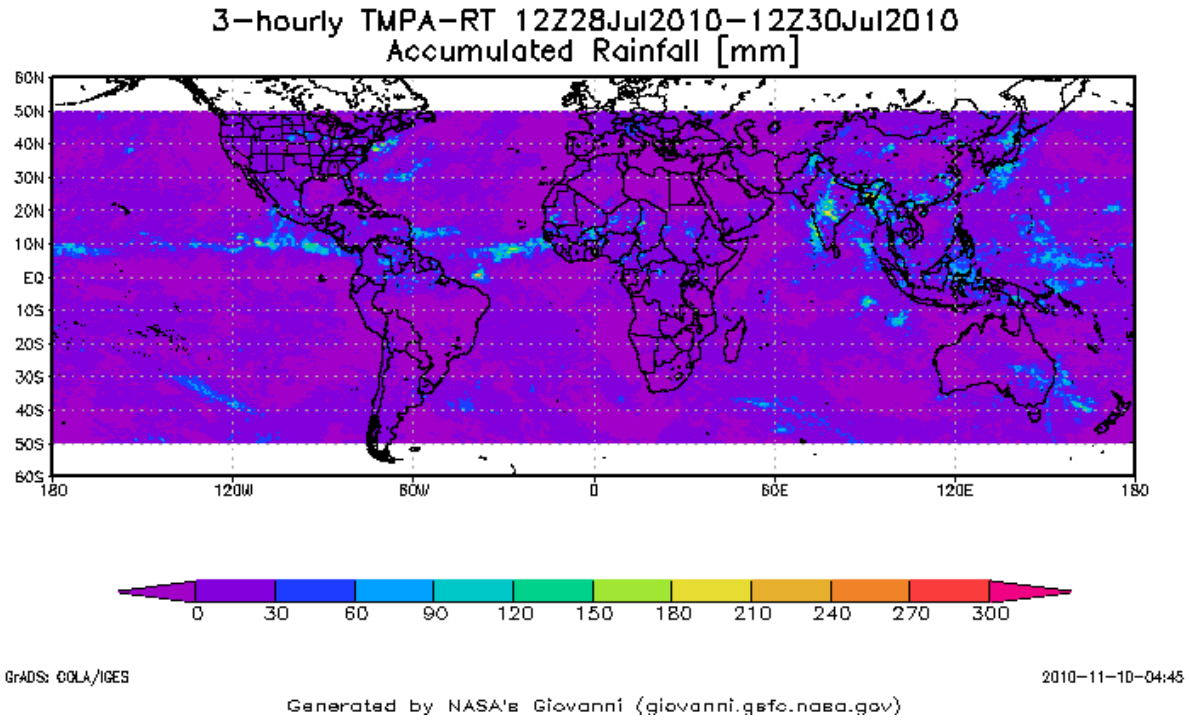

Figure 2.5 Global TRMM Multisatellite Precipitation Analysis (TMPA) rainfall estimates

2.2.4 Global Satellite Mapping Project (GSMaP)

Since 2002 the Global Satellite Mapping of Precipitation (GSMaP) was initiated by Japan Science and Technology Agency (JST) and is promoted by the JAXA Precipitation Measuring Mission (PMM) Science Team, to produce global precipitation products with high temporal and spatial resolution (Ushio *et al*., 2009). The GSMaP_MVK+ (hereafter, GSMaP) is a global hourly product with a domain covering 60^{o} N – 60^{o} S at a 0.1 x 0.1 degree grid resolution and calculated using a passive MW radiometer – IR radiometer blended algorithm (Ushio *et al*., 2009). Several satellite estimates from MW and IR are merged together to estimate the rainfall. The MW radiometer data includes TRMM/TMI, Aqua/AMSR-E, DMSP/SSMI (F13, 14, 15), NOAA/ AMSU-B (N15, N16, N17, N18). The IR data includes globally-merged (60^{o} N-60^{o} S) pixel-resolution IR brightness temperature data, merged from all available geostationary satellites (GOES-8/10, METEOSAT-7/5 & GMS) provided by NCEP/CPC. The 24 hours accumulated daily GSMaP MVK+ rainfall estimates from 2003 to 2006 were downloaded from the JAXA ftp server for the present research. There is also a near real time version (GSMaP_NRT) product the estimates of which are shown in Figure 2.6 for South Asia.

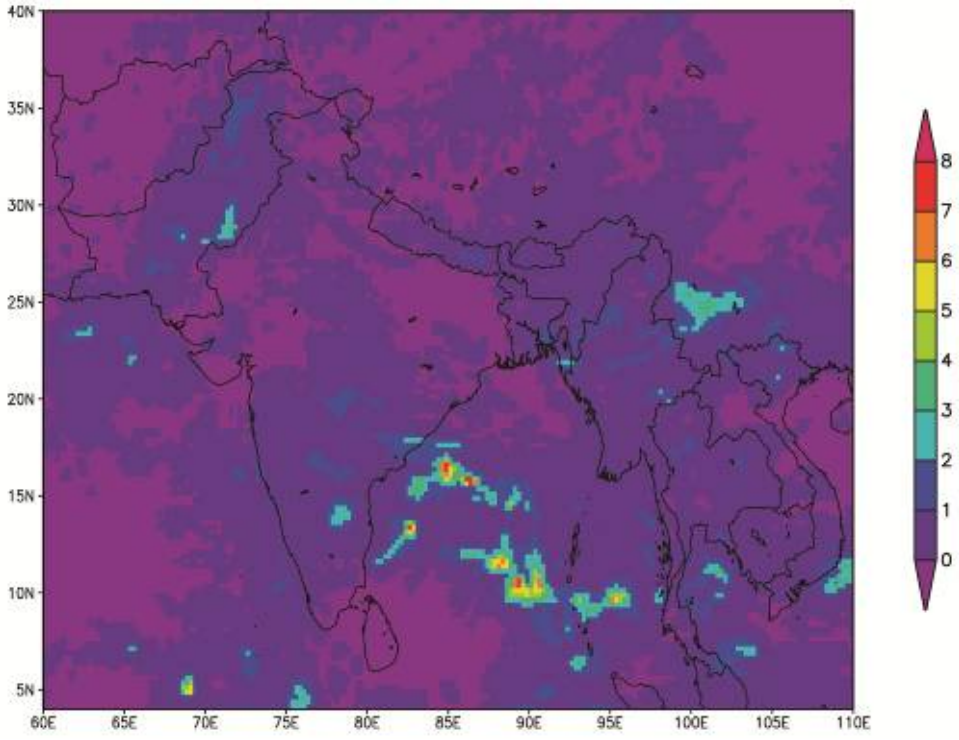

Figure 2.6 GSMaP_NRT rainfall estimates over South Asia

2.2.5 Precipitation Estimation from Remote Sensing Information using Artificial Neural Network (PERSIANN)

The Precipitation Estimation from Remote Sensing Information using Artificial Neural Network (PERSIANN) is a neural network derived rainfall estimate combining data from IR and MW observations. It computes an estimate of rainfall rate at each 0.25° x 0.25° pixel of the infrared brightness temperature image provided by geostationary satellites. An adaptive training feature facilitates updating of the network parameters whenever independent estimates of rainfall are available. The PERSIANN system was based on geostationary infrared imagery and later extended to include the use of both infrared and daytime visible imagery. Rainfall product covers 50° S to 50° N globally. The system uses grid infrared images of global geosynchronous satellites (GOES-8, GOES-10, GMS-5, Metsat-6, and Metsat-7) provided by CPC, NOAA to generate 30-minute rain rates are aggregated to 6-hour accumulated rainfall. Model parameters are regularly updated using rainfall estimates from low-orbital satellites, including TRMM, NOAA-15, -16, -17, DMSP F13, F14, F15. The product is available at a spatial resolution of 0.25° x 0.25° latitude/longitude and a temporal resolution of 30 minutes accumulated to 6-hour accumulated rainfall and the detailed description of which can be accessed through http://chrs.web.uci.edu/research/satellite_precipitation/activities00.html.

Table 2.1 A list of selected high resolution satellite-based products

Product	Description	Source Data	Temporal	Spatial	Coverage	Latency	Website/data information
CPC_RFE2.0	NOAA Climate Prediction Centre Rainfall Estimate	IR, MW	24 hrs	0.1^{o}x 0.1^{o}	60E-110E 4N-40N	17 hrs	http://www.cpc.noaa.gov/products/fews/SASIA/rfe.shtml
GSMaP	JAXA Global Satellite Mapping Project	IR, MW	hourly	0.1^{o}x 0.1^{o}	50N-50S Global	4 hrs	http://sharaku.eorc.jaxa.jp/GSMaP_crest/
TRMM	NASA Tropical Rainfall Measuring Mission	IR, PW, PR	3 hourly	0.25^{o}x0.25^{o}	50N-50S Global	6 hrs	http://disc2.nascom.nasa.gov/Giovanni/tovas/
TMPA	NASA TRMM multisatellite precipitation analysis	IR, MW, PR	3 hourly	0.25^{o}x0.25^{o}	50N-50S Global	9 hrs	http://disc2.nascom.nasa.gov/Giovanni/tovas/
PERSIANN	Precipitation estimate from remotely sensed instruments using artificial neural networks	IR, MW	6 hourly	0.25^{o}x0.25^{o}	50N-50S Global		http://chrs.web.uci.edu/research/satellite_precipitation/activities00.html
CMORPH	NOAA CPC Morphing technique	IR data, passive microwaves (DMSP 13, 14 & 15) (SSM/I), NOAA-15, 16, 17 & 18 (AMSU-B), and AMSR-E and TMI aboard NASA's Aqua and TRMM spacecraft,	3 hourly	0.25^{o}x0.25^{o}	60N-60S Global	18 hrs	http://www.cpc.noaa.gov/products/janowiak/cmorph_description.html/ (ftp://ftp.cpc.ncep.noaa.gov/precip/global_CMORPH/3-hourly_025deg)

2.3 Review of Verification of Satellite-Based Rainfall Estimates

Satellite-based rainfall estimates have been verified in several regions in the world for understanding the accuracy and its strengths and weakness. The verification of the estimates has been conducted at various spatial and temporal resolutions depending upon the expected application. A great deal of work has been done to validate climate-scale precipitation estimates against gauge data over land and for island stations (Ebert, 2002). Comparisons have been made with gauge observed rainfall from ground stations, radar and with numerical models. This section provides a review of verification of SRE with gauge observed rainfall from ground measuring stations available in published peer reviewed literature since the last two decades focusing on over land verification. It primarily looks into the verification of the satellite-based rainfall products in various regions country wise as well as for specific topographic context in detecting and quantifying the amount of rainfall rather than on the rain rate estimates.

Javanmard *et al*. (2010) evaluated TRMM 3B42 rainfall estimates with high resolution gridded precipitation datasets based on rain gauges (Aphrodite) over Iran. Comparisons were made in the Caspian sea region and in the Zagros mountains and for the entire country. Spatial distributions of mean annual average and winter rainfall were analyzed and correlation of about 0.70 was derived between TRMM 3B42 and high resolution gridded gauge based precipitation. TRMM_3B42 is found to underestimate rainfall along the Zagros Mountains and the Caspian sea.

Kubota *et al*. (2009) verified six high resolution SREs (GSMaP, CMORPH, TRMM 3B42, PERSIANN, Naval Research Laboratory (NRL) Blended, 3B42RT) around Japan with ground-based radar data for January through December 2004. In particular the GSMaP rainfall estimates were validated in detail. The 3B42 datasets best agreed to the radar data and NRL the worst when comparisons of monthly time series of SREs were performed. The better performance of 3B42 in comparison to other products is because the 3B42 datasets are adjusted by gauge information. The highest spatial correlation and lowest Root Mean Square Error (RMSE) was obtained with CMORPH and GSMaP which utilizes the morphing technique using GEO IR information. The study used a temperature threshold of 4 ^{o}C regions above were considered for the validation. In the north around the Hokaido Island the Probability of Detection (POD) was low with larger errors in rain no rain detection. Satellite estimates were poor for light and very heavy rainfall during the warm season and worst over mountainous regions influenced by orographic rain.

A number of validations with various SREs have been conducted over Africa. Asadullah *et al*. (2008) evaluated five satellite rainfall estimation products (TRMM 3B42, TAMSAT, PERSIANN, CMORPH and CPC_RFE2.0) over four regions of Uganda. Due to absence of reliable data since 1990 the SREs have been compared to the historical data from 1960-1990 to assess the ability of RFE to detect seasonal and spatial rainfall characteristics of Uganda. Products were generally able to reproduce seasonal patterns in regional rainfall amounts at the monthly scale. The verification is limited to monthly and regional scales and recommends further research at sub-regional and sub-monthly scales. CMORPH was found to match closely to the historical seasonal patterns of rainfall amounts and frequency followed by TAMSAT and TRMM 3B42. However, in terms of spatial patterns CPC_RFE2.0 showed better results in comparison to the other products. As each satellite-based product has its merits and demerits it is recommended that more than one product should be used to estimate rainfall.

A series of validation of SREs over East Africa were performed by Dinku *et al*. (2007, 2008). Dinku *et al*. (2007) conducted an extensive evaluation of 10 different satellite rainfall products over Ethiopian Highlands of East Africa at different spatial and temporal scales. Verification was made for coarse and high resolution products. The coarse resolution verification done using 2.5^{o} grid cells of monthly rainfall estimates recommends the use of additional rain gauge data to improve the SREs Verification of finer resolution SREs at 10 day accumulation (1^{o}, 0.5^{o} and 0.25^{o}) showed CMORPH and TAMSAT to have better agreement with the gauge observed datasets with CPC_RFE2.0 underestimating the rainfall. However, the best product depends upon the specific application it is intended for whether for climatologically purposes, water resources assessment or flood forecasting.

As a follow up to the previous work Dinku *et al*. (2008) evaluated high resolution satellite rainfall products at higher temporal (daily) and spatial resolution (0.25^{o}) in Ethiopia with mountainous topography and in Zimbabwe with a flatter terrain. Similar to Nepal, topography play a significant role in determining the climate of Ethiopia. The topography ranges from sea level to about 4000 m with hot deserts as well as cold highlands. As this study has explored the influence of topography in the highlands of Ethiopia the research findings is of interest to my current research. CPC_RFE, TRMM 3B42, CMORPH, PERSIANN showed good performance in detecting the occurrence of rainfall but poor in estimating the amount. The performance was better over Zimbabwe as compared with Ethiopia which may partly be due to the influence of topography.

Xie *et al*. (2007) developed a new gauge analysis product over East Asia and validated it against five high resolution SREs, CMORPH, TRMM 3B42, 3B42RT, NRL and PERSIANN. Apart from the 3B42 all of the other four products (CMORPH, TRMM 3B42RT, NRL, and PERSIANN) are based on combination of various satellite observations. The TRMM 3B42 is bias corrected using gauge observations. While all the five products performed well in capturing the spatial structure of the precipitation CMORPH provided better skill in reproducing the spatial pattern. Quantitative evaluation of the products conducted over China revealed that the performance of temporal variation of daily precipitation was better in the eastern half of China. In the quantitative assessment also CMORPH showed better skill than the rest though the TRMM 3B42 which is gauge corrected yielded higher correlation. In parts of western China and the Tibetan Plateau the correlation was very poor. Xie *et al*. (2007) infers that that the satellite algorithms tend to perform better over regions with wetter climate, while they demonstrate limited skills over arid and semiarid areas.

Hughes (2006) compared satellite-based rainfall data from PERSIANN and GPCP with gauge observed rainfall data in four basins with different climate regimes within southern Africa to explore the use of SRE in hydrological models. Monthly time steps with simple statistics (visual interpretation, r^2 and slope) were used in the comparison for use in hydrological models for water resources assessment. Preliminary analysis has provided encouraging results for further use of SRE data and suggests further research on methods to adjust the estimates for application into water resources assessment.

Barros *et al*. (2000) evaluated the skill of TRMM sensors in detecting rain-producing weather systems, and compared TRMM derived precipitation (TMI and PR) with ground based observations in the Marshyangdi catchment of Nepal. It was found that PR has better overall performance in detecting rainfall compared with TMI. PR is able to detect heavy rain in the complex Himalayan terrain however, detection is found to be better in lower altitudes compared with high altitudes. The verification was limited to detection of rainfall and not regarding quantitative amounts. For the first time over the central Himalayas the horizontal and vertical profile for a storm system was also studied.

Laurent *et al*. (1998) evaluated the performance of five satellite rainfall estimation methods with ground based precipitation over the Sahel region using the 10-day rainfall records from 1989-1993 at a 0.5^o to 1^o spatial resolution. This study is before the availability of high resolution satellite-based products such as the TRMM. The study shows that the impact of

increasing the integration of time yielded in improved and is thus is more important than space averaging. For accurate performance evaluation it is recommended that a multi error criteria approach needs to be adopted.

Table 2.2 Verification of satellite based rainfall estimates in selected regions

Region/ Country	Satellite-based rainfall products	Reference	Verification Period	Verification scale	Verification Parameters	Results/comments
Japan (2009)	GSMaP, CMORPH, 3B42, 3B42RT, PERSIANN, NRL Blended	Kubota et al. (2009)	2004	3 hrly, daily, monthly	Spatial correlation, RMSE, ETS, POD, FAR, Frequency Bias	GSMaP performed worse in mountainous areas with orographic influence
East Asia (China)	CMORPH, TRMM 3B42, TRMM 3B42RT, PERSIANN, NRL	Xie, et al. (2007)	Jan–July, 2003 (7 months)	daily	correlation	Satellite algorithms tend to perform better over regions with wetter climate, while they demonstrate limited skills over arid and semiarid areas.
Marsyangdi Valley (Nepal) (2000)	TRMM (TMI and PR)	Barros et al. (2000)	1999 (monsoon)	hrly, seasonal	POD, FAR, Skill, TS	Better detection of rain at low altitude stations compared with high elevation stations but with no quantification.
Africa Uganda	TRMM 3B42, CMORPH, TAMSAT, RFE2.0, PERSIANN		1960-1990 2003-2005	Average monthly, seasonal	Bias, correlation, efficiency, RMSE	Products are able to reflect seasonal and spatial patterns of rainfall but generally poor performance in mountainous regions. RFE2.0 shows best spatial patterns.
Sahel (Bukino Faso)	TAMSAT		1989-1993	10-days	Bias, RMSE, r, skill and scaled root mean square error	Improvement in performance with increasing the time integration from dekadel to 30 days but no significant improvement in increasing the grid cell size.
East Africa (Ethiopia)	GPCP, CMAP, TRMM-3B43, TAMSAT,	Dinku et al. (2007)	2000-2004	dekadel	Bias, RMSE, Efficiency, multiplicative bias	Best product depends on the specific application – TRMM 3B42RT performs better than CPC_RFE2

	CMORPH, CPC_RFE, TRMM 3B42					
Ethiopia Zimbabwe	RFE, TRMM 3b42, 3b42NRT, CMORPH, PERSIANN	Dinku et al. (2008)	2003-2004 (Jun – Sep) 2003 (Jan-Mar)	daily	Bias, MAE, r, efficiency, POD, FAR, ETS, HK, HSS	All products perform poorly at a pixel to pixel level comparison with underestimation of rainfall except with PERSIANN where there is overestimation. All products good in detection but not in estimation.
Southern Africa (2006)	PERSIANN GPCP	Hughes (2006)	1997-2000	monthly	Coefficient of determination, slope of the best fit regression line	Satellite data needs to be calibrated against gauge observed data to be used in conjunction with the gauge observed data for hydrological applications.
Iran (2010)	TRMM 3B42	Javanmard et al. (2010)	1998-2006	Monthly, seasonal, annual	Spatial correlation, bias, standard deviation	Relatively good correlation but varying with regions and overall underestimation of rainfall.

2.4 Summary

For application of SREs into hydrological modeling such as flood prediction it is important to have a thorough understanding of the SREs. This chapter has provided a review of the various methods available for satellite rainfall estimation the understanding of which is necessary for verification of the products. The three methods described are VIS/IR method, PMW method and merging of various satellite data. The high resolution satellite products that are now available are mostly merged products with a combination of various IR and MW satellite sensor inputs. A summary of selected high resolution SREs considered relevant for hydrological modeling has been described. Finally, verification of some of the products over various regions has been presented.

References

Adler, R.F., Chang, G.J., Ferraro, R., Xie, P., Janowiak, J., Rudolf, B., Schneider, U., Curtis, S., Bolvin, D., Gruber, A., Susskind, J., Arkin, P., Nelkin, E. (2003) The version-2 Global Precipitation Climatology Project (GPCP) monthly precipitation analysis (1979-present). *J. Hydrometeorol*. 4, 1147–1167.

Asadullah, A., Mc.Intyre, N., Kigobe, M. (2008) Evaluation of five satellite products for estimation of rainfall over Uganda. *Hydrological Sciences*, 53 (6), pp. 1137-1150.

Barros, A.P., Joshi, M., Putkonen, J., Burbank, D.W. (2000) A study of the 1999 monsoon rainfall in a mountainous region of in central Nepal using TRMM products and rain gauge observations. *Geophysical Research Letters*: Vol 27, pp. 3683-3686.

Dinku, T., Ceccato, P., Grover-Kopec, E., Lemma, M., Connor, S.J., Roplewski, C.F. (2007) Validation of satellite rainfall products over East Africa's complex topography. *International Journal of Remote Sensing*. Vol. 28, No.7, pp. 1503-1526.

Dinku, T., Chidzambwa, S., Ceccato, P., Connor, S.J., Ropelewski, C.F. (2008) Validation of high-resolution satellite rainfall products over complex terrain. *Int. J. Remote Sens*. 29(14), 4097–4110.

Ebert, E.E., Marshall, J.L. (1995) An evaluation of infrared satellite rainfall estimation techniques over Australia. *Aust. Met. Mag*. 44. Pp. 177-190.

Hsu, K.L., Gao, X., Sorooshian, S, Gupta,V. (1997) Precipitation estimation from remotely sensed information using artificial neural networks. *J. Appl. Meteor.,* **36,** 1176–1190.

Huffman, G. J., and Coauthors (1997) The Global Precipitation Climatology Project (GPCP) combined precipitation dataset. *Bull. Amer. Meteor. Soc.,* **78,** 5–20.

Huffman, G.J., Adler. R.F., Morrissey, M.M., Bolvin, D.T., Curtis, S., Joyce, R., McGavock, B., Susskind, J. (2001) Global precipitation at one-degree daily resolution from multisatellite observations. *J. Hydrometeor.,* **2,** 36–50.

Huffman, G.J., Adler, R.F., Bolvin, D.T., Gu, G., Nelkin, E.J., Bowman, K.P., Hong, Y., Stocker, E.F., Wolff, D.B. (2007) The TRMM Multisatellite precipitation analysis (TMPA): quasi-global, multiyear, combined sensor precipitation estimates at fine scales. *Journal of hydrometeorology*. Vol.8 pp. 38 – 55.

Hughes, D.A. (2006) Comparison of satellite rainfall data with observations from gauging station networks. *J. Hydrol*. 327, 399–410.

Janowiak, J. E., Xie, P. (1999) CAMS–OPI: A global satellite– rain gauge merged product for real-time precipitation monitoring applications. *J. Climate,* **12,** 3335–3342.

Javanmard, S., Yatagai, A., Nodzu, M.M., BodaghJamali, J., Kawamoto. H. (2010) Comparing high-resolution gridded precipitation data with satellite rainfall estimate of TRMM_3B42 over Iran. *Adv. Geosci.* Vol 25. pp. 119-125.

Joyce, J.J., Janowiak, J.E., Arkin, P.A., Xie, P. (2004) CMORPH: A method that produces global precipitation estimates from passive microwave and infrared data at high spatial and temporal resolution. J. Hydrometeorol. 5, 487–503.

Kidd, C., Levizzani, V., Turk, J., Ferraro, R. (2009) Satellite precipitation measurements for water resources monitoring. *Journal of the American Water Resources Association*. Vol. 45, No.3 pp. 567-579.

Kubota, T., Ushio, T., Shige, S., Kachi, M., Okamoto, K. (2009) Verification of high resolution SREs around Japan using a gauge-calibrated ground-radar dataset. *J. Meteorol. Soc.* Japan 87A, 203–222.

Laurent, H., Jobard, I., Toma, I. (1998) Validation of satellite and ground based estimates of precipitation over the Sahel. *Atmospheric Research*, 47-48, pp 651-670.

Levizzani, V., Amorati, R. (2002) A Review of Satellite-based Rainfall Estimation Methods. MUSIC – MUltiple-Sensor Precipitation Measurements, Integration, Calibration and Flood Forecasting Project. WP6 report.

NOAA (2009) The NOAA Climate Prediction Center African Rainfall Estimation Algorithm Version 2.0.

Sorooshian, S., Kuo-Lin H., Xiaogang, G., Gupta, H.V., Imam, B., Braithwaite, D. (2000) Evaluation of PERSIANN System Satellite–Based Estimates of Tropical Rainfall. *Bulletin of the American Meteorological Society*: Vol. 81, No. 9, pp. 2035–2046.

Ushio, T., Sasashige, K., Kubota, T., Shige, S., Okamota, K., Aonashi, K., Inoue, N., Takahashi, T.; Iguchi, T., Kachi, M., Oki, R., Morimoto, T., Kawasaki, Z.I. (2009) A Kalman Filter approach to the global satellite mapping of precipitation (GSMaP) from combined passive microwave and infrared radiometric data, *J. Meteorol. Soc*. , Japan, Vol.87A, pp. 137-151.

Xie, P., Janowiak, J.E., Arkin, P.A., Adler, R., Gruber, A., Ferraro, R., Huffman, G.J., Curtis, S. (2003) GPCP pentad precipitation analyses: An experimental dataset based on gauge observations and satellite estimates. *J. Climate*, 16, 2197– 2214.

Xie, P., Yatagai, A., Chen, M., Hayasaka, T., Fukushima, Y., Changming, L., Yang, S. (2007) A gauge-based analysis of daily precipitation over East Asia. *J. Hydrometeorol*. 8, 607–626.

Xie, P., Yarosh, Y., Love, T., Janowiak, J.E., Arkin, P.A. (2002) A Real-Time Daily Precipitation Analysis Over South Asia Preprints, 16th Conference of Hydrology, Orlando, FL, American Meteorological Society 12-17 January 2002.

Xie, P., Arkin, P.A. (1996) 'Analysis of global monthly precipitation using gauge observations, satellite estimates and numerical model predictions'. *Journal of Climate* 9: 840-858

CHAPTER 3

3 VERIFICATION OF SATELLITE-BASED RAINFALL ESTIMATES OVER CENTRAL HIMALAYAS OF NEPAL

From the previous chapters we have seen that in the recent years there has been rapid development of satellite-based precipitation products with various temporal and spatial resolutions and efforts to evaluate the accuracy of such estimates. Depending upon the nature of the application these products need to be verified to understand their accuracy and limitations for further use whether it is in flood forecasting, climate modelling or other hydrological water resources assessments (Ebert *et al*., 2007a). Verification of the Satellite-based Rainfall Estimates (SRE) is done by comparing the estimates against independent observed data from rain gauges and radars. One of the objectives of this research is to assess the accuracy of SRE in Nepal for suitability of applying it to flood prediction. Verification of SREs has been conducted at various levels, country as a whole region, for various physiographic regions and in selected basins. This chapter provides the verification of SRE over the central Himalayas of Nepal. This chapter is divided into two sections. The first section provides the methodology for verification of SREs. The second section provides the verification of SREs over Nepal at various levels.

3.1 Methodology for Verification of Satellite-Based Rainfall Estimates

Standard methods for verifying SRE to quantify error include bias, correlation, and Root Mean Square Error (RMSE) (Ebert *et al*., 2007b). For finer application in near real time basis for floods and flash floods forecasting more accurate estimates of rain volume, time and other indicators are needed. For example in flash floods Kidler *et al*. (2001) emphasizes the importance of correct detection of occurrence of the event along with estimate of the maximum rate rates. The standard verification techniques to compare SREs with the gauge observed rainfall includes three methods 1) visual interpretation, 2) continuous verification technique and 3) categorical verification technique (Ebert *et al*., 2007b). This section describes the verification techniques that have been used for rainfall verification in general and in specific describes the method used for this research.

3.1.1 Visual Verification

Visual comparison is one of the effective means of verification by comparing mapped estimates and observations of the same scale. The two datasets are remapped to the same projection with the same colour scale and inspected by laying them side by side. This verification technique is also known as the "eyeball" verification and is a good qualitative measure of verification. This is one of the techniques of verification used in this research.

3.1.2 Continuous Verification Technique

Continuous verification technique is quantitative in nature and used to evaluate the performance of satellite-based products in estimating the amount of rainfall. The statistical indicators such as mean error (bias), RMSE, multiplicative bias (Mbias), percentage error (PE) and correlation coefficient are used to quantify the predictive skills of the SREs. In the statistical indicators that are described below E_i designates estimated value, O_i Observed value at a given cell and N the number of samples.

Bias or Mean Error

The bias is defined as the average difference between SREs and gauge observed rainfall data. The value of bias can be positive as well as negative. A negative bias indicates underestimation of rainfall while a positive bias indicates overestimation of rainfall. The bias is given by equation 1 and normalized bias by equation 2.

$$bias = \frac{1}{N} \sum_{i=1}^{N} (E_i - O_i) \quad (1)$$

$$Normalized\ bias = \frac{\sum_{i=1}^{N} (E_i - O_i)}{\bar{O}} \quad (2)$$

Mean Absolute Error

The mean absolute error (*MAE*) measures the average magnitude of the error and is given by equation 3.

$$MAE = \frac{1}{N}\sum_{i=1}^{N}|(E_i - O_i)| \quad (3)$$

Root Mean Square Error

The RMSE measures the average error magnitude, giving greater weight to larger errors. The RMSE was differentiated into systematic (RMSEs) and unsystematic (RMSEu) error. The RMSE, RMSEs, and RMSEu parameters are defined (Wilmott, 1982) by equations 4, 5 and 6 respectively.

$$RMSE = \left[\frac{1}{n}\sum_{i=1}^{n}\left(P_i - O_i\right)^2\right]^{1/2} \quad (4)$$

$$RMSEs = \left[\frac{1}{n}\sum_{i=1}^{n}\left(\hat{P}_i - O_i\right)^2\right]^{1/2} \quad (5)$$

$$RMSEu = \left[\frac{1}{n}\sum_{i=1}^{n}\left(\hat{P}_i - P_i\right)^2\right]^{1/2} \quad (6)$$

The proportion of RMSE that arises from systematic and unsystematic error was described by RMSEs/RMSE and RMSEu/RMSE. To make cross-comparisons between models the 'index of agreement' (*d*) was used and is defined (Wilmott, 1982) by equation 7.

$$d = 1 - \left[\sum_{i=1}^{n}\left(P_i - O_i\right)^2 / \sum_{i=1}^{n}\left(|P_i'| + |O_i'|\right)^2\right], \quad 0 \le d \le 1 \quad (7)$$

where n is the number of observations, O_i is the observed value, P_i is the predicted value, $\hat{P}_i = a * O_i + b$, $P_i' = P_i - \bar{O}$ and $O_i' = O_i - \bar{O}$.

Multiplicative bias

Multiplicative bias (Mbias) is the ratio of average estimated and observed rainfall estimates and is given by equation 8. It provides an estimate of whether the satellite based rainfall estimates tend to underestimate or overestimate. A perfect value of estimate is 1.

$$Mbias = \frac{\frac{1}{N}\sum_{i=1}^{N} E_i}{\frac{1}{N}\sum_{i=1}^{N} O_i} \quad (8)$$

Correlation Coefficient

The correlation coefficient 'r' is one of the most commonly used statistics to define relationship between two values. It measures the degree of linear association between the estimated and observed values of rainfall estimates. It is recommended to be used along with other statistical measures when verifying SREs. It is given by equation 9.

$$r = \frac{\sum_{i=1}^{N}(E_i - \bar{E})(O_i - \bar{O})}{\sqrt{\sum_{i=1}^{N}(E_i - \bar{E})^2}\sqrt{\sum_{i=1}^{N}(O_i - \bar{O})^2}} \quad (9)$$

3.1.3 Categorical Verification Technique

The categorical verification technique is used to assess the rain detection capabilities of the SREs. A 2 x 2 contingency table of yes/no events, with rain/no rain, is used, as shown in Table 3.1. In Table 3.1, 'hits' (a) represents correctly estimated rain events, 'false alarms' (b) represents when rain is estimated, but did not occur, 'misses' (c) represents when rain is not estimated, but did occur, and 'correct negatives' (d) represents correctly estimated no rain events. The threshold for rain or no rain used in the contingency table can vary depending upon the nature of verification. Normally 0 mm day $^{-1}$ is considered but often variable amount such as 1, 5, 10 and 20 mm day $^{-1}$ is also considered to distinguish between rain and no rain. For the current research a threshold of 0 mm day $^{-1}$ is adopted.

Table 3.1 2 x 2 contingency table

		Satellite Rainfall (SRE)	
Gauge Observed Rainfall		No Rain (**No**)	Rain (**Yes**)
	No Rain (**No**)	(d) **Correct negatives**	(b) **False alarms**
	Rain (**Yes**)	(c) **Misses**	(a) **Hits**

The probability of detection (POD) measures the fraction of observed events diagnosed correctly. It is a ratio of hits to the sum of hits and misses. It is defined by equation 10.

$$POD = \frac{a}{(a+c)} \tag{10}$$

The false alarm ratio (FAR) gives the fraction of diagnosed events that turned out to be wrong. It is given by equation 11.

$$FAR = \frac{b}{(a+b)} \tag{11}$$

The perfect values of *POD*=1, and *FAR*=0. The *POD* and *FAR* should always be used together.

There are also other indicators for example threat score (*TS*), also known as the "critical success index", measures the fraction of all events estimated and/or observed that were correctly diagnosed. Since this score is naturally higher in wet regimes, a modified version known as the equitable threat score (*ETS*) was formulated to account for the hits that would occur purely due to random chance. The *ETS*, though not a true skill score, is often interpreted that way since it has a value of 1 for perfect correspondence and 0 for no skill. *TS* and *ETS* are defined by equation 12 and 13 respectively. The *ETS* and *TS* are not reported in this study.

$$TS = \frac{a}{a+b+c} \tag{12}$$

$$ETS = \frac{a - hits_{random}}{a+b+c-hits_{random}} \tag{13}$$

where

$$hits_{random} = \frac{1}{N}\,(a+c)\;(a+b)$$

There is no one single indicator that can determine the performance of SREs. Normally a combination of various indicators needs to be used to assess the accuracy of the estimates. The combination depends upon the use of the estimates.

3.2 Interpolation of the Observed Rainfall - Kriging

Satellite-based rainfall estimates are continuous and represent areal rainfall while gauge observed rainfall is at a particular point in location. Hence, to make comparisons between the two it is necessary to convert the point rainfall values into areal by using a suitable interpolation technique.

In mountainous areas such as in the Himalayas of Nepal orography is an important component and the spatial distribution of rainfall varies in small scales. Further the sparse and limited rainfall stations make accurate and reliable spatialization of rainfall amounts at the local scale difficult. There are various interpolation techniques available for converting point rainfall data into areal such as the inverse distance weighting method (IDW), kriging and others. The kriging interpolation technique is considered superior to IDW because prediction estimates tend to be less biased as predictions are accompanied by prediction standard errors. The kriging interpolation is found to perform better than other interpolations schemes such as Thiessen polygon, polynomial interpolation, and inverse distance method by many researchers for example Creutin and Obled (1982), Tabios and Salas (1985). This interpolation technique has also been identified as the best suited interpolation technique in the Himalayas (Basistha and Goel, 2007). In other mountain regions for example the Sannio mountain regions of southern Italy ordinary cokriging was found to be the most robust interpolation method as compared to two others (linear regression and inverse squared distance) taking into consideration topography and is recommended to be better applicable in other mountainous regions (Diodata and Caccelelli, 2005). Hence in this research the kriging technique has been utilized and is briefly described below.

Kriging is a geostatistical interpolation technique. It is a method of interpolation which predicts unknown values from data observed at known locations. This method uses variogram to express the spatial variation, and it minimizes the error of predicted values which are estimated by spatial distribution of the predicted values. It is considered to be the best linear unbiased estimate at each location and also know as BLUE. It is "linear" since the estimated values are weighted linear combinations of the available data. It is "unbiased" because the mean of error is

0. It is "best" since it aims at minimizing the variance of the errors. The difference of kriging and other linear estimation method is its aim of minimizing the error variance. A fundamental concept of geostatistics is the use of quantitative measures of spatial correlation, commonly expressed by variograms. Geosatistics offers a way of describing the spatial continuity of natural phenomenon and provides adaptation of classical regression techniques to take advantage of this continuity (Issaks and Srivastava, 1989). For the kriging interpolation a semivariogram which captures the spatial dependence between data points have been used. A semivariogram models the autocorrelation between datapoints. Kriging predicts using a weighted average of surrounding sample values. Weights are based on model and spatial correlation. This requires the assumption of stationarity i.e. the model is spatially homogeneous. For the current scope of the work the interpolation method used is ordinary kriging with a spherical variogram. Detailed information about geostatistical tools and procedures can be found in Isaaks and Srivastava (1989). All interpolation computations for this research have been performed using the Geostatistical Analyst integrated in ArcGIS 9.3 – ESRI software.

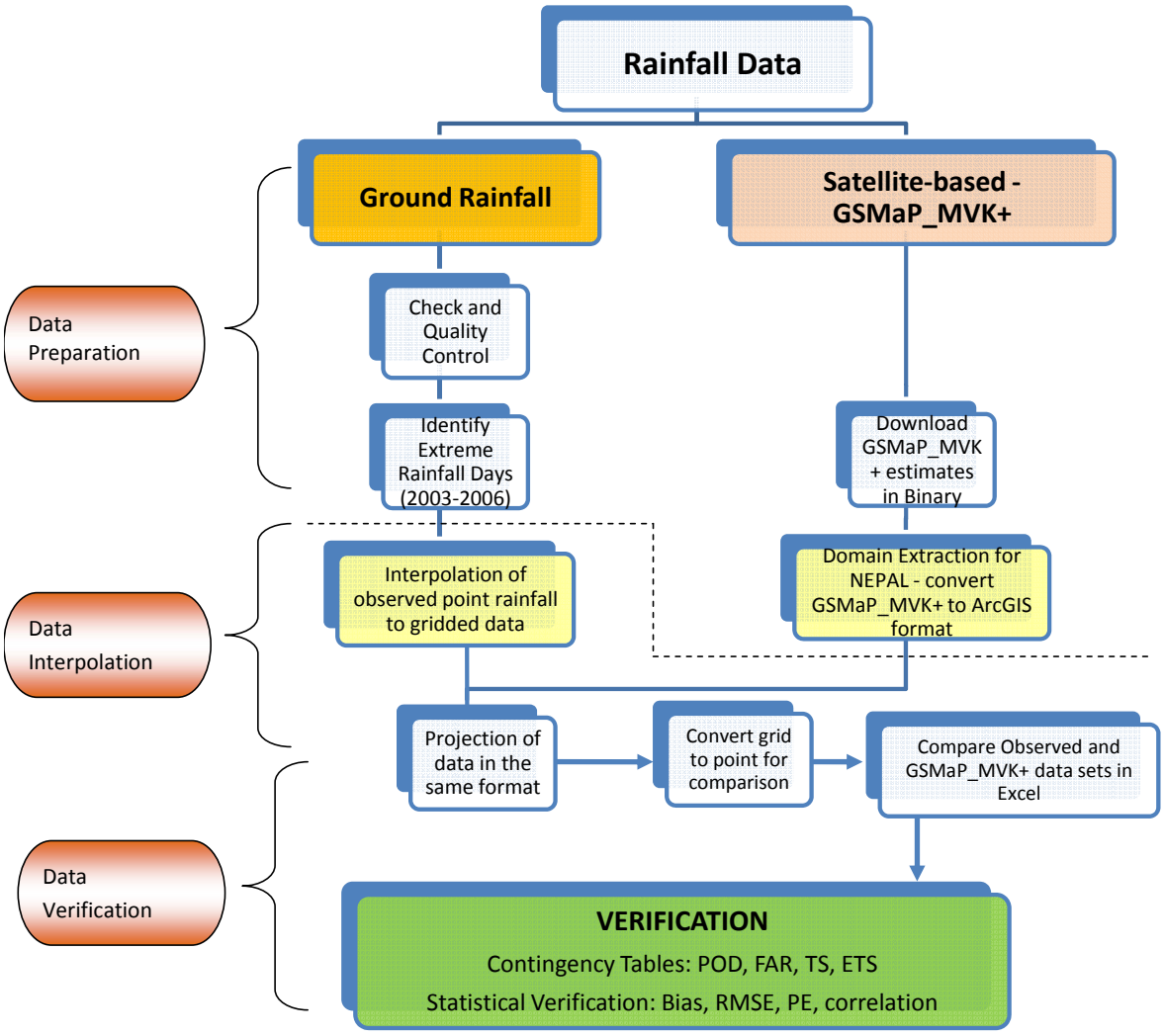

Figure 3.1 Flowchart of satellite rainfall verification

3.3 Verification of Satellite-Based Rainfall Estimates over Nepal

As we have seen from the previous chapter verification there has been limited work on assessment and application of SRE over the Himalayan region particularly in Nepal. For this research two high resolution SREs CPC_RFE2.0 from NOAA (RFE) and GSMaP_MVK+ (GSMaP) from JAXA have been evaluated. In this section we provide the verification of RFE and GSMaP. The temporal resolution is daily with a spatial resolution of 0.1^{o}x0.1^{o} latitude and longitude. The assumption is made that there is not much difference in 24 hr rainfall with about 3 hours of delay as the accumulation for the daily satellite-based rainfall is from 0Z to 0Z. Satellite data represent areal rainfall while gauge observed data represent point rainfall. To make

comparison between the two datasets the gauge observed rainfall data made available by the Department of Hydrology and Meteorology (DHM) of the Government of Nepal was interpolated to represent areal data using the krigging interpolation technique which has been found to be best suited in the Indian Himalayas and in mountainous terrain.

The SREs and gauge observed data were verified using the standard verification technique. A step wise methodology adopted for this research is provided below and shown in Figure 3.1.

3.3.1 Data Preparation

Satellite-based rainfall estimates

A substantial amount of effort and time is taken for data preparation. The first step is the familiarization with the satellite-based data formats, scale and resolution. As has been explained earlier the RFE uses merging technique, which increases the accuracy of the rainfall estimates by reducing significant bias and random error compared to individual precipitation data sources (Xie and Arkin, 1996) thereby adding value to rain gauge interpolations. The RFE rainfall estimates has been put into operation at the Climate Prediction Centre (CPC) on a near real time for South Asia since June 2001 (Xie *et al*., 2002) at a 0.1 degree spatial resolution on a daily basis ($70^oE–110^oE$; $5^oN–35^oN$). The GSMaP is a global hourly product with a domain covering 60^oN - 60^oS at a 0.1 x 0.1 degree grid resolution and calculated using a MW radiometer – infrared (IR) radiometer blended algorithm (Ushio *et al*., 2009).

The RFE has been provided by NOAA for the period 2002 to 2006. This data is in gridded binary format and can also be downloaded directly from the ftp server on a daily basis. The GSMaP has been provided by JAXA and can also be accessed through the ftp server. The GSMaP is available for four years from 2003 to 2006. There is also a near real time version known as the GSMaP_NRT which is available on an hourly basis with 4 hours latency. The downloaded binary data has to be converted for validation purposes and for application in hydrological models. For the present research, GSMaP and RFE data is extracted between latitude $26^oN – 31^oN$ and longitude $80^oE– 89^oE$ (862 grids) to cover the whole of Nepal. The data set used for the verification covers a period of 4 years from 2003–2006 with no missing data.

As the verification of SREs were conducted using ArcGIS the binary data was first converted to ASCII format. The ASCII format data was imported into ArcGIS and projected in the correct

format to carry out the verification. The gauge observed rainfall datasets were also formatted and converted into GIS format and transformed into the same projection as the SREs.

Gauge Observed Rainfall

The DHM of the Government of Nepal has provided the daily gauge observed point rainfall dataset from 176 stations for the period 2002 to 2006 (Annex 2). The distribution of the rainfall stations is shown in Figure 3.2. The gauge observed rainfall datasets have been quality checked and screened by DHM prior to making it available. However, further data quality control has been adopted by using the following process.

- The gauge data are quality controlled by removing duplicates
- Remove rain gauge data that contribute to GTS in the RFE
- Removal of the rain gauge stations which have data less than 6 months
- Considered rainfall data for the period 2002-2006 for the analysis
- Station information (especially location) should be verified, where the details are available
- The precipitation data should be checked for typing error

Using the kriging interpolation technique the quality controlled 176 rain gauges were gridded to a spatial resolution of 0.1 degree latitude longitude to match with the same resolution of the SREs. The validation data set used for the research is the daily gridded rainfall data for the whole of Nepal and used as the ground truth.

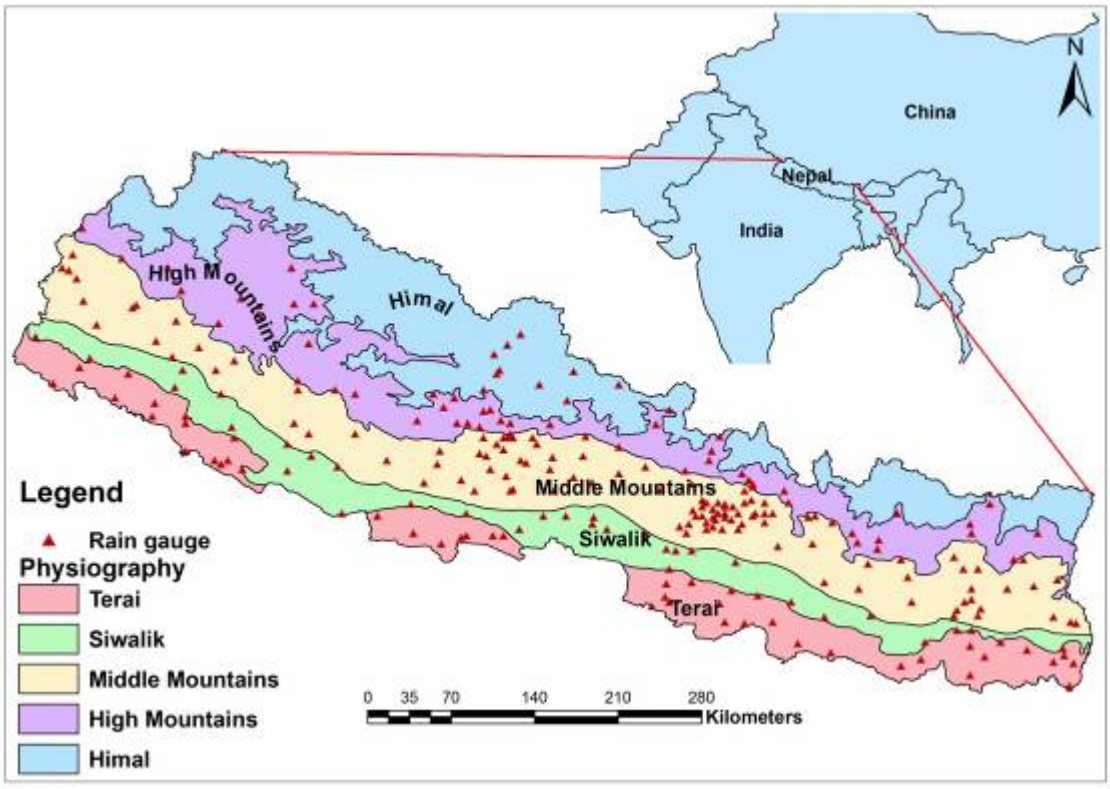

Figure 3.2 Distribution of rain gauge stations in Nepal

3.3.2 Country Level Verification - Assessment of the Accuracy of the Satellite-Based Rainfall Estimates over the Whole of Nepal

Verification of the SREs over the whole of Nepal has been conducted by comparing the rainfall estimates with the gauge observed rainfall data for January through December of 2003 to 2006 to examine the spatial distribution of precipitation. Nepal is covered by 862 grid cells of 0.1^o x 0.1^o resolution in latitude and longtitude. Comparison of the gauge observed and estimated rainfall were made in all the grid cells within the boundary of Nepal considering it as one homogeneous region. Analysis was done on a yearly basis with daily satellite-based and gauge observed rainfall data and accumulated for the four year period from 2003 to 2006.

Figure 3.3 shows the time series comparison of average daily RFE and GSMaP rainfall estimates and gauge observed rainfall from 2003 to 2006 averaged over whole of Nepal. Visual interpretation of the plot shows that both RFE and GSMaP estimated rainfall corresponds well to the gauge observed rainfall capturing the peaks but there is underestimation of the amount of rainfall. The average annual rainfall from 2003 to 2006 is 1433 mm, 1025 mm and 745 mm from

gauge observation, RFE, and GSMaP respectively. The area averaged gauge observed annual rainfall varied from 1824 to 1022 mm from 2003 to 2006 with the driest year being 2006. Similarly, the area averaged GSMaP estimate annual rainfall for the whole of Nepal varied from 816 to 665 mm from 2003 to 2006 with the driest year being 2005. For RFE the area averaged rainfall varied from 1195 to 871 with the driest year in 2005. The summary of area averaged rainfall estimates is provided in Table 3. 2. The GSMaP is found to underestimate annual rainfall by about 50 % while RFE is about 30%. Applying the standard statistical verification technique the correlation coefficient is 0.75, bias is -1.9 mm day^{-1}, RMSE is 4.1, POD is 0.98 and FAR 0.08 with GSMaP. With RFE correlation is 0.71, bias is -1.1 mm, RMSE is 4.0 mm day^{-1}, POD is 0.91 and FAR is 0.05 (Table 3.3). Table 3.2 also provides the yearwise comparison of statistical errors with GSMaP and RFE for daily area averaged rainfall. For each year from 2003 to 2006 we find that the GSMaP estimates show a better correlation with gauge observed data than RFE estimates. In an intercomparison with various SREs over Japan Kubota *et al*. (2009) also obtained better correlation with GSMaP compared to other products. However, the bias is smaller in the case of RFE which is not surprising as RFE uses gauge observed rainfall data as one of the input data sources.

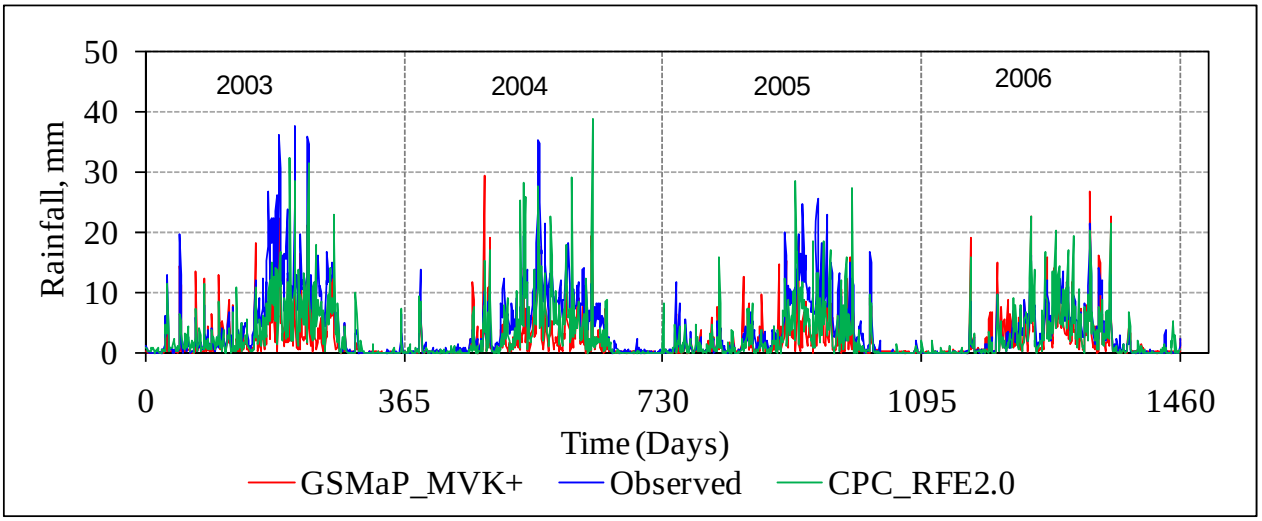

Figure 3.3 Time series comparison of GSMaP and gauge observed daily rainfall for 2003-2006 over whole of Nepal.

Table 3.2 Comparison of area averaged annual rainfall estimates over whole of Nepal using GSMaP and RFE

Year	Annual Rainfall (mm)			Percentage Error (%)	
	Observed	GSMaP	RFE	GSMaP	RFE
2003	1824.3	816.4	1195.3	-55	-33
2004	1570.8	703.4	1054.4	-55	-33
2005	1315.6	665.0	871.2	-49	-34
2006	1022.4	806.9	977.7	-21	-4
Average	1433.3	747.9	1024.7	-48	-29

Table 3.3 Time series comparison of daily area averaged rainfall from 2003 to 2006

	Bias	RMSE	correl	PE	MBias	POD	FAR
2003: GSMaP	-2.7	5.0	0.83	-54.7	0.45	1.00	0.08
RFE	-1.7	4.6	0.79	-33.5	0.66	0.91	0.06
2004: GSMaP	-2.4	4.5	0.73	-55.2	0.45	0.91	0.05
RFE	-1.4	4.6	0.67	-32.9	0.67	0.89	0.03
2005: GSMaP	-1.8	3.9	0.72	-49.2	0.51	1.00	0.12
RFE	-1.2	3.6	0.72	-33.5	0.67	0.94	0.06
2006: GSMaP	-0.6	2.4	0.81	-21.1	0.79	1.00	0.09
RFE	-0.1	2.6	0.79	-4.4	0.96	0.89	0.05
Average: GSMaP	-1.9	4.1	0.75	-47.6	0.52	0.98	0.08
RFE	-1.1	4.0	0.71	-28.4	0.72	0.91	0.05

Spatial Distribution of Annual Precipitation

In addition to the area averaged annual rainfall variation understanding the spatial distribution of rainfall is very important for various applications in water resources assessment as well as in flood forecasting. In this section we seek to understand how closely the SREs conform to the gauge observed rainfall and how good are they to represent the spatial variation. The analysis has been conducted using the daily rainfall estimates of RFE, GSMaP and gauge observation for the same period from 2003 to 2006.

In the gauge observed analysis precipitation is detected to be relatively heavy in central Nepal near Pokhara exceeding 3000 mm/yr agreeing with Kansakar *et al*. (2004) and Ichiyanagi *et al*. (2007). Kansakar *et al*. (2004) described zones of heavy precipitation also in the northeast of the Kathmandu Valley which we can also see in the 2003 to 2006 gauge observed analysis.

The highest annual precipitation amount is about 4500 mm in 2003 from the gauge observed analysis which is quite close to the average amount referred in Chalise *et al.* (1996) despite the short period of analysis from 2003 to 2006. The driest part of the country is the rain shadow area of Mustang in the transhimalayan region with below 200 mm of rainfall similar to the Tibetan plateau region.

The spatial distribution of average annual precipitation obtained from RFE and GSMaP are also similar to that of the gauge observed and in general represents the spatial distribution of rainfall well. However, there are distinct variations in the pattern in the mid mountain areas. Figure 3.4 presents the comparison of spatial distribution of mean annual precipitation (SREs using RFE and GSMaP and gauge observed rainfall) averaged from 2003 to 2006. Inspecting the satellite-based rainfall analysis for 2003 we find that the highest annual precipitation amount is about 2196 mm and 1798 mm from RFE and GSMaP respectively compared to 4500 mm with gauge observed analysis. There is underestimation of the amount by both SREs. Further, it is found that in the SREs the heavy precipitation tends to be more towards the southern belt rather than in the mid mountain regions. This variation may be due to the orographic influence on precipitation in the mid mountain areas which the SRE seem to not detect well. There are also some local variations in pattern for example in the far eastern and western region of Nepal where gauge observation shows higher precipitation while SREs seem to not capture this variation. The observed trend is decrease in precipitation from east to west while this is not adequately reflected in the SREs. The better quantitative estimate of RFE compared to GSMaP is quite likely because the RFE estimate is gauge merged SREs and utilizes the WMO observed rainfall datasets while the GSMaP is based on satellite observations only.

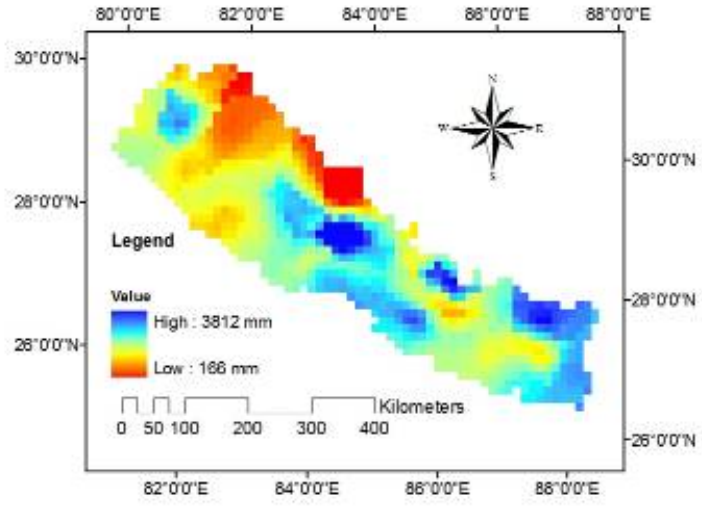

(a)

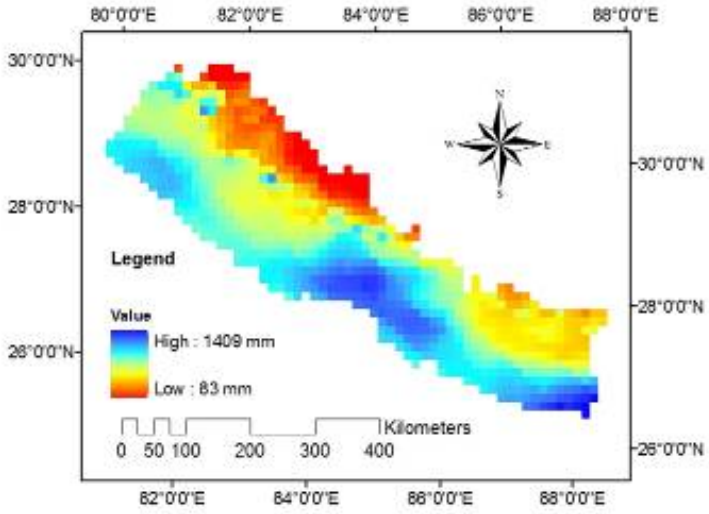

(b)

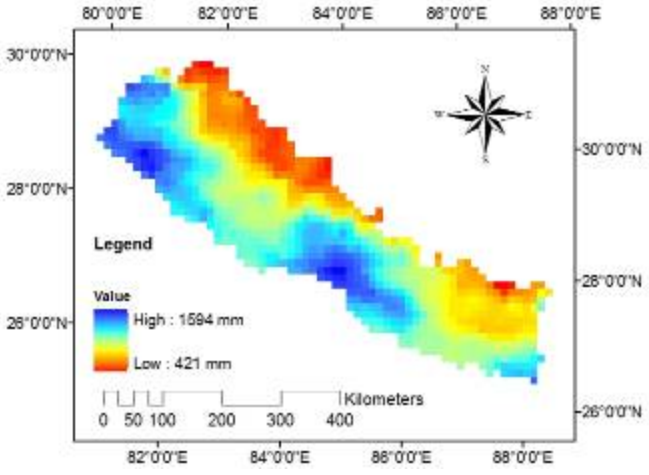

(c)

Figure 3.4 Spatial distribution of average annual precipitation from 2003 to 2006, a) gauge observed, b) GSMaP and c) RFE

Figure 3.5 presents the average annual rainfall bias map using GSMaP and RFE rainfall estimates. As we have seen both the products are significantly underestimating the amount of rainfall. However, it is interesting to observe the difference in the bias between the two products GSMaP is found to have larger underestimation of rainfall in the central region compared to RFE as seen in Figure 3.5. In the central north region in the trans-himalayas both products are found to have positive bias though RFE has higher positive bias. In the central far east of Nepal GSMaP and RFE have negative bias with GSMaP having higher negative bias.

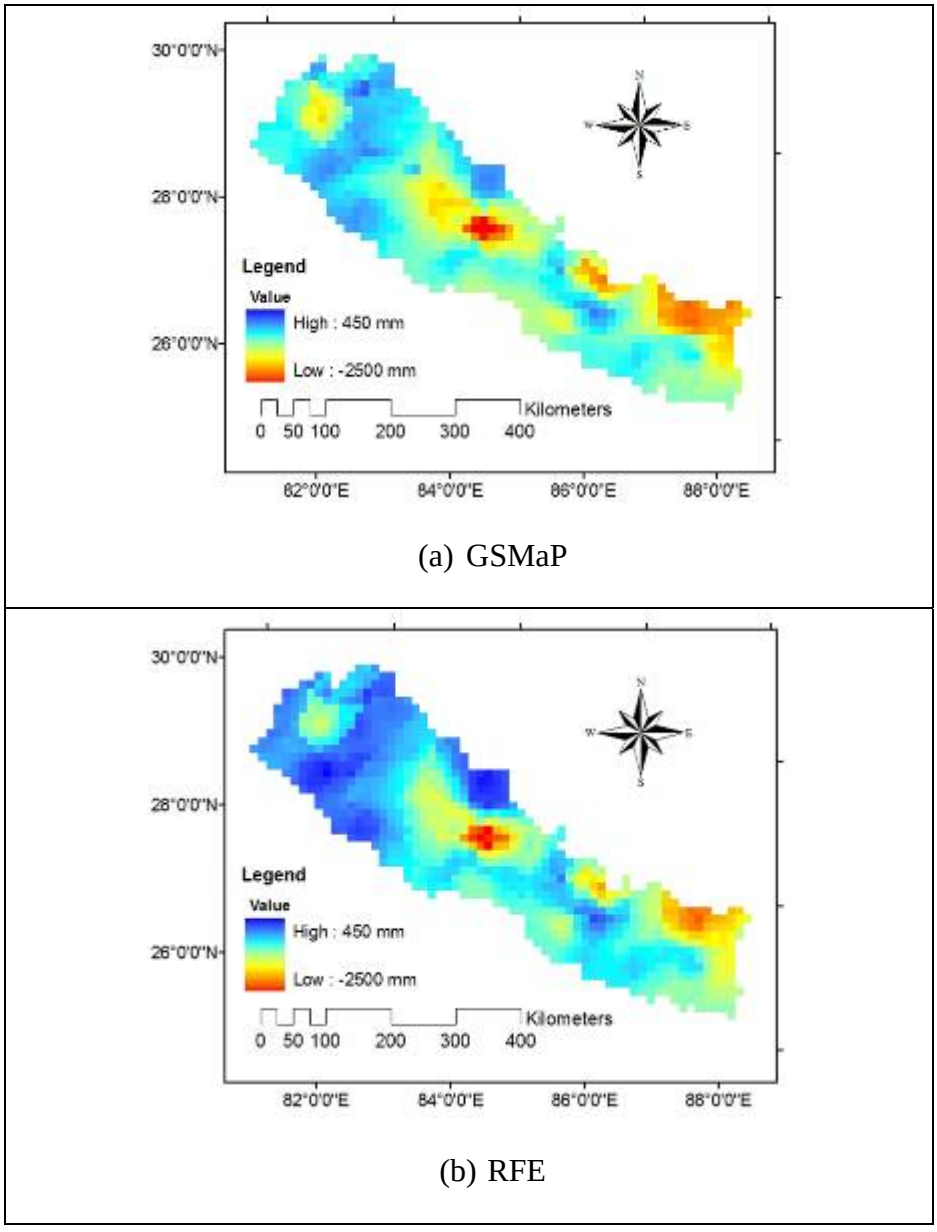

Figure 3.5 Bias Map of average annual precipitation for 2003-2006, a) GSMaP and b) RFE

Figure 3.6 presents the spatial distribution of average annual precipitation year wise from 2003 to 2006 for GSMaP, RFE and gauge observed rainfall. For every year SREs using RFE and GSMaP underestimates the annual precipitation.

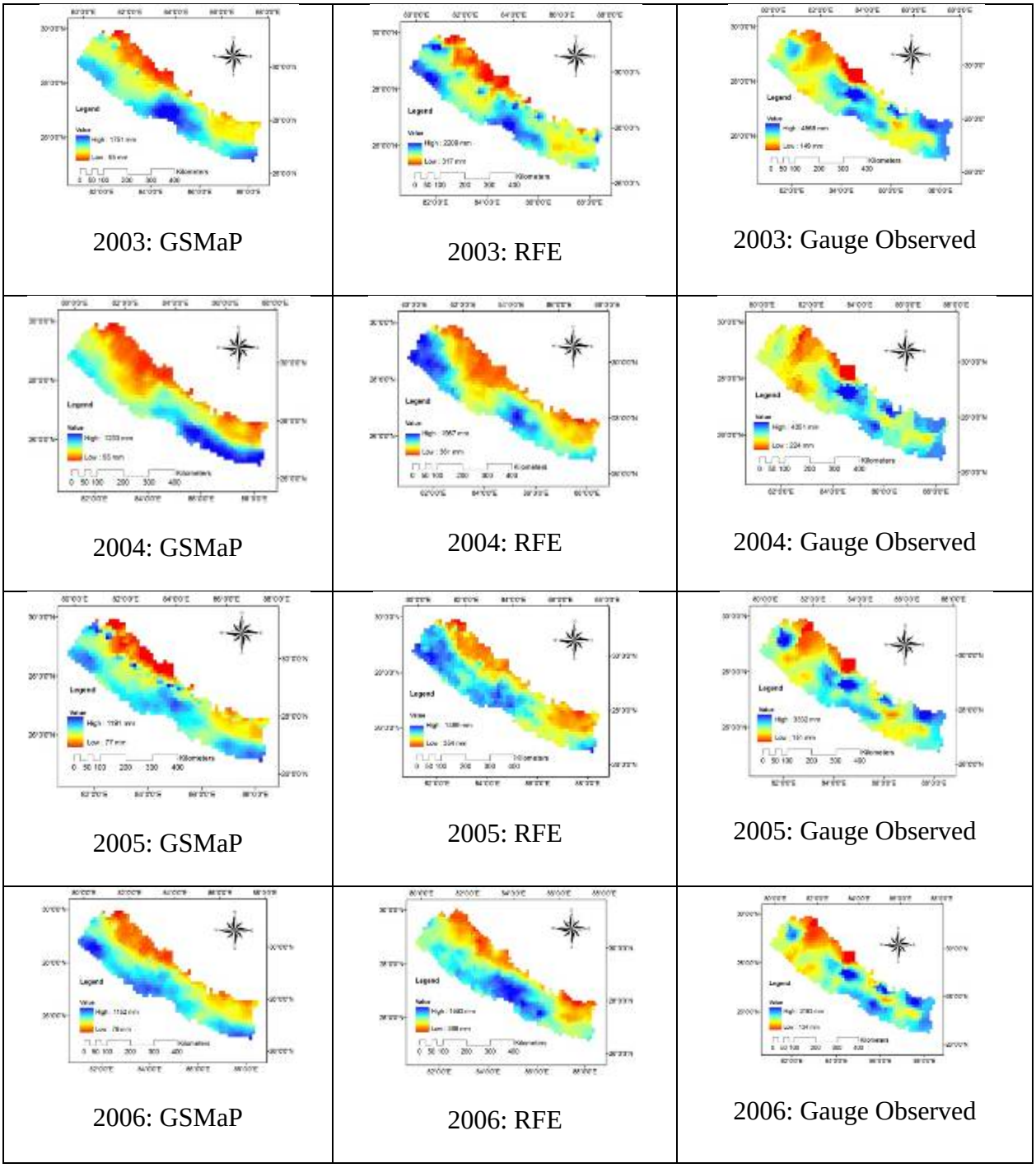

2003: GSMaP | 2003: RFE | 2003: Gauge Observed

2004: GSMaP | 2004: RFE | 2004: Gauge Observed

2005: GSMaP | 2005: RFE | 2005: Gauge Observed

2006: GSMaP | 2006: RFE | 2006: Gauge Observed

Figure 3.6 Spatial distribution of annual precipitation with GSMaP, RFE and gauge observed rainfall for 2003 to 2006

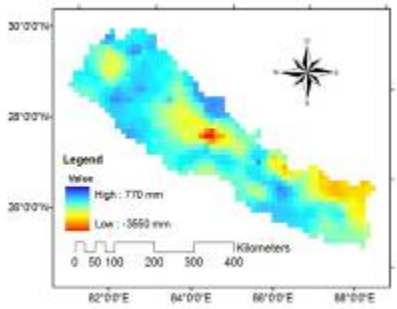

2003: GSMaP Bias Map

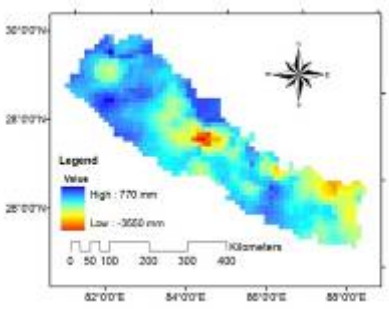

2003: RFE Bias Map

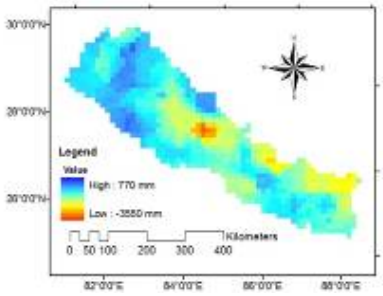

2004: GSMaP Bias Map

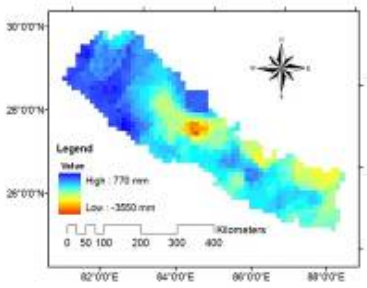

2004: RFE Bias Map

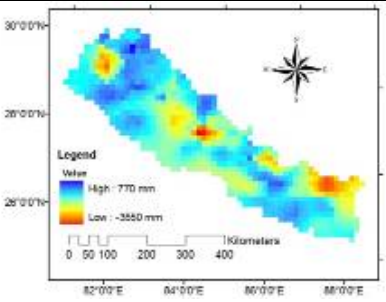

2005: GSMaP Bias Map

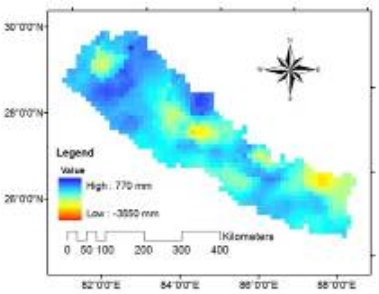

2005: RFE Bias Map

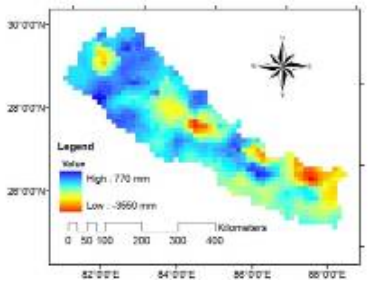

2006: GSMaP Bias Map

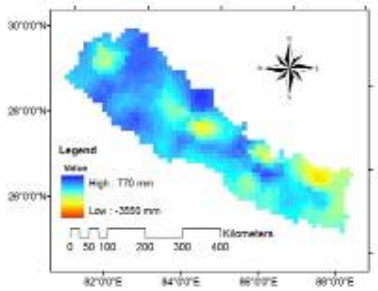

2006: RFE Bias Map

Figure 3.7 Annual bias map for each year from 2003 to 2006 with GSMaP and RFE

Figure 3.7 presents the bias map of average annual precipitation showing yearly variation in the bias. In general the positive and negative biases for both satellite-based products are similar

in trends. However, the significant negative bias of GSMaP is high rainfall areas (Pokhara valley area) is very prominent from inspecting these bias maps.

Spatial Distribution of Seasonal Precipitation

The average accumulated rainfall for four season premonsoon (March, April, May), monsoon season, (June July, August, September), post monsoon (October, November) and winter (December, January and February) were analysed for 2003-2006. The monsoon season is of primary interest to this study as more than 80% of the rain falls during this period and is important for flood prediction. Therefore, only the monsoon (JJAS) rainfall analyses are reported. Figure 3.8 shows the variation of spatial distribution of average JJAS rainfall over Nepal. Inspection of RFE, GSMaP and gauge observed maps shows that patterns of rainfall are similar as heavy rainfall is detected in the south western and central region. But as in the annual maps there are some distinct local differences for example the orographic heavy rainfall is not detected in the southern part of Annapurna range around Pokhara valley which is the highest rainfall area in Nepal. The rainfall estimates from satellite data are more concentrated in the flatter areas of Terai and Siwaliks both in the case of RFE and GSMaP. There are also some variations in the north east region and in some areas such as Bajura, Khaptad and Mangalsen in far western region where local topography and orography plays a role (Shrestha *et al*., 2010).

Figure 3.9 shows the average JJAS bias map from 2003-2006 using GSMaP and RFE. The general trend of bias is very similar to the annual bias map with underestimation in the high rainfall areas and overestimation in low rainfall and rainshadow areas. GSMaP rainfall product is found to have larger underestimation in heavy rainfall areas and lesser positive bias in rain shadow areas compared to RFE estimates.

Figure 3.10 shows the comparison of JJAS average rainfall maps for each year from 2003 to 2006 using GSMaP, RFE and gauge observation. There is a year to year variation in the agreement between SREs and gauge observations. Figure 3.11 shows the bias map for each year from 2003 to 2006. Negative bias in the high rainfall area and positive bias in the low rainfall areas are quite evident from these figures.

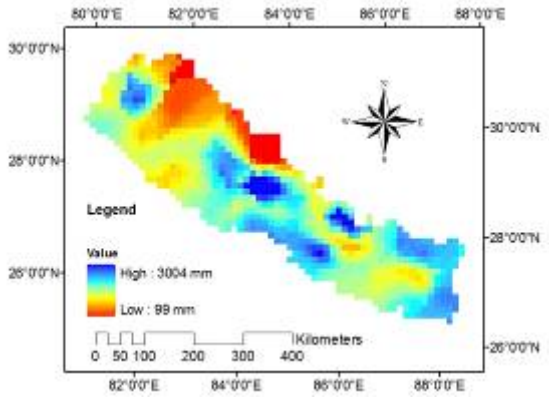

(a) Gauge Observed

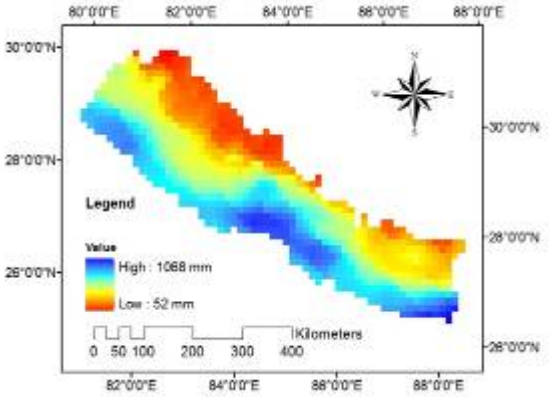

(b) GSMaP

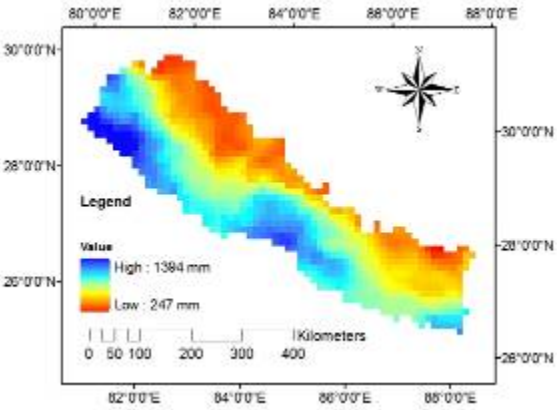

(c) RFE

Figure 3.8 Spatial distribution of June, July, August and September (JJAS) average rainfall map for 2003-2006 a) gauge observed, b) GSMaP and c) CPC_RFE2.0.

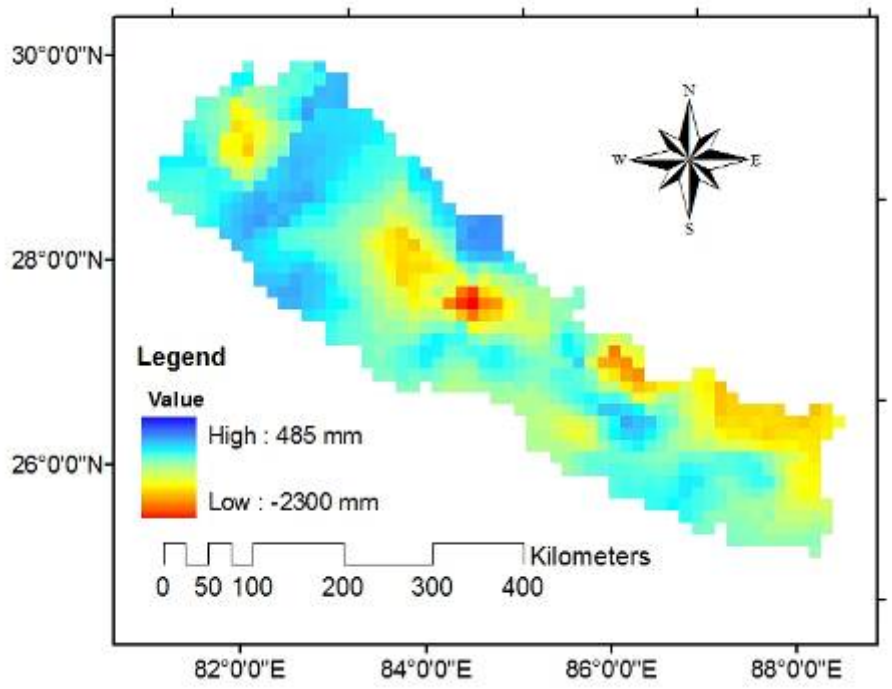

(a) Bias with GSMaP

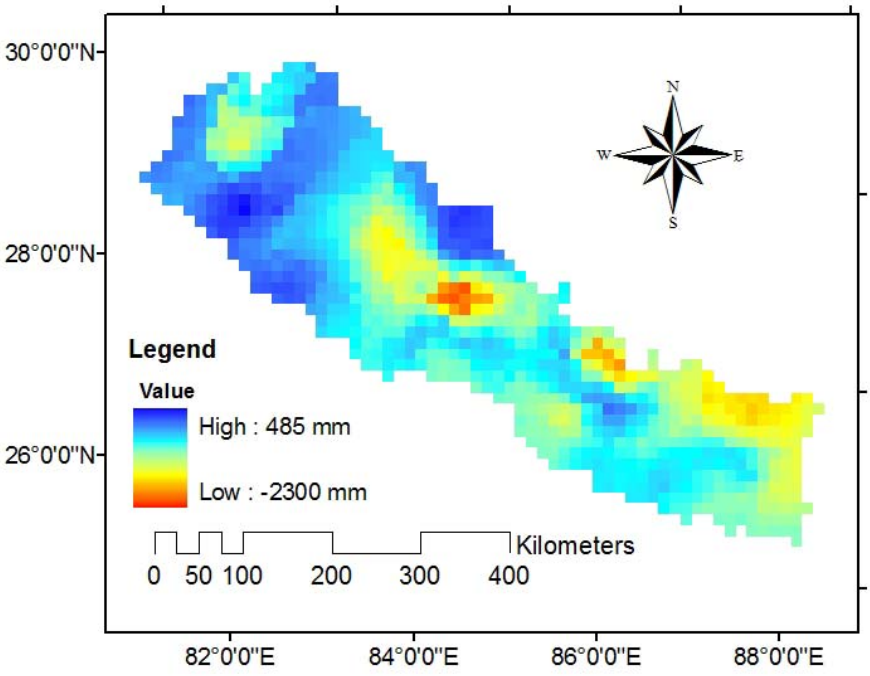

(b) Bias with RFE

Figure 3.9 Bias Map of average JJAS precipitation for 2003-2006, a) GSMaP and b) RFE

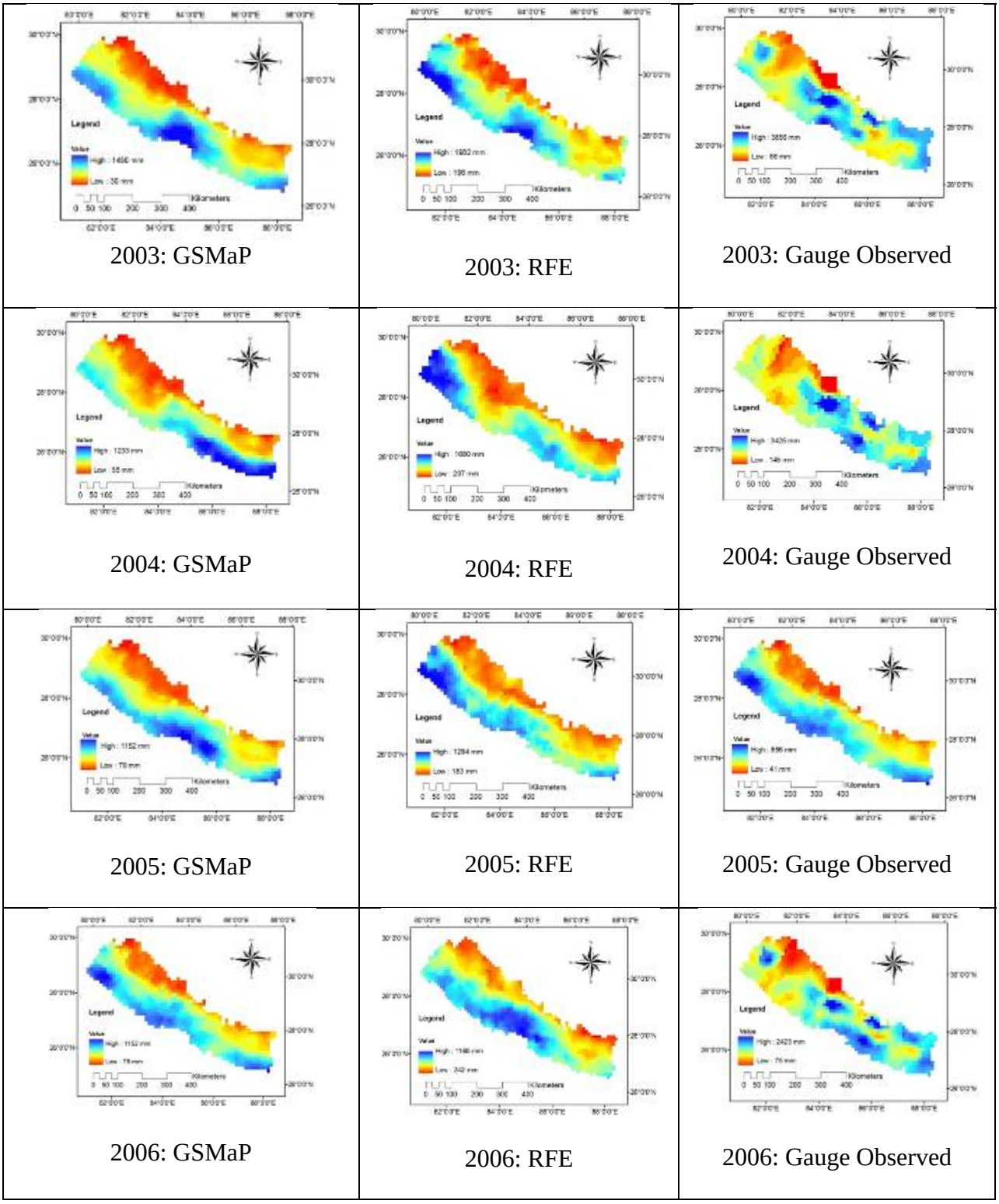

Figure 3.10 Spatial distribution of year wise average JJAS rainfall using GSMaP, CPC_RFE2.0 and gauge observation over Nepal for 2003 to 2006.

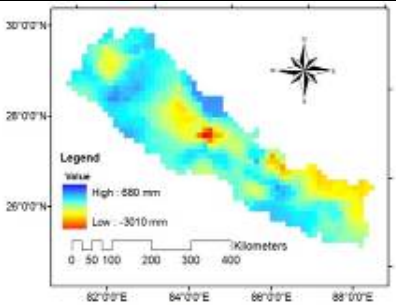

2003: Bias GSMaP

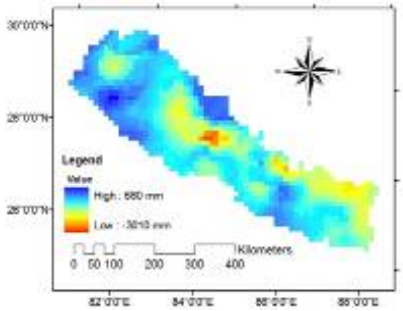

2003: Bias RFE

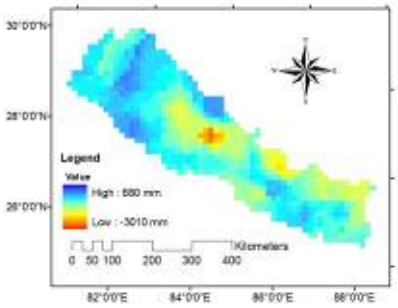

2004: Bias GSMaP

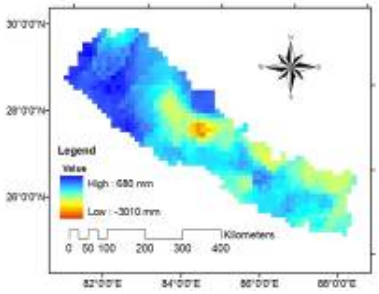

2004: Bias: GSMaP

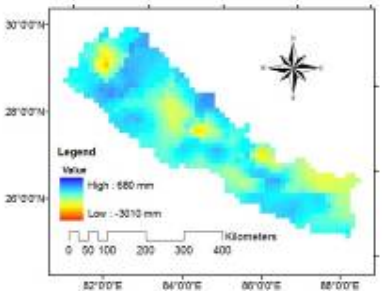

2005: Bias GSMaP

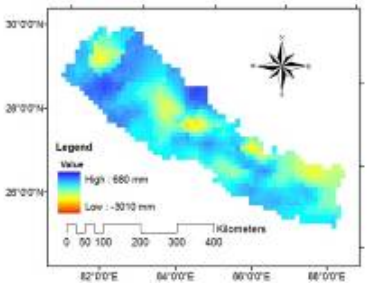

2005: Bias RFE

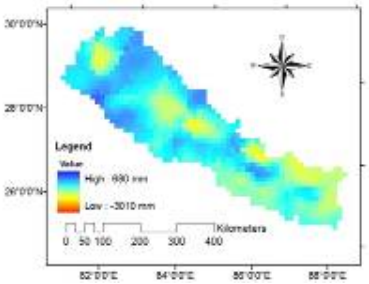

2006: Bias GSMaP

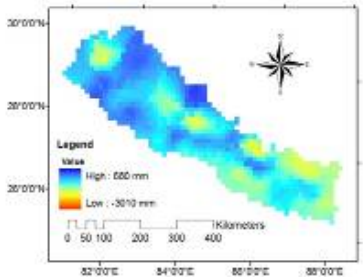

2006: Bias RFE

Figure 3.11 Bias Map of JJAS precipitation for 2003-2006, a) GSMaP and b) RFE

Scatter plots of area averaged daily rainfall for the monsoon (JJAS) for 2003 to 2006 for GSMaP and RFE estimates are shown in Figure 3.12. For the area averaged daily rainfall for the period 2003 to 2006 the correlation coefficient is 0.79, bias is -5.0 mm day^{-1}, and RMSE is 5.6 for GSMaP and 0.72, -2.9 mm day^{-1} and RMSE is 4.0 mm for RFE respectively (Table 3.4). The bias is less in the RFE estimates than the GSMaP, however, the GSMaP has a higher correlation coefficient.

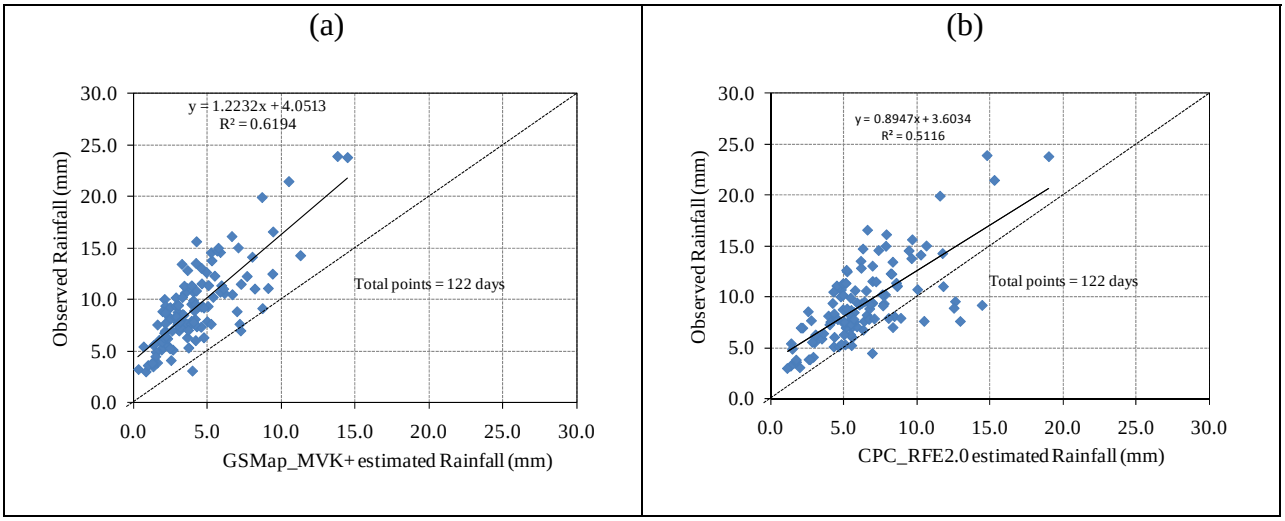

Figure 3.12 Scatter plot of area averaged daily rainfall for monsoon (JJAS) of 2003-2006 from a) observed and GSMaP, (b) observed and RFE.

Table 3.4 Statistical error of daily area average rainfall from 2003-2006 for JJAS

	Bias	RMSE	PE	correl	MBias	POD	FAR
RFE	-2.9	4.0	-31.9	0.72	0.68	1.00	0.00
GSMaP	-5.0	5.6	-54.1	0.79	0.46	1.00	0.00

Figure 3.13 shows the scatter plot of average accumulated rainfall for each 0.1^{o} x 0.1^{o} grid cell (862 grid cells in total) for JJAS for 2003 to 2006 for GSMaP and RFE estimates. For the average accumulated monsoon rainfall (JJAS) of each 0.1^{o} x 0.1^{o} grid cell the correlation coefficient is 0.46, bias is -609.7 mm and RMSE is 736.5 with a percentage error of -54.2% for GSMaP and 0.35, -352.0 mm, 569.8, -31.3% for RFE respectively. Table 3.5 shows that the bias is less in the RFE estimates than the GSMaP, however, the GSMaP has a higher correlation coefficient. The underestimation of rainfall is consistent with previous finding (Shrestha *et al*., 2008; Dinku *et al*., 2008; Ebert *et al*., 2007a). In the case of Ethiopia, with a complex terrain similar to the study area, Dinku *et al.* (2008) investigated the performance of various satellite

rainfall products and found that satellite-based estimates did well in detecting the occurrence of rainfall, but were not good in estimating the amount of daily rainfall. Table 3.5 presents the statistical error of accumulated rainfall for monsoon (JJAS) from 2003-2006 at each grid cell.

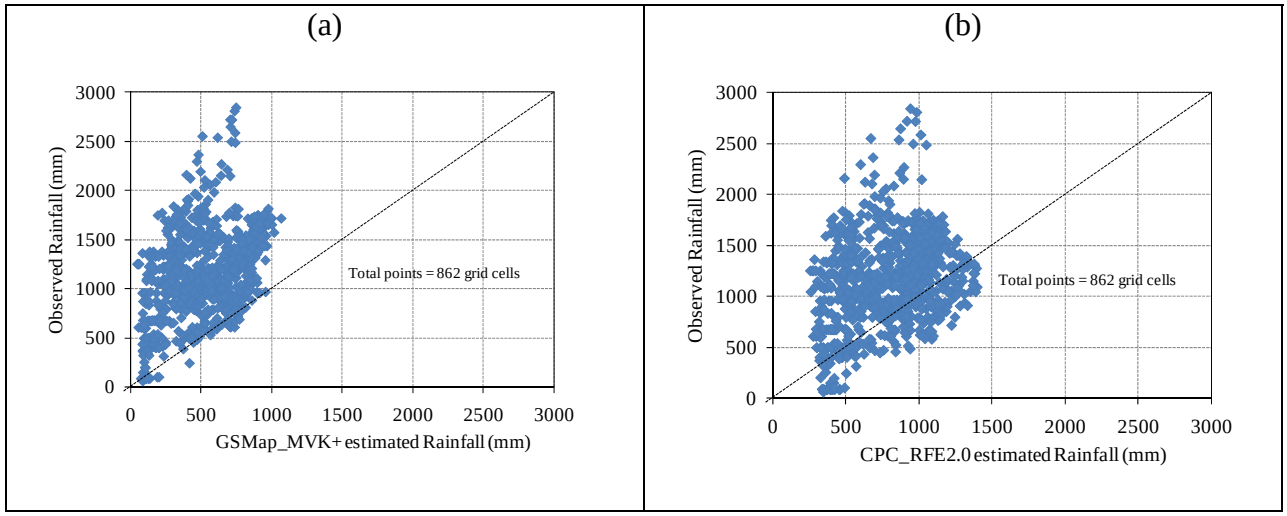

Figure 3.13 Scatter plot of accumulated average rainfall for JJAS of 2003-2006 from a) GSMaP and b) CPC_RFE2.0for each 0.1^{o}x0.1^{o} grid cell.

Table 3.5 Statistical error of accumulated rainfall for monsoon (JJAS) from 2003-2006 at each grid cell

	Bias	RMSE	PE	correl	MBias	POD	FAR
RFE	-352.0	569.8	-31.3	0.35	0.69	1.0	0.0
GSMaP	-609.7	736.5	-54.2	0.46	0.46	1.0	0.0

The monthly, seasonal and annual total rainfall is computed from the daily analyzed values. The year 2003 is selected over the whole observation period as 2003 is the wettest year and SREs from GSMaP. Using the 0.1^{o}x0.1^{o} data set of individual grids the total annual rainfall in 2003 is 1824.3 mm from gauge and 816.4 mm from the GSMaP. There is a negative bias of 1007.9 mm $year^{-1}$ (Table 3.6). During the monsoon (JJAS) there is an accumulated rainfall of 1501.8 mm from gauge and 605.3 mm from GSMaP with a highest negative bias of 896.5 mm compared to other seasons. The correlation coefficient between the gauge observed and the GSMaP annual rainfall estimates is 0.48 and for the monsoon is 0.47 (Shrestha *et al*., 2010).

Table 3.6 Comparison of GSMaP and gauge observed rainfall for 2003

	Gauge Observed (mm)	GSMap (mm)	bias (mm)	RMSE (mm)	Correl	PE (%)	Mbias	POD	FAR
Jan	28.4	9.3	-19.1	24.0	0.18	-67.3	0.33	0.93	0.00
Feb	68.0	33.2	-34.8	46.0	0.39	-51.1	0.49	0.99	0.00
Mar	48.4	43.4	-5.0	36.5	0.24	-10.3	0.90	0.99	0.00
Apr	58.0	71.6	13.6	46.6	0.61	23.5	1.23	1.00	0.00
May	74.9	31.4	-43.6	62.1	0.36	-58.1	0.42	0.99	0.00
Jun	312.9	140.0	-172.9	216.3	0.53	-55.3	0.45	1.00	0.00
Jul	513.7	211.5	-302.2	352.9	0.60	-58.8	0.51	1.00	0.00
Aug	374.4	132.2	-242.2	276.4	0.43	-64.7	0.35	1.00	0.00
Sep	300.9	121.7	-179.2	210.2	0.38	-59.6	0.40	1.00	0.00
Oct	29.1	13.9	-15.3	28.7	0.78	-52.4	0.48	0.71	0.00
Nov	1.0	2.4	1.3	6.6	0.01	-125.2	2.25	0.40	0.16
Dec	14.5	5.9	-8.6	15.3	-0.09	-59.3	0.41	0.93	0.01
Annual	1824.3	816.4	-1007.9	1172.5	0.48	-55.3	0.45	1.00	0.00
Monsoon (JJAS)	1501.8	605.3	-896.5	1033.3	0.47	-59.7	0.40	1.00	0.00
ON	30.2	16.2	-14.0	30.6	0.67	-46.3	0.54	0.75	0.00
DJF	110.9	48.4	-62.5	76.8	0.22	-56.3	0.44	1.00	0.00
MAM	181.4	146.4	-35.0	106.2	0.51	-19.3	0.81	1.00	0.00

The RMSE is 1172.5 for the annual rainfall and 1033.4 for JJAS. Percentage error on an annual basis is quite large about -55.3 % and is -59.7 % during monsoon. The probability of detection (POD) remained high throughout the year varying between 1.0 and 0.71 and the false alarm ratio close to 0 except for November. The multiplicative bias is 0.40 in the monsoon indicating more than 50 % underestimation of rainfall by GSMaP.

3.3.3 Physiographic Level Verification - Assessment of the Accuracy of the Satellite-Based Rainfall Estimates for Various Physiographic Regions

To have a better understanding of how the performance of the SREs varies with elevation further verification according to physiographic regions has been conducted. The verification has been done for four physiographic regions High Mountains, Mid Mountains, Siwaliks and Terai at a spatial resolution of 0.1 degree with 2003 GSMaP datasets. Each physiographic region is clipped from the whole Nepal dataset to make this verification. The Terai area is covered by a total of 122 grids, Siwaliks by 122 grids, Mid Mountains by 251 grids and High Mountains by 170 grids. Accordingly the distribution of rainfall stations is 31 in Terai, 18 in Siwaliks, 78 in Mid Mountains and 45 in High Mountains (Figure 3.14). The Himals with elevation higher than 4000 m is not included in the verification due to fewer number of rainfall stations which would significantly influence the accuracy of interpolated gauge observed rainfall used as ground truth for all the analysis.

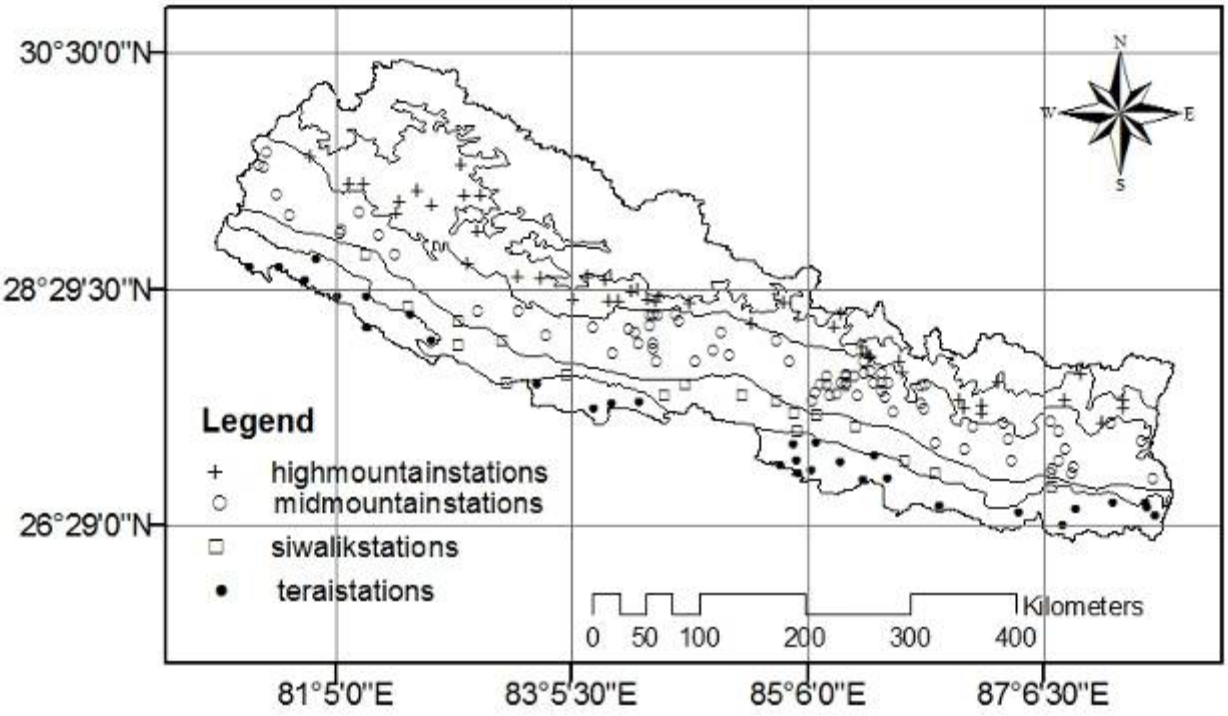

Figure 3.14 Location of rainfall stations in various physiographic regions of Nepal

Table 3.7 presents the comparison of annual GSMaP and gauge observed rainfall in the four physiographic regions of Nepal. In the Terai and Siwaliks area where the elevation is fairly low less than 1500 m the correlation coefficient between the GSMaP and gauge observed rainfall is high above 0.8. In the Mid Mountains and High Mountain areas where orography plays an important role the correlation coefficient decreases to about 0.4 on average with increasing RMSE. In the High Mountains the RMSE is 1470.1 and in the Mid Mountains 1070.4. Despite the relatively denser network of rainfall stations the prediction in the Mid Mountain area is less than in the Terai and Siwaliks. The percentage error an indicator of how close the predictions are to observed values also is minimum in the Terai (-38.8%) and maximum in the High Mountains (-67.4%). The correlation coefficient is highest in the Siwlaki (0.85) and Terai (0.84) regions while it decreases to 0.83 in the mid mountain region and to 0.47 in the High mountains. The multiplicative bias is higher in the Terai and Siwalik region and decreases rapidly to less than 0.4 in the High mountains indicating the performance of satellite based rainfall estimates to deteriorate with higher altitude region where influences of orography is high. The accuracy of prediction in the Terai and Siwalik is about 38% while with increase in elevation this accuracy

decreases to 49% in the middle mountains and more than 67% in the high mountain regions (Shrestha *et al*., 2010).

Table 3.7 Error statistics of area averaged annual GSMaP and gauge observed rainfall in various physiographic regions for 2003.

	bias	RMSE	Correl	PE	Mbias	POD	FAR
Terai	-743.4	784.6	0.80	-38.8	0.61	1.00	0.00
Siwaliks	-697.6	764.7	0.88	-37.0	0.63	1.00	0.00
Mid Mountains	-931.9	1070.4	0.37	-49.0	0.51	1.00	0.00
High Mountains	-1313.1	1470.1	0.43	-67.4	0.33	1.00	0.00

Table 3.8 Error statistics of monsoon (JJAS) GSMaP and gauge observed rainfall in physiographic regions for 2003.

	bias	RMSE	Correl	PE	Mbias	POD	FAR
Terai	-662.4	697.2	0.76	-41.4	0.59	1.00	0.00
Siwaliks	-645.9	721.8	0.83	-40.9	0.59	1.00	0.00
Mid Mountains	-832.5	943.3	0.40	-53.0	0.47	1.00	0.00
High Mountains	-1151.1	1277.9	0.46	-72.5	0.27	1.00	0.00

For the monsoon (JJAS) similar results are obtained as shown in Table 3.8. The correlation coefficient is high in the Siwaliks and Terai region on an average of about 0.8 while in the Middle and High Mountain region the correlation coefficient sharply drops to about 0.4. The RMSE is lowest in the Terai (697.2) and highest in the High Mountains (1277.9). This result clearly illustrates that GSMaP performs well in the flatter terrain with better prediction (Shrestha *et al*., 2010). While with increasing elevation the accuracy of predicting rainfall by GSMaP algorithm is found to become lower. Worse performances of the SREs over mountainous regions of Japan were indicated by previous works (Kubota *et al*., 2009; Shiraishi *et al*., 2009). This may be due to the impact of orographic enhancement of rainfall despite denser network of stations in the Mid Mountain region. The GSMaP uses a statistical database of precipitation vertical profiles classified into 10 types (Aonashi *et al*., 2009), but currently it cannot reflect profiles of localized precipitation systems. The profiles of heavy orographic rainfall are unique and largely different from those in the database, which can lead to large errors (Kutota *et al*., 2009).

Table 3.9 shows the error statistics of daily area averaged GSMaP and gauge observed rainfall during JJAS in various physiographic regions. Similar to the accumulated rainfall comparison the correlation is high in the Terai and Siwalik regions and reduces significantly in

the High Mountains. The error in detection is also lowest in the Terai and Siwalki region and increases to about 70% in the High Mountains. The daily bias in the Siwalik is half of that of the High Mountain region.

Table 3.9 Error statistics of daily GSMaP and gauge observed rainfall during JJAS in various physiographic regions for 2003.

		RMSE	Correl	PE	Mbias	POD	FAR
Terai	-2.0	5.5	0.84	-38.0	0.62	0.73	0.01
Siwaliks	-1.8	5.1	0.85	-35.9	0.64	0.73	0.00
Mid Mountains	-2.5	5.1	0.83	-48.3	0.52	0.70	0.01
High Mountains	-3.6	6.8	0.47	-67.0	0.33	1.00	0.12

Figure 3.15 illustrates the scatter plot of accumulated rainfall for JJAS of 2003 from observed and GSMaP for each grid cell. The poor performance of SREs in the high mountains is quite evident. We see that the High mountain regions show greater underestimation of rainfall compared to Siwalik and Terai regions. It is quite clear from this analysis that at higher elevation where orographic influence is evident the performance of the SREs decreases. However, the decrease in the performance cannot be solely attributed to orography only because other factors such as wind, slope and aspect are also important. Figure 3.16 shows the scatter plots of area averaged rainfall for the various physiographic regions of Nepal.

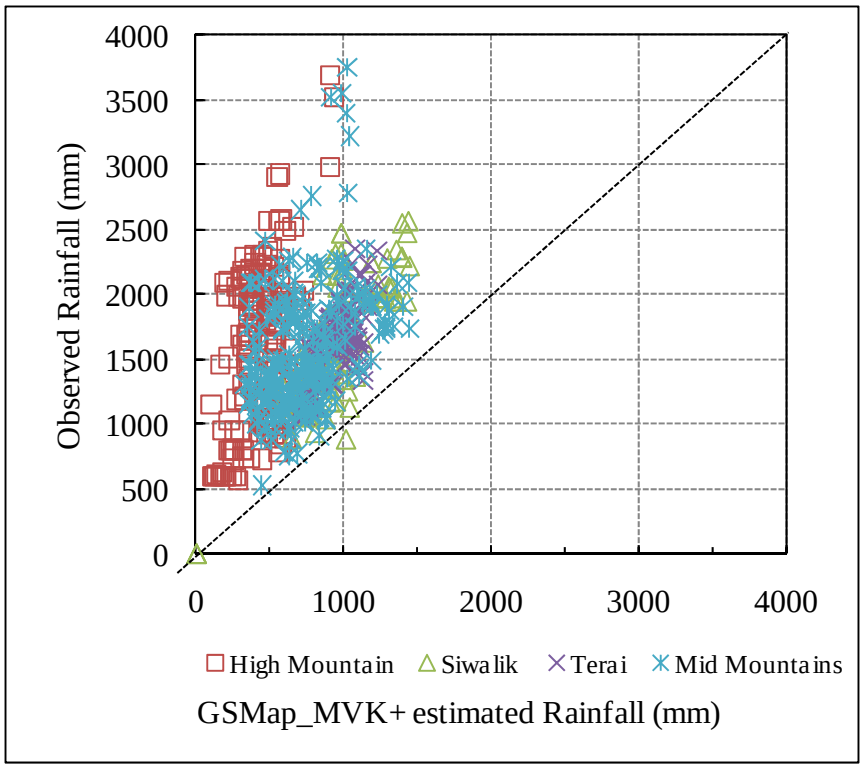

Figure 3.15 Scatter plot of accumulated rainfall for JJAS of 2003 from observed and GSMaP for each 0.1^{o}x0.1^{o} grid cell.

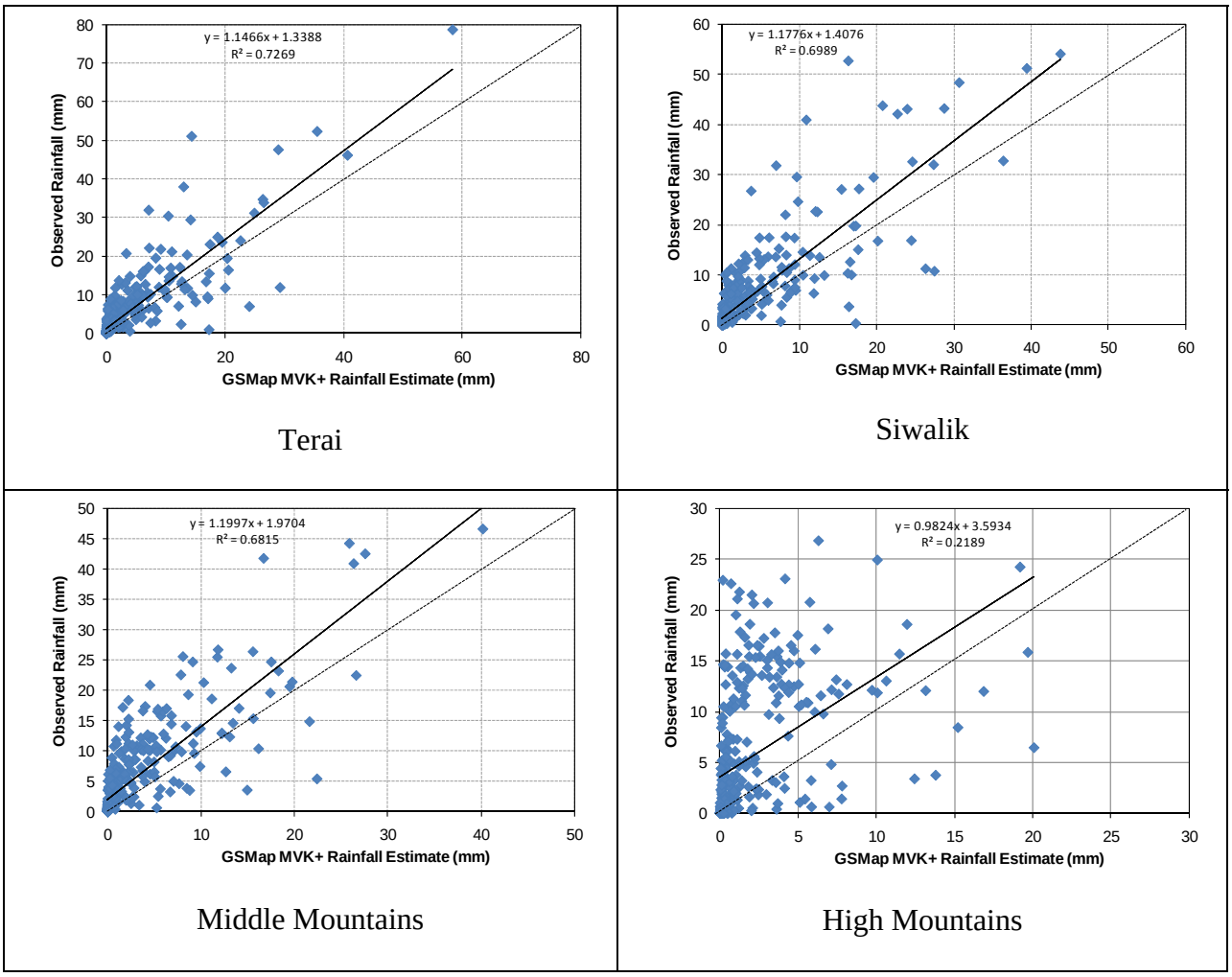

Figure 3.16 Scatter plots of area averaged rainfall for various physiographic regions of Nepal

3.3.4 Basin Level Verification in the Bagmati and Narayani Basins

There are three major river basins in Nepal the Koshi, Narayani and the Karnali. Apart from these river basins there are other river basins like Bagmati, East Rapti as shown in Figure 3.17. For the current research, basin level verification has been done for two basins Bagmati and Narayani. These two basins were selected to study the performance of SRE considering the flood vulnerability of the basin as well as the catchment sizes and topographic extent. Narayani Basin is a snow fed basin with more than 15 % of catchment area above 5000 m while the Bagmati Basin is below 2700 m with a catchment area of 2800 km^2. However, in both the basin flooding

causes adverse impacts to people's lives and livelihoods on a regular basis. It is anticipated that the study of these two basins will enable a better understanding of the performance of SREs for flood prediction purposes. The characteristics of the two basins are provided in Table 3.10.

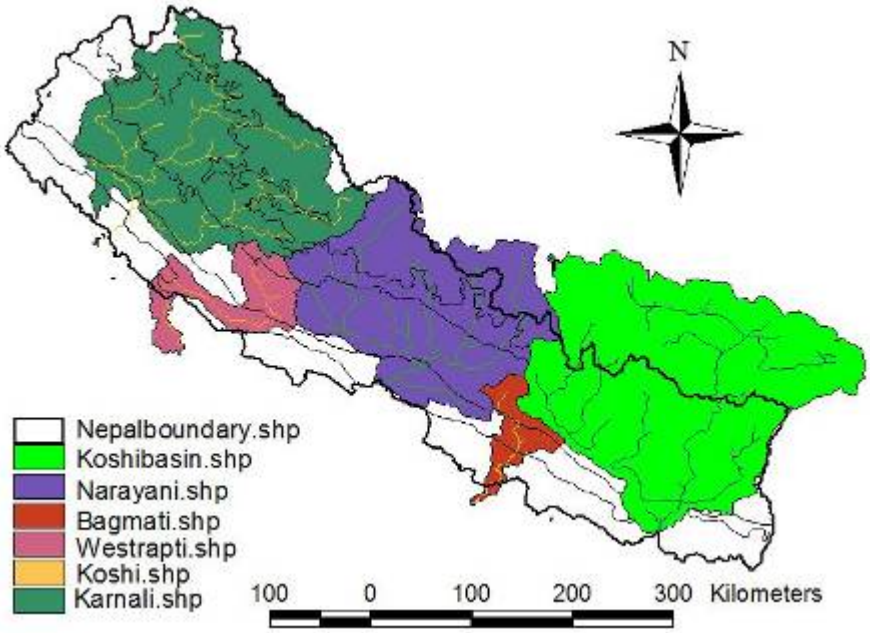

Figure 3.17 Major river basins of Nepal

Table 3.10 Characteristics of Bagmati and Narayani Basins

	Bagmati	Narayani
Catchment Area [km^2]	2800 (at Pandheradovan)	32000 (at Devghat)
Altitudinal range [m]	70 – 2700	100 - >8000
Physiography	Terai, Siwalik and Middle mountains (alluvial plain to the mid mountains)	Terai, Siwaliks, Middle mountains, High Mountains and Himal (alluvial plain to the himal with tundra conditions)
Dominant land use	Forest and agriculture	Forest and agriculture
Annual rainfall [mm]	1800	2000
Range of annual rainfall[mm]	1200 - 2000	200 - 6000

Bagmati Basin

The Bagmati Basin originates in the Mahabhararat range of the Middle Mountains of Nepal at elevation of around 2700 m and drains southward into the state of Bihar in India to join the Ganges River. It has a catchment area of about 3550 km^2 upto the Nepal India border and has

been classified into three physiographic regions. The upper part of the Bagmati Basin covers the whole of Kathmandu Valley. The middle part of the catchment extends downstream of the Chovar gorge to the Terai area at Pandhera Dovan near Karmaiya where the catchment area is about 2800 km^2. Further downstream beyond Pandhera Dovan gauging station the river then flows through the third part of the catchment with the lowest elevation of the Bagmati River at the Nepal India border at about 70 m above mean sea level (Figure 3.18). The catchment area of the Bagmati Basin lying below 1000 m inside Nepal is about 2050 km^2 and that lying between 1000 m and 3000 m is about 1500 km^2. The location of the basin is shown in Figure 3.17. The average elevation of the basin is about 1350 m. The total length of the river from its origin to Nepal India border is 170 km. The average slope of the river is about 1% which flattens down to 0.03% in the Terai area. The catchment lies in eight districts of Nepal; Kathmandu, Lalitpur, Bhaktapur, Sindhuli, Kavre, Makwanpur, Rautahat, and Sarlahi.

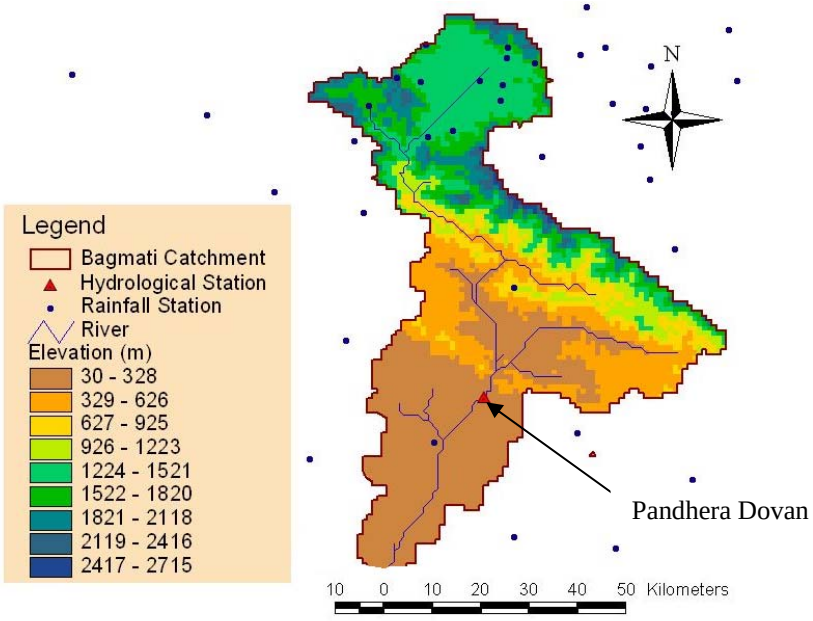

Figure 3.18 Location of rainfall station in the Bagmati Basin and its vicinity and discharge gauging station at Pandhera Dovan

Assessment of the accuracy of the RFE estimates

The rainfall observed at the rain gauge stations was higher than the concurrent RFE. Figure 3.19 shows an example of a rainfall event on July 23, 2002 along with the details of the statistical analysis. The probability of detection is 1 and the false alarm ratio is 0 showing that the RFE is capturing the rainfall event quite well qualitatively in terms of occurrence. However, the

estimated rainfall is lower than the observed amount indicating a negative bias. Figure 3.20 shows the comparison of the gauge observed rainfall and RFE for the 38 days period from July 1 to August 7, 2002. The RFE captures the rainfall trends well but underestimates the amount. However, the RFE almost completely miss to register any significant rainfall on day 204, a day when the rain gauges network showed the second highest rainfall amount of the period illustrating the random errors in the RFE (Shrestha *et al*., 2008).

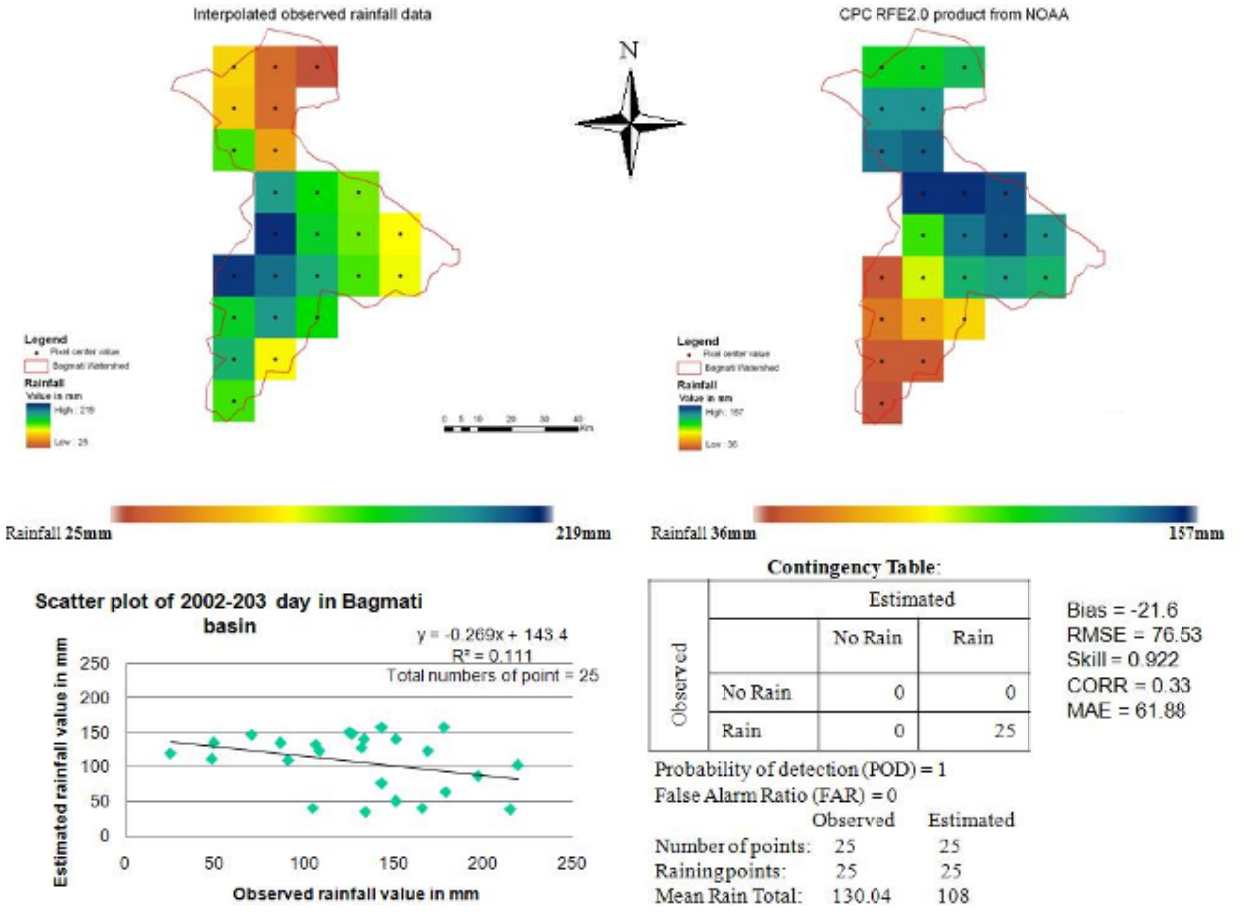

Figure 3.19 Comparison of rain gauge observed and RFE for the Bagmati Basin on July 23, 2002

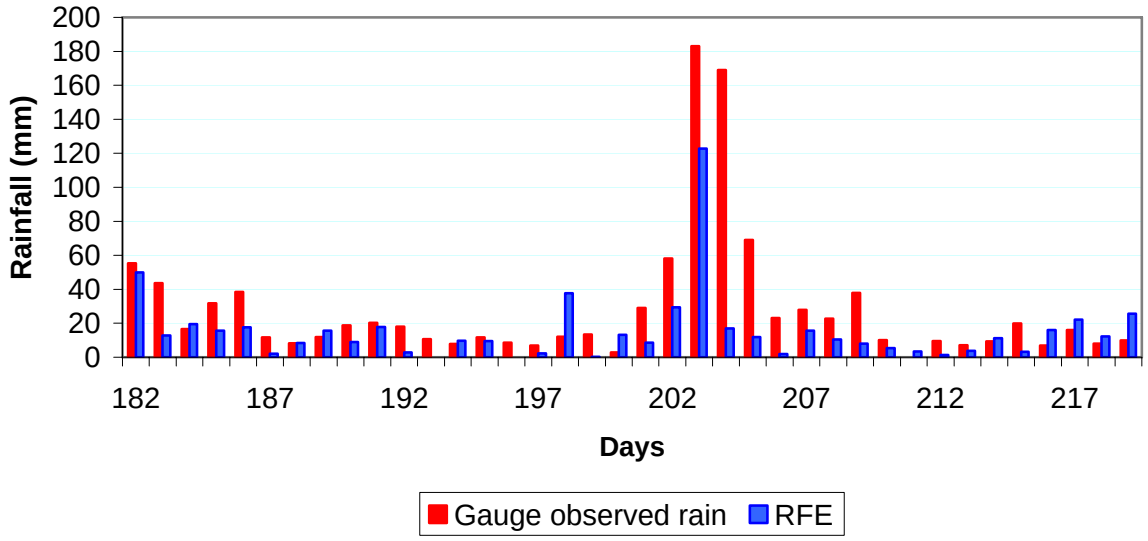

Figure 3.20 Basin average rainfall of Bagmati Basin for 2002

The daily accuracy of RFE was determined comparing the daily basin average rainfall for June, July, August and September (JJAS) from 2002 to 2006 (Figure 3.21). Table 3.11 provides the yearwise statistics of the performance of RFE compared to the gauge observed data of daily basin average rainfall. The correlation coefficient between the RFE and gauge observed daily basin average rainfall for JJAS was found to vary from 0.49 to 0.68 for each year with an average correlation of 0.60. The daily area averaged bias is -3.6 mm, RMSE is 13.1 mm and percentage error is -30.7 for the period 2002 to 2006. Figure 3.21 illustrates the underestimation of daily basin average rainfall from RFE compared to gauge observed rainfall for JJAS from 2002 to 2006. A histogram of daily basin averaged rainfall for 2003 is shown in Figure 3.22. The RFE showed relatively good agreement on some days while on other days, the RFE completely failed to register any significant rainfall when the rain gauge network showed high rainfall amounts.

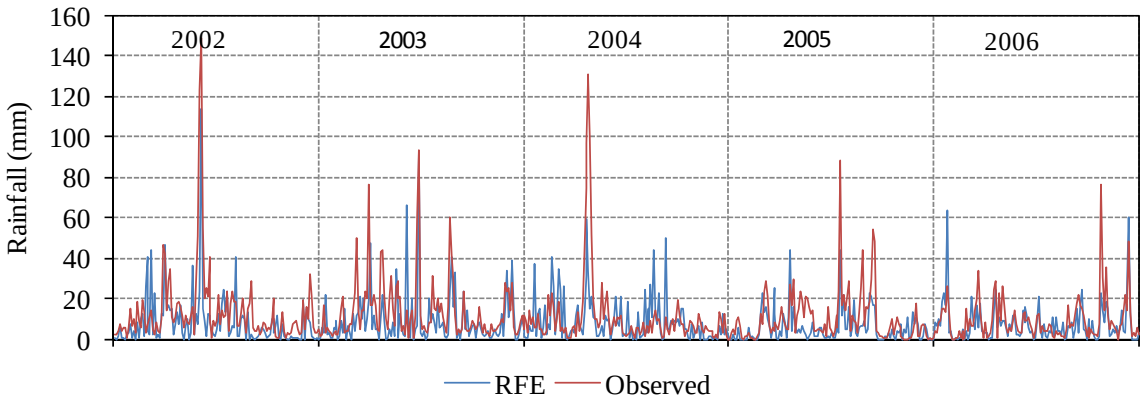

Figure 3.21Time series comparison of gauge observed and RFE daily basin average rainfall for monsoon (JJAS) from 2002 to 2006 in the Bagmati Basin

Table 3.11Statistics of performance of daily RFE compared to gauge observed data for JJAS from 2002 to 2006

Year	Bias (mm/day)	RMSE (mm/day)	r	PE (%)	Mbias
2002	-5.4	14.9	0.68	-39.1	0.61
2003	-4.2	13.5	0.58	-31.2	0.69
2004	-2.1	16.3	0.49	-18.8	0.81
2005	-4.3	10.3	0.64	-42.7	0.57
2006	-1.8	8.7	0.63	-19.3	0.81
Average (2003-2006)	-3.6	13.1	0.60	-30.7	0.69

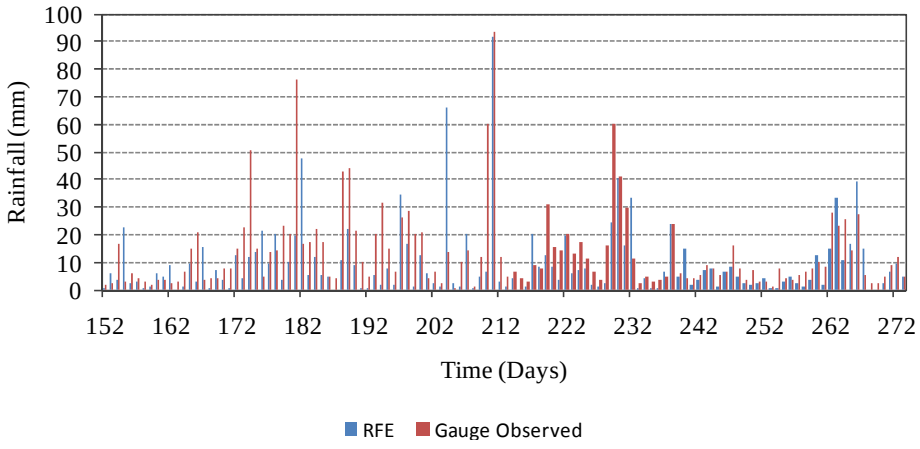

Figure 3.22 Daily basin averaged gauge observed rainfall with RFE for JJAS of 2003 in the Bagmati Basin

Narayani Basin

The Narayani Basin lies in the Western Development Region of Nepal (Figure 3.17). The Narayani river system has five major tributaries, the Kali Gandaki, Seti Gandaki, Marsyandi, Budhi Gandaki, and Trisuli. The Trisuli and Budhi Gandaki originate in the Tibet Autonomous Region of China, while the other three originate within Nepal. The Kali Gandaki is the main river in this drainage system. After the confluence of its five tributaries, the Narayani flows through Devghat and meets the Ganges in India. Geographically, it is located between longitudes 82.88^{o} to 85.70^{o} east and latitudes 27.36^{o} to 29.33^{o} north and passes through 19 districts of Nepal. It has a total drainage area of 32,000 km^2 at the Devghat hydrometric station.

The basin has high topographic variation with elevation ranging from 60 m in the south to higher than 8000 m in the north where it passes through the high Himalayas, which contain the Dhaulagiri (8167 m) and Annapurna (8091 m) peaks. The Narayani Basin contains all five physiographic regions of Nepal: the Terai (the northward extension of Indo-Gangetic plain), the Siwalik (Chure Hills), Middle Mountains, High Mountains, and Himal. The Terai covers an area extending from an altitude of less than 500 m (9.2%), the Siwaliks from 501 to 1500 m (31.1%), the Middle Mountains from 1501 to 3,000 m (18.2%), High Mountains from 3001 to 5000 m (26.5%) and Himals above 5000 m (14.9%). Given the topographic variation the climate varies from subtropical in the Terai to alpine conditions in the Himal. There is pronounced temporal and spatial variation in precipitation in the basin; the mean annual precipitation varies from 200 mm to more than 5000 mm (Sharma, 1977; Chalise *et al.*, 1996). The upper basin of the Kali Gandaki lies in the Trans Himalayan region, which has arid conditions. The main rainy season is the monsoon from June to September.

The Narayani Basin is one of major development hubs of Nepal contributing about 50 per cent of the total hydropower production of the country (NEA, 2008). In 1993, a large flood occurred in the Narayani Basin with record high rainfall of 540 mm in 24 hours and intensity exceeding 70 mm/hr, during which more than 1050 people lost their lives. Bhusal and Bhattarai (2002) noted that had there been a flood forecasting system in place the loss of lives would have been minimized. Hence, SREs now available at a higher resolution provides an opportunity for flood prediction.

Assessment of the accuracy of the RFE estimates

Verification of the RFE rainfall estimates over the Narayani Basin was conducted by comparing with the gauge observed rainfall data for selected high rainfall days from 2003 and 2004. The Narayani Basin is covered by 234 grids of 0.1 degree resolution; 41 of the grids contain one or more rainfall stations (Figure 3.23). Comparison of the gauge observed and estimated rainfall in those grids with one or more stations shows that, on average, the observed rainfall was higher than the concurrent rainfall estimates in all cases considered. Figure 3.23 shows an example of a rainfall event on 9 July 2003, along with the statistics.

The RFE captures the rainfall spatial trends well, but underestimates the amount on average by more than 50 per cent. The POD was 0.97 and the FAR was 0.05. The RMSE was 45.2 mm; using the Wilmott method (Wilmott, 1982; Wilmott *et al*., 1985), 34.7 mm was unsystematic RMSE (0.59), and 28.9 mm was systematic RMSE (0.41). The RFE estimated rainfall was lower than the gauge observed rainfall amount with bias of 33.7 mm. The random and systematic errors observed in the RFE estimates result from the uncertainty in estimates from the individual data sources used to produce the RFE product (Xie *et al*., 2002). The satellite data used in the production of the RFE are from microwave imagers and infrared imagery. The SSM/I and AMSU-B are the primary passive microwave data included in the RFE estimates. These data have a strong physical relationship to the hydrometeors that result in surface precipitation, but each individual satellite provides a very sparse sampling of the time-space occurrence of precipitation (Huffman *et al*., 2007). The random error observed in the rainfall estimates could partly be associated with this limited sampling of satellite observations.

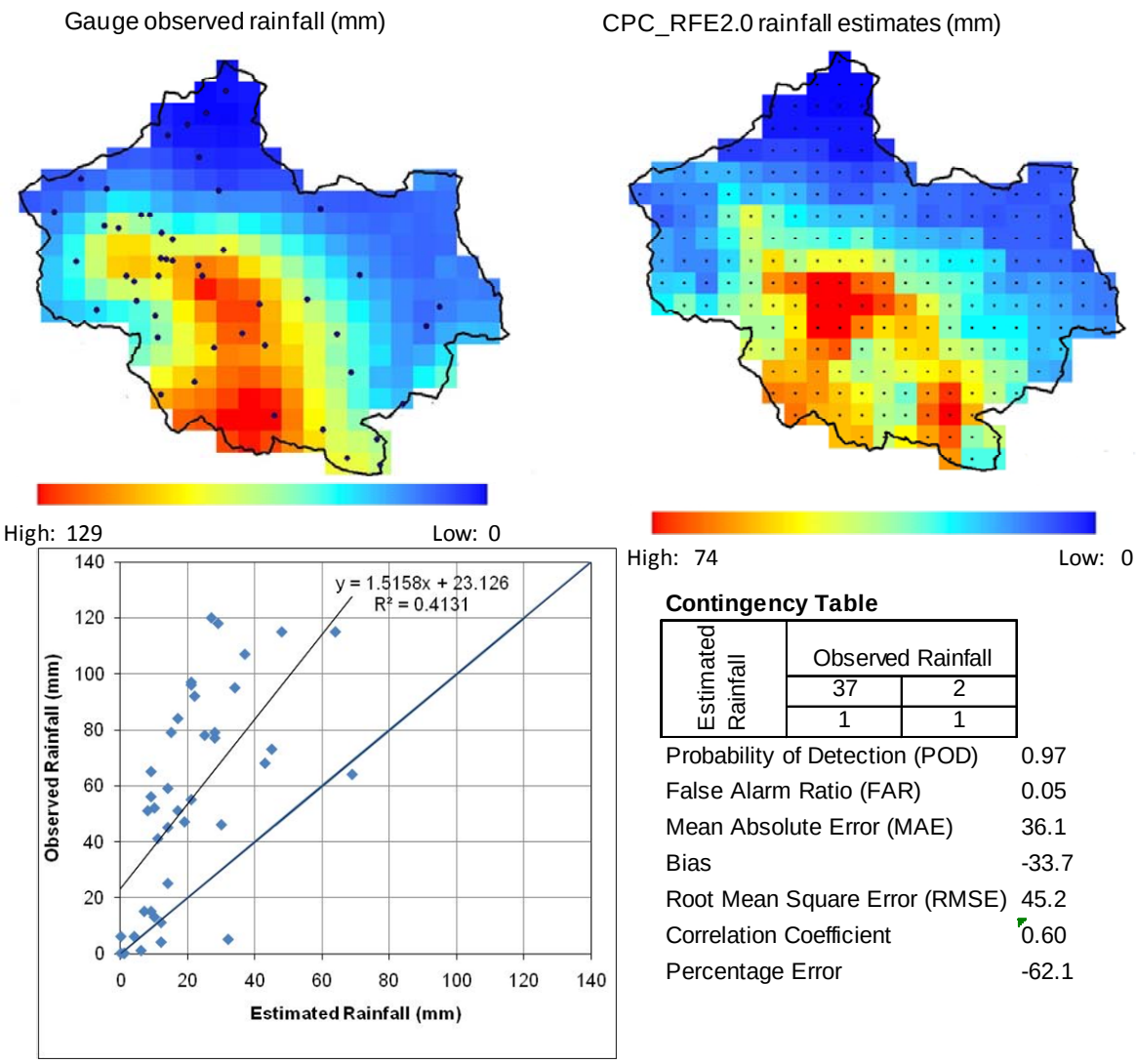

Contingency Table

Estimated Rainfall	Observed Rainfall	
	37	2
	1	1

Probability of Detection (POD)	0.97
False Alarm Ratio (FAR)	0.05
Mean Absolute Error (MAE)	36.1
Bias	-33.7
Root Mean Square Error (RMSE)	45.2
Correlation Coefficient	0.60
Percentage Error	-62.1

Figure 3.23 Comparison of gauge observed and RFE for 9 July, 2003 in the Narayani Basin

The daily accuracy of RFE was determined comparing the daily basin average rainfall for June, July, August and September (JJAS) from 2002 to 2006 (Figure 3.24). Table 3.12 provides the yearwise statistics of the performance of RFE compared to the gauge observed data of daily basin average rainfall. The correlation coefficient between the RFE and gauge observed daily basin average rainfall for JJAS was found to vary from 0.40 to 0.69 for each year with an average correlation of 0.50. The daily basin averaged bias is -4.9 mm, RMSE is 8.8 mm and percentage error is -43.4 for the period 2002 to 2006. Figure 3.25 illustrates the underestimation of daily basin average rainfall from RFE compared to gauge observed rainfall for JJAS from 2002 to 2006. A histogram of daily basin averaged rainfall for 2003 is shown in Figure 3.25. The RFE showed relatively good agreement on some days while on other days, the RFE completely

failed to register any significant rainfall when the rain gauge network showed high rainfall amounts. This random nature of the SRE was also noted in the Bagmati Basin.

In both the basins there is a consistent underestimation of rainfall by RFE except for some days where the satellite-based rainfall exceeds the gauge observed rainfall and shows false detection. The bias is smaller in the Bagmati Basin compared to the Narayani. However, the percentage error in the Narayani is larger than that observed in the Bagmati, suggesting that the SREs perform better in the basins located in the Terai and Siwalik regions compared to basins with substantial area in the Mid Mountain and High Mountain areas. The underestimation of rainfall is consistent with previous studies (Dinku *et al*., 2008; Ebert *et al*., 2007; Harris *et al*., 2007; Shrestha *et al*., 2008; Hughes, 2006). This underestimation of rainfall in the Narayani Basin, may be further attributed to the orographic effects prevalent in the basin where rainfall varies in small spatial scales between 200 mm to over 5000 mm which may not be adequately represented in the current rain profile algorithms of the SRE. To accurately predict floods the RFE thus needs to be adjusted.

Table 3.12 Statistics of performance of daily RFE compared to gauge observed data for JJAS from 2002 to 2006.

Year	Bias (mm/day)	RMSE (mm/day)	r	PE (%)	Mbias
2002	-6.7	12.0	0.41	-51.6	0.48
2003	-5.9	8.7	0.69	-44.2	0.56
2004	-5.7	8.9	0.40	-49.5	0.50
2005	-4.2	7.1	0.55	-46.2	0.54
2006	-2.1	6.7	0.50	-23.8	0.76
Average (2003-2006)	-4.9	8.8	0.50	-43.4	0.57

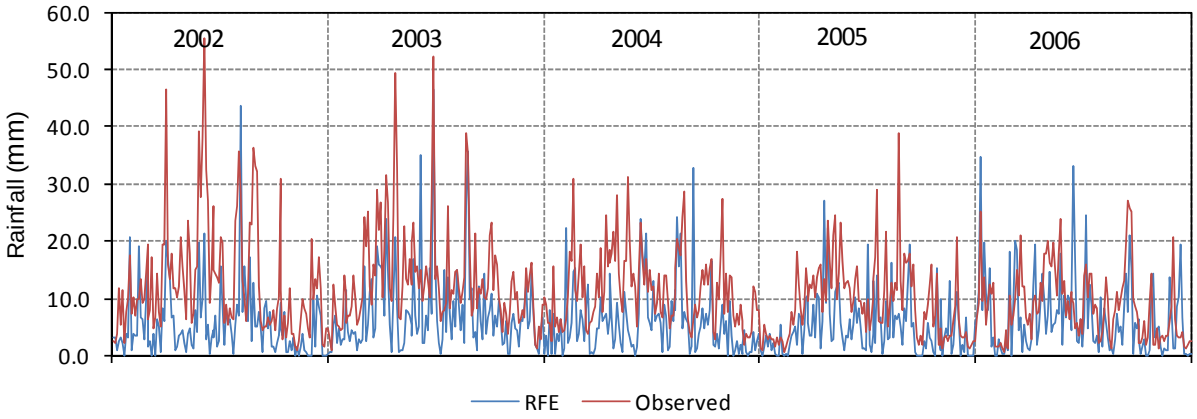

Figure 3.24 Time series comparison of gauge observed and RFE daily basin average rainfall for monsoon (JJAS) from 2002 to 2006 in the Narayani Basin

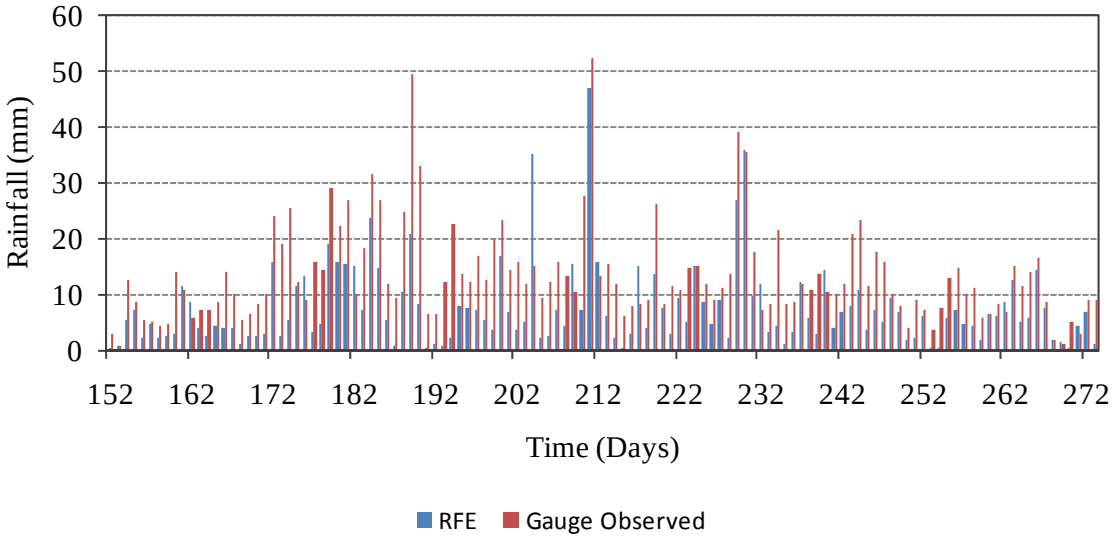

Figure 3.25 Daily basin averaged gauge observed rainfall with RFE for JJAS of 2003 in the Narayani Basin

3.4 Summary

Verification of SREs using two products, the RFE and GSMaP has been conducted at three levels. The first set of verification was conducted at a country level. The GSMaP estimates were found to underestimate the annual rainfall by 48 % and RFE by 30%. The GSMaP however showed better correlation with the observed data as compared to RFE. The second level of verification was conducted for various physiographic regions to assess the performance of RFE

is various regions. Both SREs performed better in the flatter regions in the Terai and Siwalik regions. The performance deteriorated with higher elevations with the minimum performance in the High Mountain region. The middle mountain regions despite the dense network of stations showed poorer performance of SREs. Finally, verification was also conducted at a basin level in two basins Bagmati and Narayani which differ in catchment areas and general characteristics. On a daily basis the Bagmati Basin has a lower bias than the Narayani. The percentage error is also smaller in the Bagmati compared with the Narayani, suggesting that RFE performs better in basins lying in the Siwaliks and the Terrai region compared to the Middle Mountains and High Mountain areas. In all three levels of verification the SREs were found to be generally lower than the gauge observed data indicating the need to adjust the rainfall estimates for further application.

References

Aonashi, K., Awaka, J., Hirose, M., Kozu, T., Kubota, T., Liu, G., Shige, S., Kida, S., Seto, S., Takahashi, N., and Takayabu, Y. N.: GSMaP passive, microwave precipitation retrieval algorithm: Algorithm description and validation. *J. Meteor. Soc.*, Japan, Vol.87A, pp. 119-136, 2009.

Basistha, A.; Arya, D. S.; Goel. N.K. (2007) Spatial Distribution of Rainfall in Indian Himalayas – A Case Study of Uttarakhand Region, *Water Resour Manage* DOI 10.1007/s11269-007-9228-2.

Chalise, S.R., Shrestha, M.L., Thapa, K.B., Shrestha, K.B., Bajracharya, B. (1996) *Climatic and hydrological Atlas of Nepal*. Kathmandu: ICIMOD

Creutin, J.D., Obled, C. (1982) Objective analysis and mapping techniques for rainfall fields: an objective comparison. *Water Resour. Res.* **18** 2, pp. 251–256.

Diodato, N.; Ceccarelli, M. (2005) Interpolation processes using multivariate geostatistics for mapping of climatological precipitation mean in the Sannio Mountains (southern Italy). *Earth Surf. Process. Landforms* 30, pp. 259–268

Ebert, E.E. (2007a) Methods for verifying satellite-based precipitation estimates *Measuring Precipitation from Space*, V. Levizzani et al. (eds) Eurainsat and the Future, pp. 345-356.

Ebert, E.E.; Janowiak, J.E.; Kidd, C. (2007b) Comparison of near-real-time precipitation estimates from satellite observations and numerical models. *Bull. Amer. Meteorol. Soc.* 88(1), 47–64.

Ebert, E.E.; McBride, J.L. (2000) Verification of precipitation in weather systems: Determination of systematic errors. *J. Hydrology*, **239**, 179-202.

Hughes, D.A. (2006) Comparison of satellite rainfall data with observation from gauging station networks. *J. Hydrol*. 327, pp. 399-410.

Ichiyanagi, K.; Manabu, D.;Yoshitaka, Y.; Murajic, Y.; Vaidya, B.K. (2007) Precipitation in Nepal between 1987 and 1996 *International Journal of Climatology*. **27**, pp. 1753–1762

Isaaks, E. H., Srivastava, R.M. (1989) *An Introduction to Applied Geostatistics*. Oxford Univ. Press, New York, Oxford.

Kansakar, S.R.; Hannah, D.M.; Gerraed, J.; Rees, G. (2004) Spatial pattern in the precipitation regime of Nepal. *International Journal of Climatology* **24**, 1645–1659.

Kubota, T.; Ushio, T.; Shige, S.; Kachi, M.; Okamoto, K. (2009) Verification of high resolution SRE around Japan using a gauge-calibrated ground-radar dataset. *J. Meteorol. Soc*., Japan 87A, pp. 203–222.

Shiraishi, Y., Fukami, K., Inomata, H. (2009) The proposal of correction method using the movement of rainfall area on satellite-based rainfall information by analysis in the Yoshino River basin. *Annual Journal of Hydraulic Engineering,* Vol.53, pp. 385-390.

Shrestha, M.S., Artan, G.A., Bajracharya, S.R. and Sharma, R.R. (2008) Applying satellite based rainfall estimates for streamflow modelling in the Bagmati Basin, Nepal. *J. Flood Risk Management,* Vol.1, pp. 89-99.

Shrestha, M.S., Takara, K., Kubota, T., Bajracharya, S. (2011) Verification of GSMaP rainfall estimates over the Central Himalayas. *Annual Journal of Hydraulic Engineering*, JSCE, Vol. 55 (to be published).

Tabios, G.Q.; Salas, J.D. (1985) A comparative analysis of techniques for spatial interpolation of precipitation. *Water Resources Bulletin* 21, pp. 365–380.

Ushio, T.; Sasashige, K.; Kubota, T.; Shige, S.; Okamota, K.; Aonashi, K.; Inoue, N.; Takahashi, T.; Iguchi, T.; Kachi, M.; Oki, R.; Morimoto, T.; Kawasaki, Z.I. (2009) A Kalman Filter

approach to the global satellite mapping of precipitation (GSMaP) from combined passive microwave and infrared radiometric data, *J. Meteorol. Soc*. , Japan, Vol.87A, pp. 137-151.

Wilmott, C.J. (1982) Some comments on the evaluation of model performance. *Bull. Amer. Meteorol. Soc*. 88, 1309–1313.

Xie, P.; Arkin, P.A. (1996) Analyses of global monthly precipitation using gauge observations, satellite estimates and numerical model predictions. *J. Clim*., Vol.9, pp. 840-858, 1996.

CHAPTER 4

4 RAINFALL-RUNOFF MODELLING USING SATELLITE-BASED RAINFALL ESTIMATES

4.1 Introduction

There are a range of rainfall-runoff models for discharge prediction based on rainfall inputs (Maidment, 1993). The rainfall-runoff process can depict a catchment response based on meteorological inputs (rainfall, evapotranspiration) and catchment parameters including soil, landuse and landcover. The rainfall-runoff models are used for a number of applications for example flood forecasting, prediction of the effects of proposed changes of the catchment including climate change and, in general for water resources management. Since the 1960s after the development of the Stanford Watershed model which is based on water-balance accounting there has been a wide number of rainfall-runoff models developed. Literature review indicates that there are many rainfall-runoff models like the HEC-HMS, TOPMODEL, OHYMOS, NAM, TANK, GeoSFM, and others that have been applied in for runoff prediction. We can find in literature many comparisons of these models examining their performance. Moore and Bell (2001) has provided a review of the rainfall-runoff models used for flood forecasting purposes mainly in the United Kingdom. With the rapid technological advancement in computation rainfall-runoff processes have been modelled using distributed hydrologic modelling techniques.

Precipitation is one of the most important inputs that feed into the rainfall-runoff models for hydrological modelling. However, in many regions the number of ground measuring stations is very limited and unevenly distributed making it difficult for flood prediction. In areas with limited or no rain gauge network, like the Himalayan region, satellite-based rainfall estimation could provide information on rainfall occurrence, amount, and distribution (Hong *et al*., 2007; Shrestha *et al*., 2008). A few studies have looked into the application of satellite-based rainfall estimates (SRE) in hydrological modelling. Artan *et al*. (2007a) investigated the utility of SREs for flood forecasting purposes. Yilmaz *et al*. (2005) evaluated the utility of SREs for hydrologic forecasting. Hughes (2006) evaluated SREs with gauge observed data at a monthly time step for application in hydrological modelling. Hong *et al*. (2007) proposed

the application of satellite rainfall data in near real time using TRMM in global monitoring system for early warning of floods and landslides. Harris and Hossain (2008) investigated the optimal configuration of conceptual hydrologic models for flood predictions based on satellite rainfall data using a 970 km^2 catchment in Kentucky in the United States. Considerable caution is recommended in application of satellite rainfall data when the scale of available satellite rainfall data is comparable to the overall size of the basin. Wilk *et al*. (2006) developed a long-term rainfall dataset by combining gauge and satellite datasets for various periods for the data sparse Okavango River Basin in Africa and applied it in a hydrological model for runoff estimation to provide decision support in water management. Asante *et al*. (2007a) demonstrated the usefulness of SRE in the detection of extreme flood events for wide area flood monitoring to enhance the ability of water managers to provide early warnings, but the accuracy of the estimates were not assessed. The usefulness of SRE to hydrological modelling on a daily time scale has been further demonstrated in several basins around the world including Bagmati and Narayani Basin in Nepal using the United States Geological Survey (USGS) hydrological model, the Geospatial Stream Flow Model (GeoSFM) (Artan *et al*., 2007a; Asante *et al*., 2007a; Shrestha *et al*., 2008; Shrestha *et al*., 2010). Results using SRE have shown underestimation of flows (Artan *et al*., 2007a; Harris *et al*., 2007; Shrestha *et al*., 2008). This chapter describes the GeoSpatial Streamflow model (GeoSFM) used for the study and provides calibration and validation of the model and application of SRE as an input for flood prediction.

4.2 The GeoSFM Model

4.2.1 Introduction

The GeoSFM is a semi distributed hydrologic model developed by USGS, Earth Resources Observation and Science (EROS) Centre. The GeoSFM simulates the dynamics of runoff processes by using remotely sensed and widely available global datasets. The GeoSFM model assimilates spatially distributed data to simulate streamflow on a daily basis. The model is a physically-based catchment scale hydrologic model (Artan *et al*., 2007a). The model runs in ArcView environment with a Graphical User Interface (GUI) and a rainfall-runoff simulation component. The general framework of the GeoSFM model is illustrated in Figure 4.1.

The GeoSFM GUI component runs within the GIS for model input and data preparation and visualization of model outputs. Topographic, land cover and soil information are the basic inputs to derive and parameterize the hydrologic modeling units. On the basis of Digital Elevation Model (DEM) hydrologic parameters such as slope, aspect, flow direction and accumulation are derived. After the data parameterization and end of the hydrologic simulation run the GeoSFM provides a module through which flow statistics outputs can be generated in a tabular form which includes maximum, minimum, mean, standard deviation and percentile flows of each catchment. Through the GUI these values can be viewed through a visual map. Flow status maps of each catchment can be viewed in a color coded map.

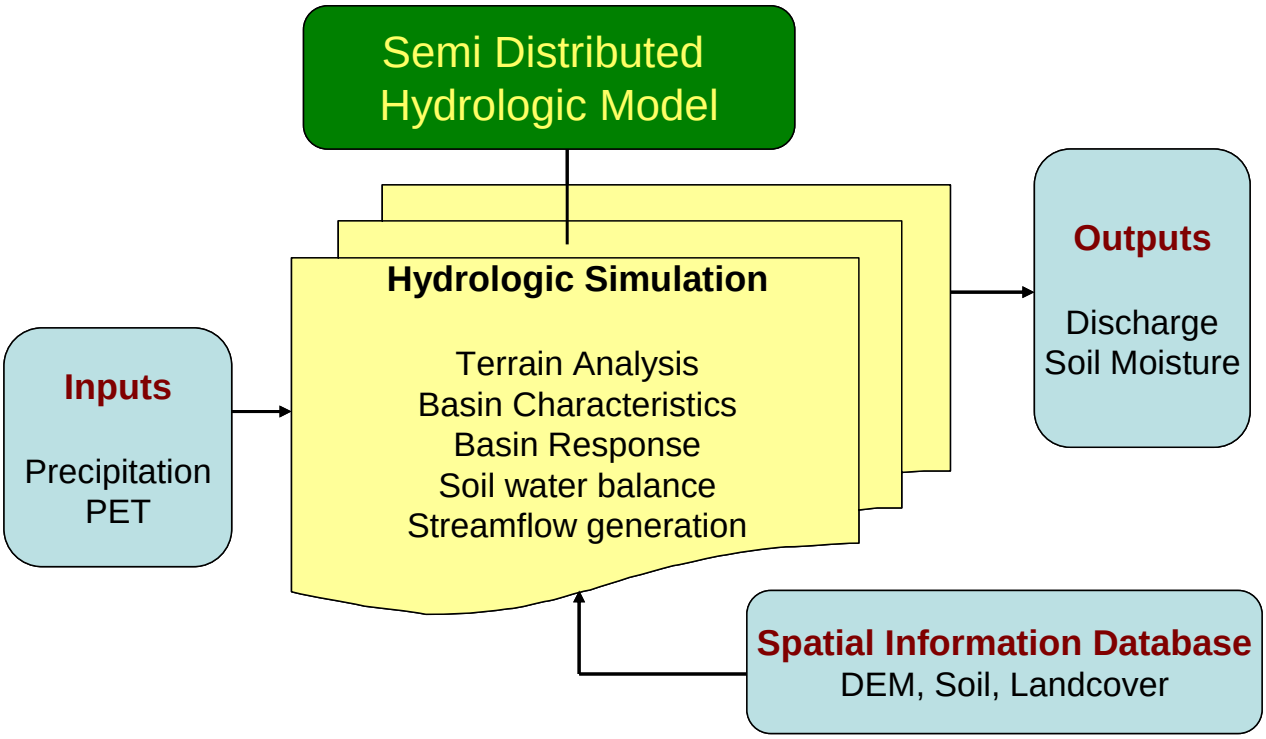

Figure 4.1 General framework of the GeoSFM model

4.2.2 Model Formulation

The GeoSFM rainfall-runoff component has three main modules: water balance, catchment routing, and distributed channel routing (Artan *et al*., 2007a; Asante *et al*., 2007a). In the water balance module, the sub-basins are the subject of a daily water balance calculation. This calculation determines how much water enters the stream network from each sub-basin. In the water balance module, the soil is conceptualized as composed of two zones: (a) an active soil layer where most of the soil– vegetation–atmosphere interaction processes take place, and (b) the groundwater zone. The active soil layer is divided into an upper thin soil layer where evaporation and transpiration both occur and a lower soil layer where only transpiration takes place. The catchment runoff mechanisms considered in the model are excess precipitation runoff, direct runoff from impermeable areas of the basin, rapid subsurface flow (interflow), and base flow contribution from groundwater.

The model has several excess runoff generation options; in the present study the Soil Conservation Service Curve Numbers (CN) method is used to model the surface runoff generation process. CN were estimated from a land use and land cover data layer and were dynamically updated to reflect the state of the soil moisture. The runoff produced by the water balance module is routed in two phases. First, the catchment runoff is routed at the sub-basin level to its outlet, and then the flow is routed through the main river channel network. In the sub-basins, the subsurface runoff is routed using a set of two conceptual linear reservoirs. According to Artan *et al*. (2007a) in the GeoSFM model the surface runoff routing is carried out using a diffusion wave equation modified for use in a GIS environment, the land cover and DEM data are used to determine the rate at which runoff is transported from the point of generation to the catchment outlet. When runoff generated within a given catchment arrives at the catchments outlet, it enters the river network and travels downstream to the basin outlet. The GeoSFM model supports two linear namely pure translation and the diffusion analog, and one non-linear method, the Muskingum–Cunge for flow routing. The GeoSFM has been used in several basins around the globe with good results (Artan *et al*., 2007b; Asante *et al*., 2007b). Figure 4.2 provides the process map and system diagram for the GeoSFM Model

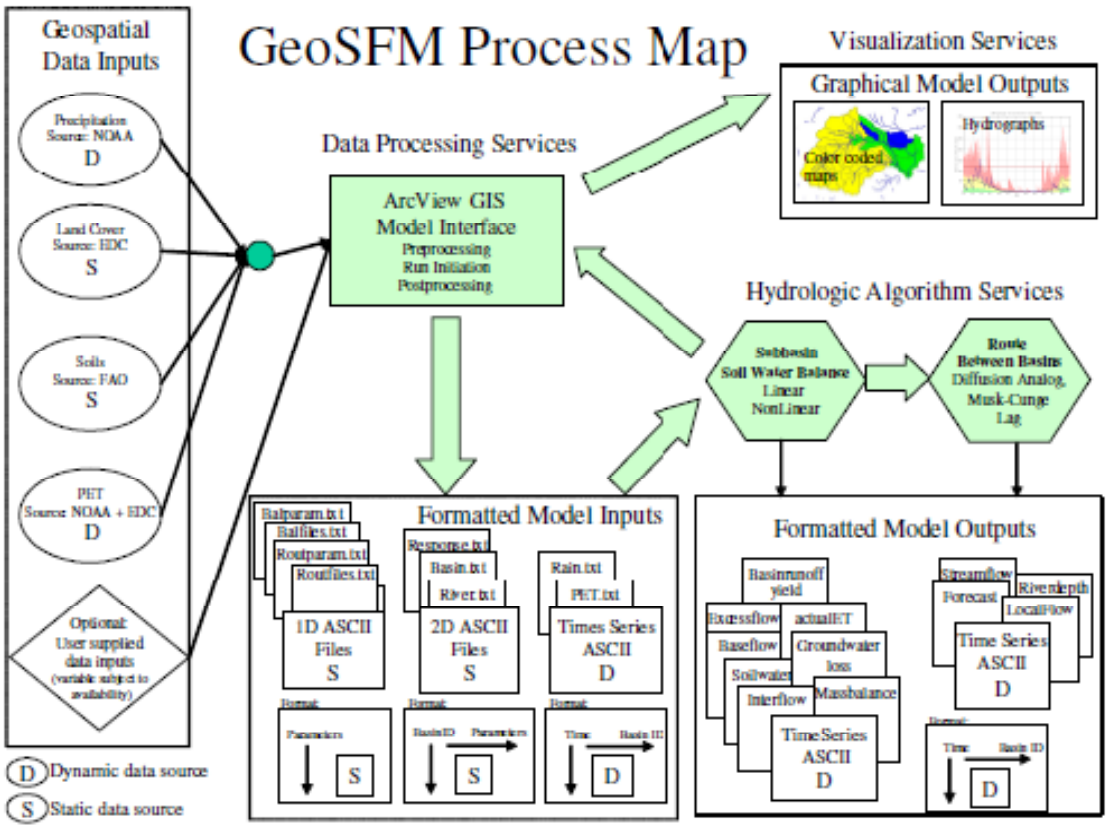

Figure 4.2 Process Map and System Diagram for the GeoSpatial Streamflow Model (Source: Asante *et al*. 2001)

4.3 Data Inputs

4.3.1 Digital Elevation Model

The GeoSFM uses a digital elevation model (DEM) for the delineation of hydrologic modeling units. The model supports the use of DEM of any resolution. In this study the DEM of 1-kilometer resolution Hydro1k produced by the USGS EROS data centre is used which provides a hydrologically corrected DEM of the HKH region.

4.3.2 Soil Data

The response of a river basin to a rainfall event depends heavily on the nature and condition of underlying soils. In the GeoSFM model the static parameters and the dynamic parameters of soil characteristics are required. In particular the model requires soil water holding capacity, hydrologically active soil depth, texture, average saturated hydraulic conductivity and runoff curve number (Artan *et al*., 2007a). The curve number determines the amount of incident

precipitation that becomes surface runoff. Model-required soil parameters (i.e., soil water holding capacity, saturated soil hydraulic conductivity, hydrologically active soil layer depth, and soil texture) were extracted from the Digital Soil Map of the World (FAO, 1995). All the data are in geographic projection and are produced from original map sheets with a scale of 1:5,000,000.

4.3.3 Land Cover Data

The nature of vegetation on the land surface influences the flow velocity and hence runoff generation and overland flow processes. The USGS Global Land Cover Characteristics (GLCC) database is used in the GeoSFM modeling. The GLCC data were derived from 1km Advanced Very High Resolution Radiometer (AVHRR) data and are presented in the Lambert Equal Area Azimuthal projection.

4.3.4 Evaporation Data

Evaporation is a process by which water is extracted from the soil column. The rate of evaporation depends upon the amount of water present in the soil column. The potential evapotranspiration (PET) depends upon the prevailing weather conditions including temperature, radiation, atmospheric pressure, relative humidity, wind speed as well as factors like soil moisture availability and type of vegetation. The GeoSFM uses the data from the Global Data Assimilation System (GDAS) to solve the Penman-Monteith equation to generate grids of PET at a daily time step. The GeoSFM contains a procedure for processing the PET grids and computing actual daily evapotranspiration based on antecedent soil moisture conditions.

4.3.5 Rainfall Data

Precipitation is the most essential input to the GeoSFM. In the current study the SRE as well as the observed rainfall from ground based gauges have been used for the modeling. The NOAA CPC-RFE 2.0 (RFE) rainfall estimates over the Central Himalayas for the period 2002-2006 has been used for the study. The daily observed rainfall data are from 176 rainfall stations over Nepal for the 2002 to 2006 period obtained from the DHM. The gauged observed rainfall data were checked for consistency and accuracy. Incomplete and duplicates datasets were discarded.

The datasets were then formatted to GIS format and transformed to the same projection as the RFE data sets. The gauged data was then interpolated using the kriging spatial interpolation technique at a 1^o x 1^o spatial resolution.

4.4 Methodology - Geospatial Processing and Hydrologic Computations

4.4.1 Preprocessing Modules

The preprocessing module includes the terrain analysis, unit hydrograph response and daily weather data assimilation.

Terrain Analysis

The main input parameter in the terrain analysis is DEM. The direction and rate of movement of water over the land surface is highly influenced by underlying topography. The analysis of topographic data for hydrologic modeling applications relies on the simple principle that water flows in the direction of steepest descent. Flow direction in GeoSFM is assigned using the eight direction pour point model in which each grid cell is assigned one of eight compass directions depending on which of its eight neighboring cells it discharges flow into. The computation of a flow direction grid paves the way for the determination of other parameters of hydrologic interest such as upstream contributing area, distance to the basin outlet and the slope of the land surface. It also allows for the definition of hydrologic modeling units such as basins and river reaches.

Unit Hydrograph Response

For each catchment a unit hydrograph is developed to simulate the response of the catchment. Based on the catchment slope and land cover an overland velocity is computed for the catchment. The distance along the flow path from each grid cell in the catchment to the outlet is also computed. On the basis of this the travel time is computed. The distribution of discharge at the catchment outlet is given by the probability function of travel times in the catchment. All these computations are done through an algorithm built inside the GeoSFM.

Daily Weather Data Assimilation

The primary data required by GeoSFM for daily simulations are precipitation and evapotranspiration. Daily rainfall values (RFE and gauge observed rainfall grids) are used to compute mean areal precipitation and mean areal evapotranspiration values for each sub-basin.

On the basis of antecedent soil moisture conditions and the data from the GDAS evaporation time series are generated.

4.4.2 Hydrologic Simulation Modules

The hydrologic simulation modules include soil moisture accounting, channel flow routing and computing spatial statistics.

Soil Moisture Accounting

Soil moisture condition on a daily basis is computed for each catchment. The soil parameters of each catchment are extracted from the DMSW produced by FAO and UNESCO. In the model there are two soil moisture accounting routines: the single layer soil model and the two layer soil model. Where there is limited data availability the single layer model is widely used which however does not account for land cover within a catchment. In areas where finer resolution data is available the two layer soil model is used which has a more complete representation of subsurface processes by creating separate soil layers within which interflow and baseflow processes occur.

Channel Flow Routing

When runoff generated within a given catchment arrives at the catchment outlet, it enters the river network and works its way downstream to the basin outlet. Within the GeoSFM model there are three methods for routing, two linear methods namely pure translation and diffusion analog, and one non-linear method, the Muskingum Cunge. For the current study the diffusion analog routing method has been used given its simplicity and better generation of results compared to other two routing methods.

Diffusion Analog Routing

The diffusion analog method is a linear transport routine. It is similar to the lag routing except that it accounts for both flow advection (using a flow time or celerity) and attenuation (using a flow dispersion coefficient). The diffusion analog equation is in fact the linear solution of the Advection-dispersion equation (also known as the Navier-Stokes equation) for a plane rectangular source (Maidment, 1993). Mathematically, the diffusion analog equation can be expressed by using a series of equations as described below.

$$\frac{\delta Q}{\delta x} + \frac{\delta A}{\delta t} = q \qquad (1)$$

$$\frac{\delta y}{\delta x} = S_o - S_f \tag{2}$$

where Q is discharge at location x along the channel, A is channel cross-sectional area, q is the lateral inflow, and the friction slope, S_f can be parameterized using Mannings's equation

$$S_f = \frac{n^2|Q|Q}{A^2R^{1.33}} \tag{3}$$

$$S_f = \frac{|Q|Q}{A^2C^2R} \tag{4}$$

where C is the Chezy's coefficient.

For a rectangular channel the continuity and momentum equation can be written as

$$\frac{\delta Q}{\delta t} = D\ \frac{\delta^2 Q}{\delta x^2} - c\ \frac{\delta Q}{\delta x} + cq \tag{5}$$

where D is the Diffusion coefficient and is estimated as

$$D = \frac{{K_c}^2}{2QB} \tag{6}$$

where v is an advective velocity estimated as

$$v = \frac{Q}{BK_c}\frac{dK_c}{dy} \tag{7}$$

where K_c is the conveyance given as

$$K_c = Q\sqrt{S_f} \tag{8}$$

And finally the Diffusion equation is given by

$$Q(t) = I(t_0)\left(\frac{1}{2(\pi D)^{0.5}}\frac{x}{(t-t_0)^{1.5}}\right)\exp\left[-\frac{(v(t-t_0)-x)^2}{4D(t-t_0)}\right] \quad (9)$$

where *x* is the location for forecast point downstream or the length of the river reach in m.

D is the dispersion coefficient in m^2/s

V is the advection velocity or the flow celerity in m/s

x is the length of the river reach in m

t_o is the time of the input event in seconds

t is the present time in seconds

π is the numerical constant Pi and has a value of 3.14159

Q(t) is the discharge at the downstream end of the river reach

$I(t_o)$ is the inflow at the upstream end of the river reach.

4.4.3 Post Processing Modules

The post processing module in the GeoSFM includes calibration, sensitivity, flow statistics and flow status maps.

Sensitivity Analysis

Sensitivity analysis (SA) is an important step towards model calibration. Sensitivity analysis has a dual purpose of testing which sensitive parameters should be used for calibration as well as analyzing feasible parameter ranges. Sensitivity analysis allows us to see if there is a change in model results when the parameter values are changed. The SA result can be used to test the model structure, if parameters assumed to have a strong impact on model results do not show any sensitivity, the model structure should be reassessed.

Model Calibration

The purpose of calibration is to adjust the model parameters so that the model closely matches the real system. Although many GeoSFM model parameters are derived from spatially

distributed observed data, uncertainties in parameter adjustment to differences in scale, uncertainty in deriving the parameter values from observed data, and uncertainties in the structure of the model require that parameters be adjusted to overcome what we do not know, and cannot measure about the watershed. These issues apply to all hydrologic models. Built within the GeoSFM is a parameter calibration module which includes a sensitivity analysis routine and a model calibration routine. The sensitivity analysis determines which parameters are to be adjusted during the calibration process. There are twenty parameters in the model (eg. soil water holding capacity, hydraulic conductivity, soil depth, curve number, river loss coefficients, pan coefficient, etc) and the sensitivity analysis thus significantly reduces the time taken to calibrate the model. The model calibration routine is an automatic calibration process using the Multiobjective Shuffled Complex Evolution Metropolis (MOSCEM) Algorithm. It is an automatic optimization process which finds the optimum parameters to minimize the difference between the model simulated output and the observed output values. There are several objective functions available within the model for example RMSE, NSCE among others to carry out the optimization of the parameters. Manual calibration of the model can also be conducted by adjusting the parameters identified during the sensitivity analysis by trial and error process.

Flow Statistics

At the end of a simulation run, flow statistics provides a summary of the results. GeoSFM includes a tool for computing a variety of flow statistics including the maximum, minimum, mean, standard deviation, median, 25^{th}, 33^{rd}, 66^{th}, and 75^{th} percentile flows for each basin. The results of the flow statistics computations are stored in the form of tables which are linked to the basin data layer.

Flow Status Maps

Flow Percentile Map

Visual maps are considerably easier to interpret than tabular time series data particularly when dealing with large river basins. GeoSFM contains a tool for displaying the results of simulations for any given date in a visual map. The stream flow values on a user-selected date are presented in the form of indices which present the values in the context of predefined criteria. The default criterion for differentiating between low and normal flow is the 33^{rd} percentile flow for the analysis period, while the 66^{th} percentile flow is the minimum threshold separating normal flow and high flows. However, the user can define other criteria such as return period flow or

predetermined drought and flood warning levels for the classification of flows. Each basin is assigned a flow status index of 1, 2 or 3 to signify the respective low, normal and high flow conditions. A color-coded map is then produced showing the flow status of each basin for the select day.

Flow Hydrographs

GeoSFM contains a graphing tool for plotting hydrographs at the completion of a simulation run. The tool can be activated from either a program menu or the tool menu bar. The user can then visually select the basin for which a hydrograph is required by clicking on the basin in the visual interface. The program automatically matches the spatial information with the time series and produces a hydrograph. The flexibility of this tool is limited by ArcView's rather limited charting capabilities. The user is consequently encouraged to import the ASCII files resulting to flow simulations into spreadsheet programs such as Microsoft's Excel for more sophisticated time series plotting capabilities.

4.5 Model Performance Indicators used for the Study

There is no single model performance indicator that determines the strengths and weakness of a particular model. For determining the model performance it is desirable to adopt a variety of different statistics and tests and decisions be made on the basis of these tests (Weeks and Hebbert, 1980). A variety of tests, including those described by Aitken (1973), Nash and Sutcliffe (1970) were utilized in this study to evaluate the performance of the GeoSFM model. In the model performance indicators that are described below Q_o and Q_s are observed and simulated discharge, $\bar{Q}_o$ and $\bar{Q}_s$ are the mean of the observed and simulated discharge. *N* is the number of samples.

4.5.1 Correlation Coefficient

The standard correlation coefficient is one of the indicators used to describe the agreement between the observed and simulated flows. It is defined as

$$r = \frac{\sum(Q_o - \bar{Q}_o)(Q_s - \bar{Q}_s)}{\sqrt{\sum(Q_o - \bar{Q}_o)^2 \sum(Q_s - \bar{Q}_s)^2}} \qquad (10)$$

4.5.2 Nash Sutcliff Coefficient of Efficiency (NSCE)

The Nash-Sutcliffe Coefficient of Efficiency (NSCE) (Nash and Sutcliffe, 1970) is commonly used to evaluate the fit of the predicted hydrograph with observed. The perfect value is 1. It is calculated as:

$$NSCE = 1 - \left[\frac{\sum_{i=1}^{N} \left[Q_s - \overline{Q_o} \right]^2}{\sum_{i=1}^{N} \left[Q_o - \overline{Q_o} \right]^2} \right] \quad (11)$$

4.5.3 Bias

The bias is the difference between the simulated and observed discharge and is defined as

$$Bias = \frac{\sum_{i=1}^{N} (Q_s - Q_o)}{N} \quad (12)$$

4.5.4 Root Mean Square Error (RMSE)

The RMSE provides greater emphasis on larger error and is defined as

$$RMSE = \sqrt{\frac{\left(\sum_{i=1}^{N} (Q_s - Q_o)^2\right)}{N}} \quad (13)$$

4.5.5 Peak Flow Error

The accuracy of flood prediction is evaluated using the peak flow error which is expressed in percentage. The peak flow error is defined as

$$E_p = \sum_{i=1}^{n} \frac{(Q_{ps} - Q_{po})}{Q_{po}} \times 100 \quad (14)$$

where E_p is the peak flow error in %, Q_{ps} is the peak simulated discharge, Q_{po} is the peak observed discharge and n is the number of peaks above a defined threshold corresponding to the discharge of the warning water level of the river.

4.6 GeoSFM Model of the Bagmati Basin

The location and general characteristics of the catchment has been provided in chapter 3. The river system of the Bagmati is illustrated in Figure 4.3. The Bagmati basin can be divided into three climatic zones: the subtropical subhumid zone below 1000 m, the warm temperate humid zone between 1000 and 2000 m and the cool temperate humid zone between 2000 and 3000m (Jha, 2002; Dulal *et al*., 2006). The average rainfall of the basin is about 1800 mm. The upper part of the watershed is mainly cultivated with limited forest and a few other land uses. Urban areas include Kathmandu, Bhaktapur and Patan of the Kathmandu Valley, which lies within the upper part of the watershed. The middle part of the watershed is a combination of cultivation and forest, with the greater part covered with forest. The lower part of the catchment in the Terai is predominantly cultivated. Forest accounts for 58% of the total basin area, while cultivated land accounts for about 38%. The dominant soil type is loamy soil.

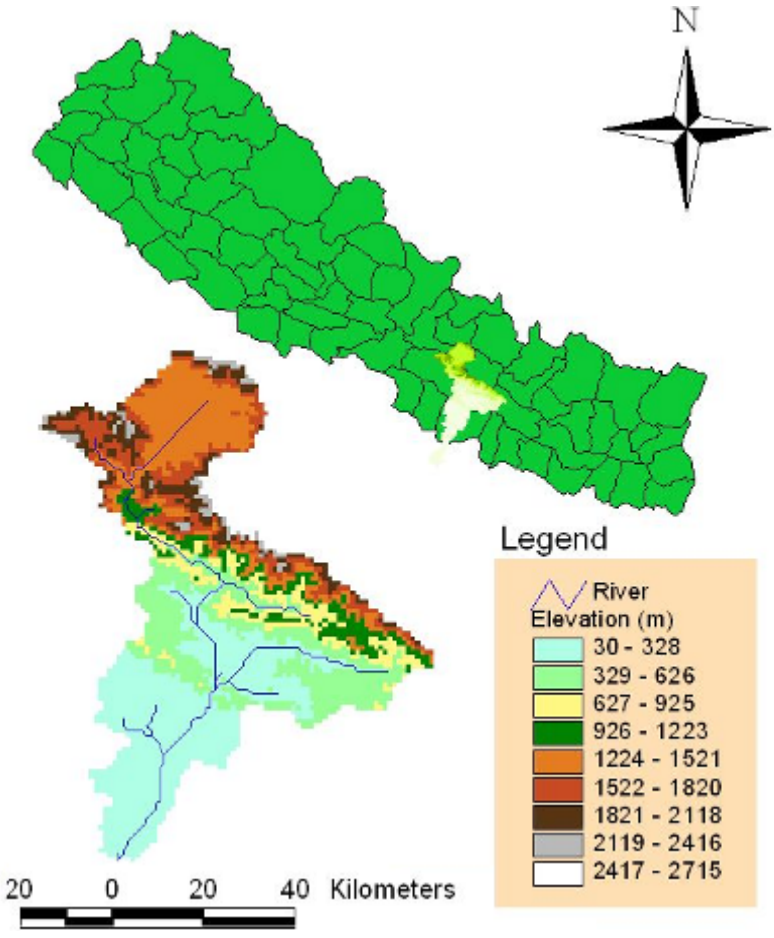

Figure 4.3 River system of the Bagmati Basin

4.6.1 Data Parameterization and Analysis

For the current study, the Bagmati Basin boundary was delineated and clipped from this global digital elevation model Hydro1k. Model-required soil parameters (i.e., soil water holding capacity, saturated soil hydraulic conductivity, hydrologically active soil layer depth, and soil texture) were extracted from the Digital Soil Map of the World (FAO, 1995). The USGS Global Land Cover Characteristics (GLCC) database derived from 1km AVHRR data projected in the Lambert Azimuthal Equal Area projection is used in the GeoSFM modelling. The rainfall station data and streamflow gauge data were provided by DHM of the Government of Nepal. The daily rainfall data covered the period 2002 through 2004 and was provided for 176 stations over Nepal including 14 stations within the Bagmati Basin. The daily discharge data of Bagmati Basin at Pandhera Dovan from 2002 to 2004 was also available for the study. The locations of the hydrological and meteorological stations in the Bagmati Basin and its vicinity are shown in Figure 4.4.

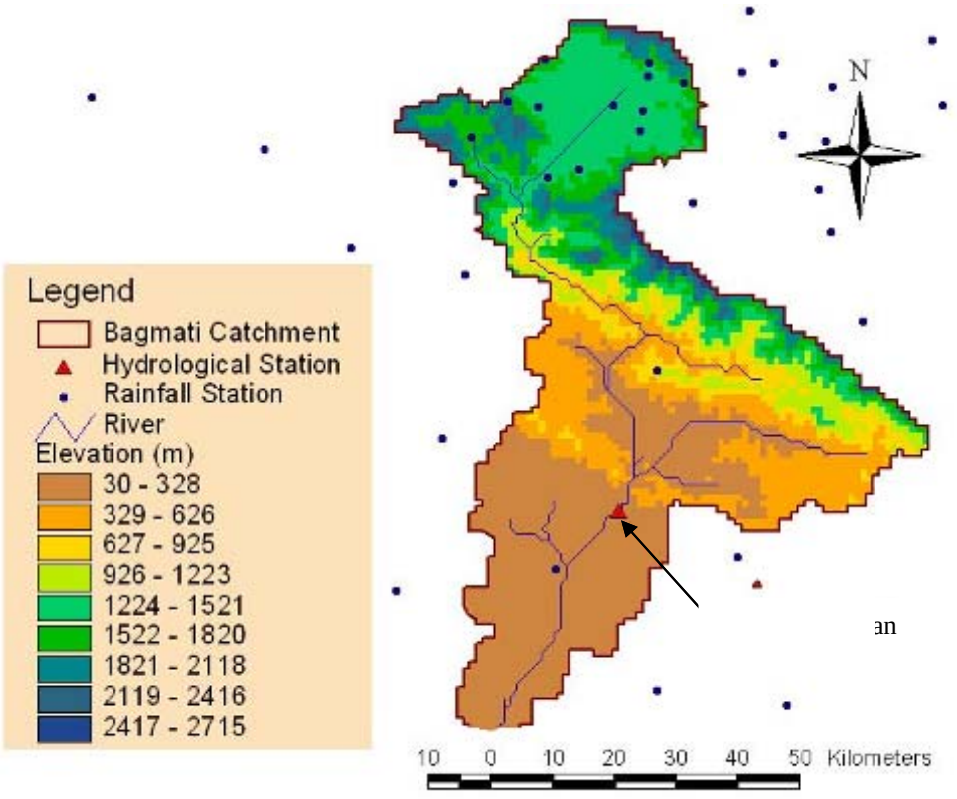

Figure 4.4 Location of rainfall and discharge gauging stations in the Bagmati Basin and its vicinity

The GeoSFM model was applied for three different cases:

1. Case 1: With the gauged observed rainfall over a peak flooding period. The run was for 38 days period, July 1 – August 7, 2002. The run was during monsoon caused peak flood period.

2. Case 2: With the RFE data over the same 38 days period

3. Case 3: With the RFE for 2002 to 2004 period.

4.6.2 Results and Discussion

Simulated streamflow with gauge observed rainfall of July 2002

The simulated hydrograph over the 38-day period in 2002 (July 1 to August 7) using the gauge observed rainfall compares well with the observed flows (Figure 4.5). The magnitude of the daily simulated flow and timing matched well the observed flow magnitude and timing during the high flow period (Figure 4.5). The high NSCE (0.91) and correlation (0.95) indicate a good fit between observed and simulated flows. The scatter plot of the simulated and observed flows is presented in Figure 4.6. Our findings of good correlation and performance of the model with gauged observed rainfall data is consistent with the findings of previous studies (Hapuarachchi *et al*., 2007; Kafle *et al.*, 2006; Sharma *et al*., 2007; Artan *et al*., 2007b). The excellent match at the peaks between simulated and observed flows indicates that the model can be used effectively for flood forecasting.

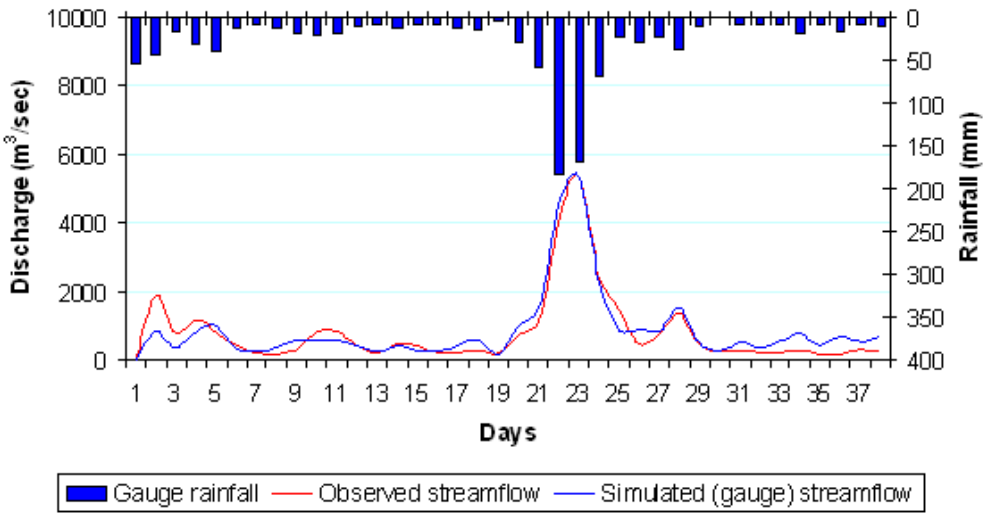

Figure 4.5 Observed and simulated daily flows at Panheradovan, the daily flows were simulated using gauge observed rainfall data (July 1 – August 7, 2002)

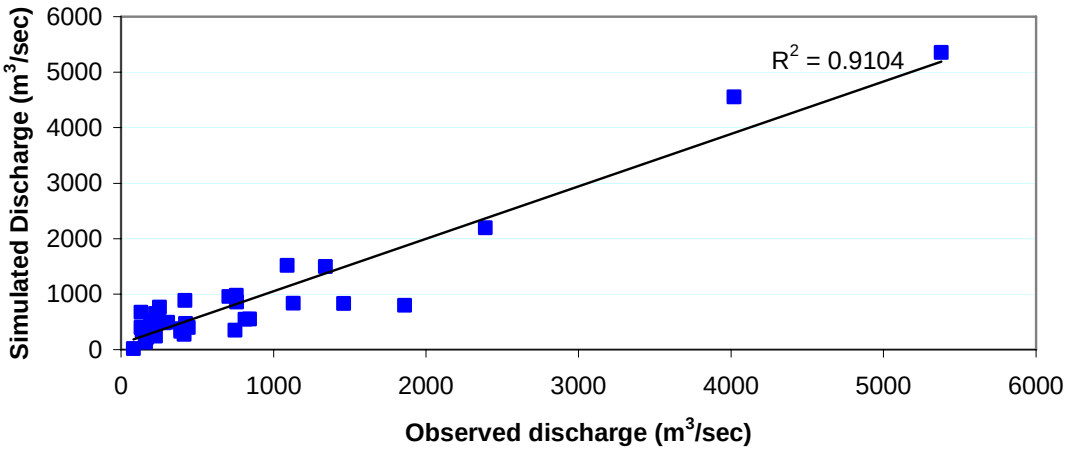

Figure 4.6 Scatter Plot of daily Observed and Simulated Discharge (July 1 – August 7, 2002)

Results of Model with the RFE Rainfall of July 2002

For the same period from July 1 to August 7, 2002 without readjusting the GeoSFM parameters the model was driven with the RFE data. The comparison of observed and simulated flows is presented in Figure 4.7. We find that with the RFE data the GeoSFM underestimates the peak flow compared with observed gauge rainfall. We can also observe that there is a shift in the timing and the sharpness of the peak. The NSCE of 0.15 and correlation of 0.50 were achieved. The scatter plot of the simulated and observed flows is presented in Figure 4.8. Hapuarachchi *et al.* (2007) explored the applicability of satellite-based precipitation data for near real-time flood forecasting considering satellite based products from CMORPH, TRMM 3B42RT and GSMaP. A grid based distributed hydrological model (BTOP) was used to generate river flow of Yoshino basin in Japan. With gauged precipitation the NSCE was 0.84 while with CMORPH, 3B42RT and GSMaP were 0.06, 0.52 and -0.06 respectively. The findings of the current study are consistent with Hapuarachchi (2007) with the gauged precipitation performing well compared to the RFE. Artan *et al*. (2007b) found poor agreement between the observed and RFE simulated flows for the Se Done basin, a tributary of the Mekong River in Laos when the model was calibrated with rain gauge measured rainfall data. Similarly when applied to the Nyando basin in Kenya, tributary to Lake Victoria, the model with the RFE data considerably loses predictive skills in contrasts to if gauged observed rainfall are used. The Se Done and Nyando are midsize basins (6000 and 2600 km^2) as the Bagmati Basin. The poor results for simulated flows with

RFE suggest that the RFE is not a suitable rainfall data for input to hydrologic models for basin with the size of the Bagmati Basin.

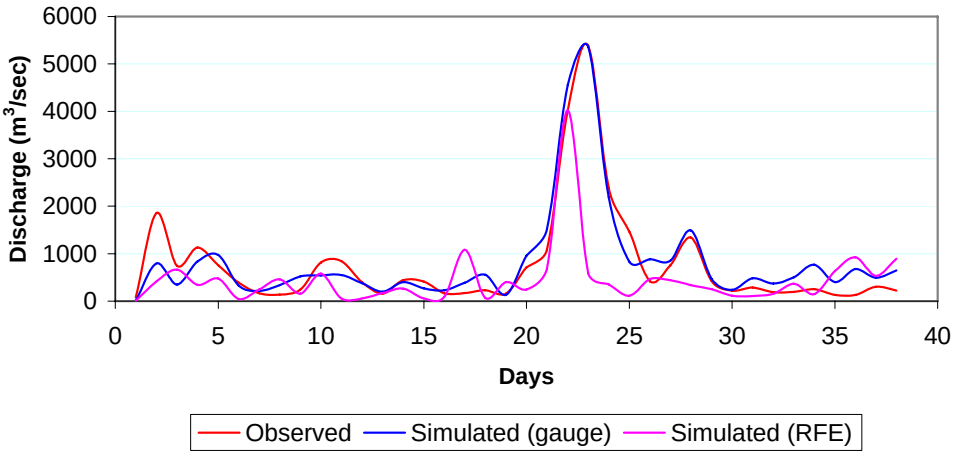

Figure 4.7 Comparison of observed and simulated daily flows at Pandheradovan using gauge observed rainfall and RFE data as an input rainfall (July 1 – August 7, 2002)

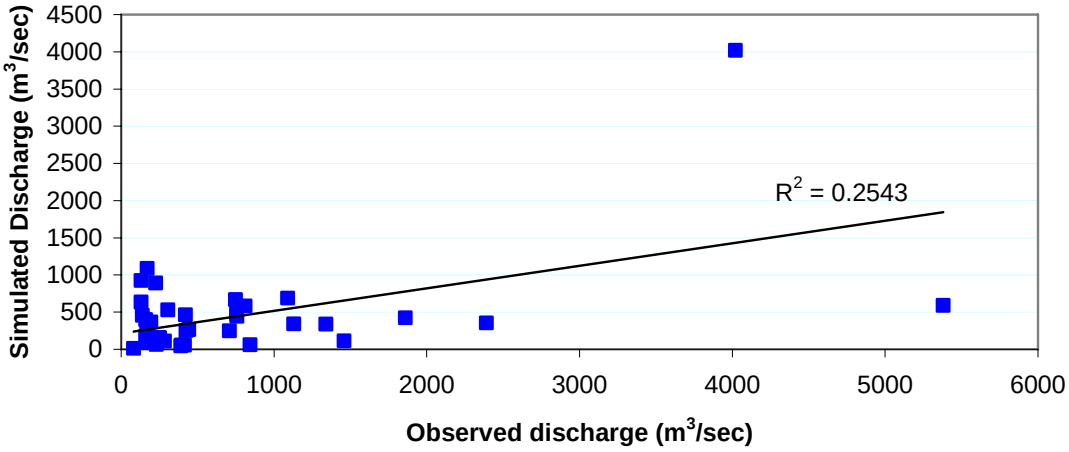

Figure 4.8 Scatter plot of observed and simulated discharge when the GeoSFM was driven with RFE (July 1 – August 7, 2002)

Streamflow Simulation using RFE for 2002, 2003 and 2004

As poor agreement was found between the gauge observed and RFE simulated flows for Bagmati Basin when the model was calibrated with rain gauge measured rainfall data further analysis was done to recalibrate the GeoSFM with RFE. As three years of daily discharge data was available the period 2002 to 2003 was taken as the calibration period and 2004 for validation. Parameters were adjusted to provide the best simulated results using the RFE. The calibration was considered to be complete when no further improvement or very little change

was observed in the predicted flows even when varying the parameters. This involved successive changes in the parameter values identified as sensitive during the sensitivity analysis until the best fit was obtained. Comparison of observed and simulated hydrographs from the model is summarized in Figure 4.9. The year 2002 and 2003 the agreement between the observed and simulated flows was marginal. The NSCE was 0.23 with a correlation of 0.59.

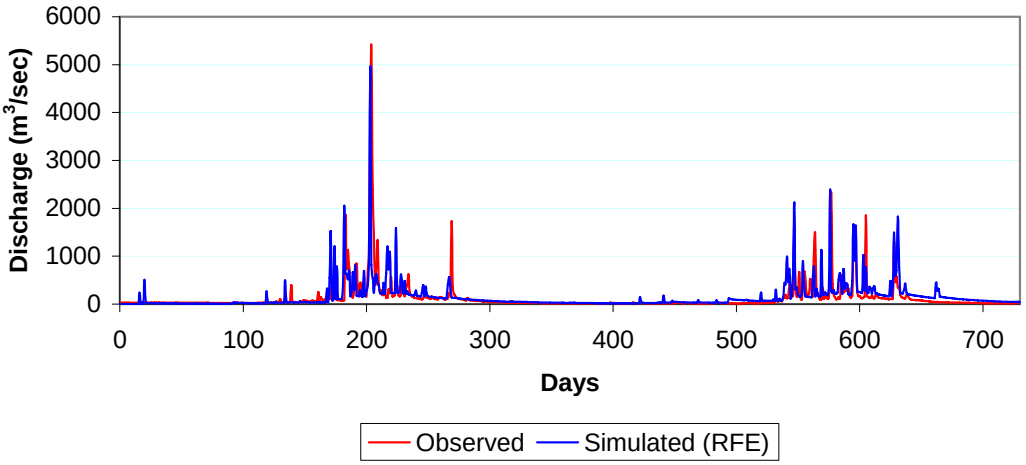

Figure 4.9 Observed and simulated streamflows using RFE from 2002 to 2004 (calibration)

Using the same parameters from the calibration period the GeoSFM was run for 2004 using 2004 RFE. The predicted peak flows in 2004 were extremely low compared to the observed flows as presented in Figure 4.10. The performance of the validation period was not satisfactory. When the model is driven with an RFE it under predicted considerably the flows. When the model was calibrated with the RFE soil water holding capacity (SWHC) value becomes significantly lower than the at prior estimated values at around 100 mm per 1 meter of soil. Figure 4.11 shows a box plots of the SWHC that were estimated when the two rainfall data were use. Where the SWHC estimated from the calibration of the gage data is reasonable of what could be expected for the dominant soil types present in the basin (silty clay loam and clay loam soil types).

The poor performance of the results could be due to a number of reasons. Firstly, the calibration period i.e. 2002 to 2003 may not have been appropriate or long enough. Secondly, the

quality of data/RFE is questionable at best. Thirdly, the 2004 RFE must be significantly underestimating rainfall resulting in an amplification of error into a large flow underestimation.

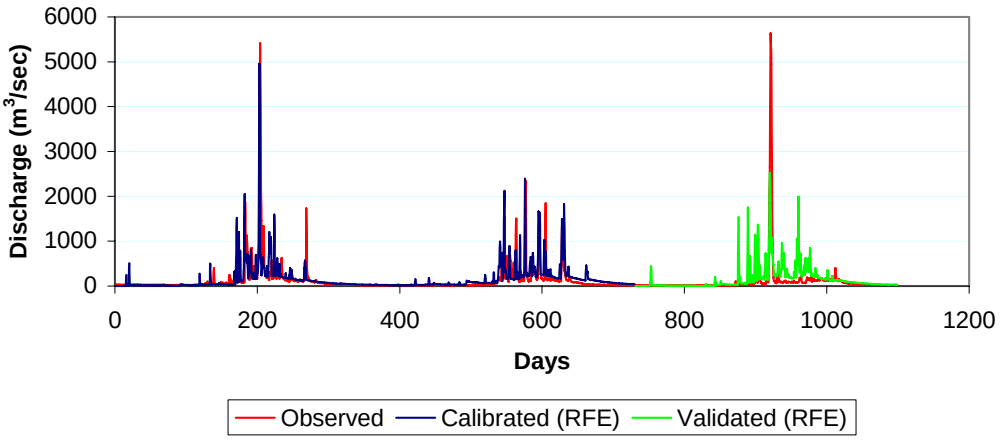

Figure 4.10 Observed and simulated flows for 2002-2005

In a study conducted by Hughes *et al*. (2006) the results of the validation period using the satellite rainfall data were poorer compared to the calibration period in the Okavango river. The current results also indicate similar findings.

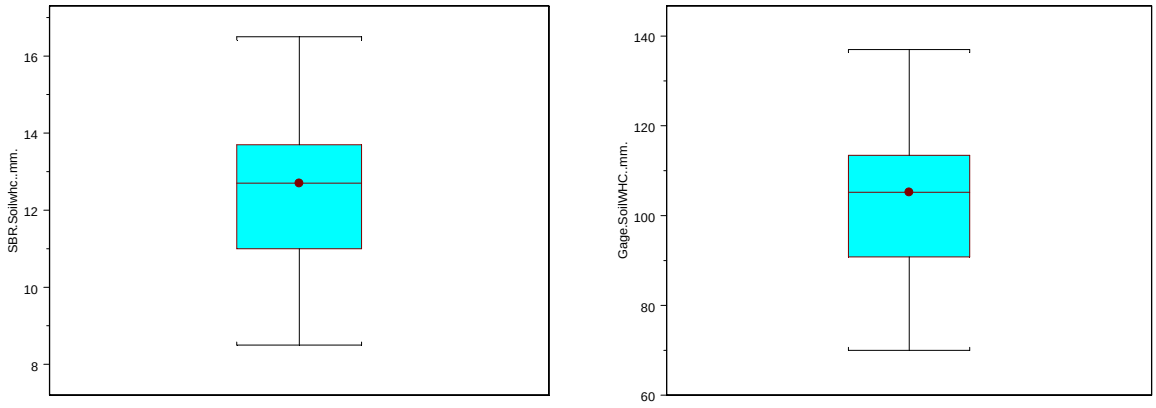

Figure 4.11 Average soil water holding capacity of the 21 sub-basins modelling units when the GeoSFM (a) is calibrated with satellite-based rainfall fields, and (b) when the model is calibrated with rain

In the past several studies have been done to assess the runoff of the Bagmati Basin using various rainfall-runoff models and satellite data. Kafle (2007) used the HEC-HMS hydrologic model with TRMM and rain gauge data to simulate flows of the Bagmati. Sharma *et al*. (2007) has made comparison with TRMM 3B42RT data and rain gauge data and applied the results to predict floods in the Bagmati Basin. He observed that the TRMM data has underestimated the

monsoon rainfall peaks. The findings of these studies in the past are in agreement with the current findings where with the rain gauge data the model predicted the peak discharge fairly accurately while the satellite data underestimated the discharge significantly as was observed from the one month simulation in 2002. This indicates that the accuracy of the RFE has to be improved further to realistically predict the floods of the basin and become useable product for an operational flood forecasting system for the Bagmati River.

4.7 GeoSFM Model of the Narayani Basin

The location and general physiographic description of the Narayani Basin has been presented in the previous chapter. The location of the rainfall stations in and within the vicinity of the Narayani Basin is shown in Figure 4.12.

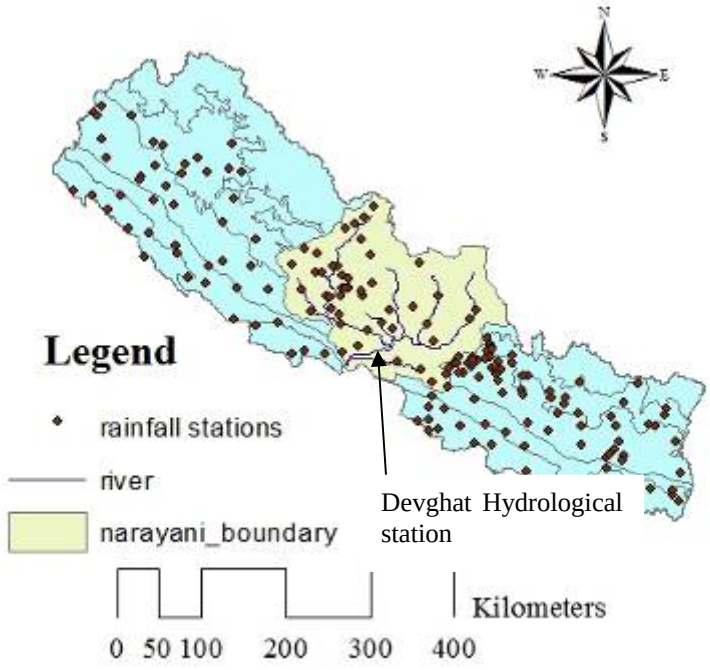

Figure 4.12. Location of the rainfall stations within and in the vicinity of the Narayani Basin

4.7.1 Data Parameterization and Analysis

The Narayani Basin boundary was delineated and clipped from this global digital elevation model Hydro1k. Similar to the Bagmati Basin the model-required soil parameters (i.e., soil water

holding capacity, saturated soil hydraulic conductivity, hydrologically active soil layer depth, and soil texture) were extracted from the Digital Soil Map of the World (FAO, 1995). The USGS Global Land Cover Characteristics (GLCC) database derived from 1km AVHRR data projected in the Lambert Azimuthal Equal Area projection is used in the GeoSFM modelling. The rainfall station data and streamflow gauge data were provided by DHM of the Government of Nepal. The daily rainfall data covered the period 2002 through 2006 and was provided for 176 stations over Nepal including 45 stations within the Narayani Basin. The daily discharge data of Narayani River at Devghat from 2002 to 2006 was also made available by DHM for the study. The locations of the hydrological and meteorological stations in the Narayani Basin and its vicinity are shown in Figure 4.12.

This focus of this study is the four months of the monsoon June, July, August, and September when floods occur in the basin. The gridded gauge observed rainfall data for the monsoons of 2003 and 2004 were used in the GeoSFM to predict floods. Daily observed river discharge data from the 2003 monsoon were used for GeoSFM model calibration and data from 2004 for validation. The reliability of the RFE rainfall estimates for flood prediction was evaluated using the 2003 monsoon data.

4.7.2 Results and Discussion

Calibration and validation of the GeoSFM with gauge observed rainfall

The calibration of the GeoSFM for the Narayani Basin was performed using daily gauge observed rainfall data from June to September 2003. A high NSCE (0.84) and a highly significant correlation (0.94) indicate a relatively robust calibration with a good fit between observed and simulated discharge. The RMSE was 754.3 with an average discharge error of -3 % over a threshold of 7500 m^3/sec. The threshold discharge of 7500 m^3/sec corresponds to the warning level of 6.8 m at the Devghat hydrological station. The average peak discharge error was -7.6% for the three peaks. Overall, the magnitude and timing of the simulated peak discharge matched well with the observed. Figure 4.13 presents the comparison and scatter plot of the simulated and observed discharge. In the Bagmati Basin about ten times smaller than the Narayani Basin a similar high NSCE of 0.91 and r of 0.95 were obtained (Shrestha *et al*., 2008). The GeoSFM therefore predicts the flows accurately when gauge observed data are applied and calibrated in small and large basins indicating reliable application to flood forecasting with improved quality of rainfall estimates.

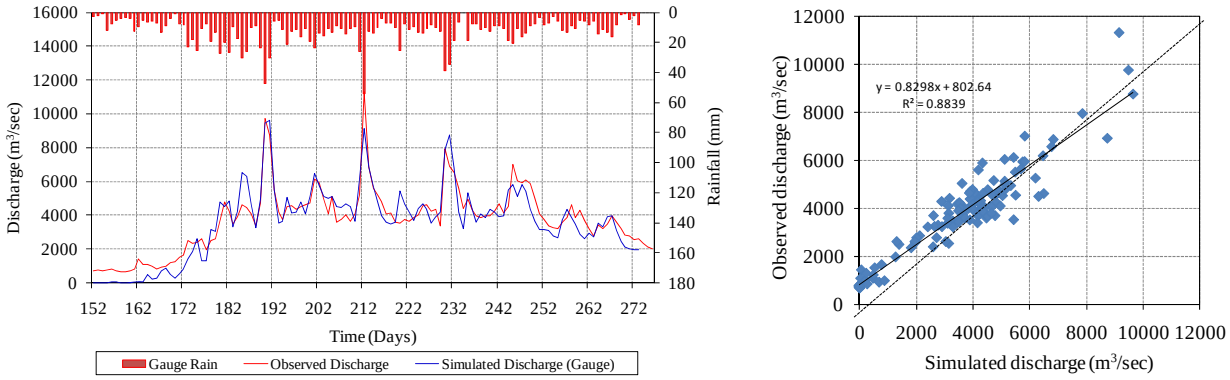

Figure 4.13 Comparison and scatter plot of observed and simulated discharge at Devghat using 2003 monsoon gauge observed rainfall (June to September)

The validation of the GeoSFM was performed using rainfall data from June to September of 2004. An NSCE of 0.77, RMSE of 697.1 and a highly significant correlation coefficient of 0.94 were achieved. The peak flow error was about -3%. All flood peaks during this year was lower than the threshold discharge corresponding to the warning level so no discharge error above the threshold was computed. Figure 4.14 presents the comparison of simulated and observed hydrographs and scatter plot indicating a fairly good fit.

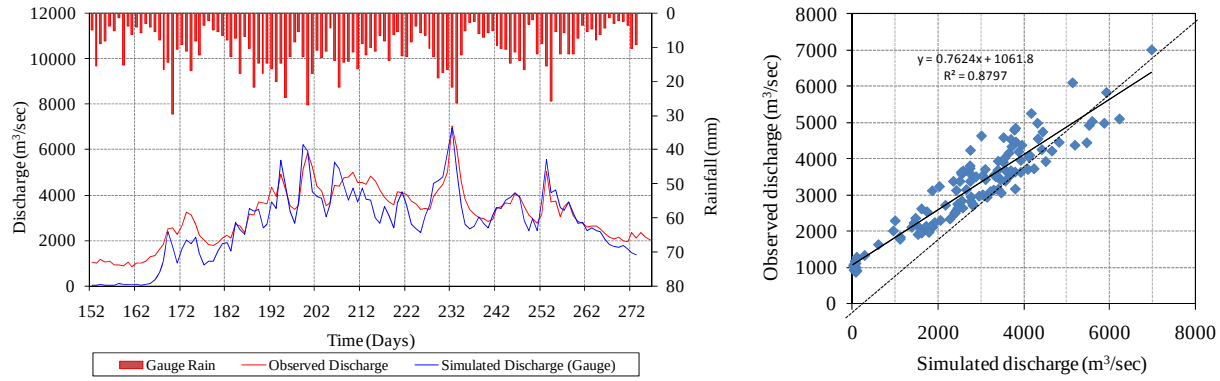

Figure 4.14 Comparison and scatter plot of daily observed and simulated discharge at Devghat using 2004 monsoon gauge observed rainfall (June to September)

Flood Prediction using CPC_RFE2.0 (RFE) rainfall estimates

A simulation run of the GeoSFM model forced with the RFE for the period June to September 2003 was obtained. The model parameters obtained from the calibration of the GeoSFM with the gauge observed rainfall data were not readjusted. The hydrograph simulated with the RFE

considerably underestimated the peak flows when compared with the hydrograph simulated with gauge observed rainfall (Figure 4.15). Also, the fact that RFE simulated streamflow missed some of the peaks, points to the presence of random errors in the RFE data. A low NSCE of -1.17, a high RMSE of 2805 and correlation coefficient of 0.69 were achieved indicating a significant underestimation of flow but still with a relatively significant correlation. The average peak discharge error using RFE was -53%. The average error above the threshold discharge corresponding to the warning level was -61%. Figure 6 shows the scatter plot of the simulated and observed flows (R^2 = 0.47) with significant underestimation of flows. In the Bagmati Basin (which is about ten times smaller than the Narayani), RFE simulated hydrographs showed an underestimation of flows with a NSCE of 0.15 and a correlation of 0.50 (Shrestha *et al.*, 2008). The increased correlation obtained in the Narayani Basin simulation suggests better performance of GeoSFM in larger basins. But, the reduced NSCE, increased RMSE and peak discharge error compared to the Bagmati indicates deterioration in flood prediction using the RFE rainfall estimates in the Narayani Basin where the terrain is complex with a large proportion of basin area in the high mountains with greater influence of orography.

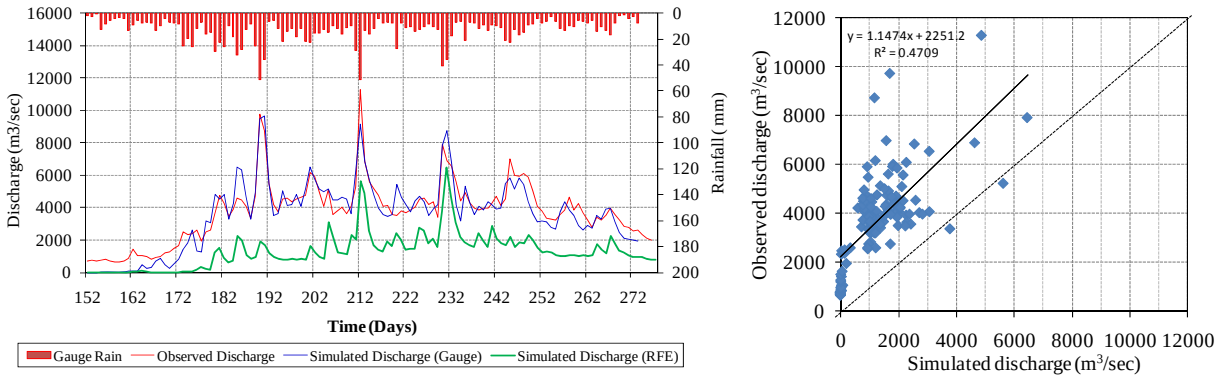

Figure 4.15 Comparison and scatter plot of daily observed and simulated discharge at Devghat using gauge observed rainfall and RFE data as input rainfall (June to September 2003)

Therefore, the poor skills of the GeoSFM hydrological model to predict the magnitude of the floods when using the RFE, compared to when using gauge observed rainfall, suggest that the increased uncertainty of flood prediction is a result of inaccurate satellite-based rainfall inputs rather than the modelling of the hydrological processes, thus, making imperative the de-biasing or improvement of the SRE prior to use in predicting floods.

Flood Prediction using CPC_RFE2.0 (RFE) rainfall estimates calibrated model

A simulation run of the GeoSFM model forced with the RFE rainfall estimates for the period June to September 2003 was obtained. In this simulation the model was calibrated using the RFE estimates instead of using the parameters obtained from the calibration of the GeoSFM with the gauge observed rainfall data. By recalibrating the model with RFE a slight improvement in the performance of the model is seen though the hydrograph simulated with the recalibration still underestimates the peak flows when compared with the hydrograph simulated with gauge observed rainfall (Figure 4.16). The NSCE increases from -1.17 to -0.36 and correlation coefficient from 0.69 to 0.76 while the RMSE decreases from 2805 to 2174. The average error above the threshold discharge corresponding to the warning level was decreases to -41% from -61%. Figure 4.16 shows the scatter plot of the simulated and observed flows (R^2 = 0.58) with significant underestimation of flows. The improvement in the results indicates that the model has to be recalibrated with the RFE rainfall estimates for discharge prediction with RFE. However, even with improvement the RMSE and peak flow error are large with the recalibrated model suggesting that the RFE has to be bias-corrected before further use in discharge prediction.

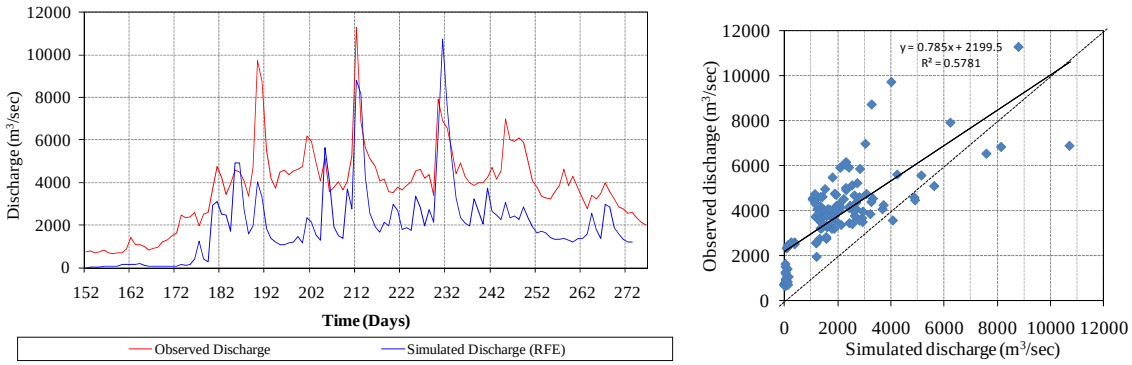

Figure 4.16 Hydrograph and scatter plot of daily observed and simulated discharge at Devghat with RFE calibrated model from June to September 2003

4.8 Summary

The GeoSFM, a semi-distributed physically based hydrological model developed by the USGS was used to simulate the discharge using remotely sensed and widely available global datasets for the Bagmati and Narayani Basins in Nepal. Bagmati has a catchment area of 2800 km^2 at the Padheradovan gauging station while the Narayani is about 32,000 km^2 at Devgaht gauging station. The interpolated gauge observed rainfall data and SRE from NOAA at 0.1 x 0.1 degree

spatial resolution on a daily basis were used to simulate the flows. The GeoSFM model was calibrated using the gauge observed monsoon data from June to September 2003 for the Narayani Basin and for from 1st July to 7th August 2002 for the Bagmati Basin. Satisfactory validation of the model was obtained using the gauge observed monsoon data. The same parameters obtained during the calibration were used for the validation of the model which showed good agreement with the observed. Thus we can infer that GeoSFM predicts the flows accurately when observed rain gauge data have been applied and calibrated indicating reliable application to flood forecasting with improved quality of rainfall estimates.

Discharge was then simulated with RFE using the calibrated parameters from the 2002 and 2003 monsoon data for Bagmati and Narayani respectively, which showed underestimation of flood prediction. The hydrograph simulated with the RFE considerably underestimated the peak flow when compared with the hydrograph simulated with gauge observed rainfall. The accuracy in RFE estimates was assessed by comparing the gauge observed and estimated rainfall in those grids with one or more stations. The RFE captures the rainfall spatial trends well, but underestimates the amount on average by more than 50 per cent.

As the magnitude of the rainfall is much lower in the RFE compared to the gauged observed rainfall there is underestimation of simulated flows when the RFE dataset is used to force the hydrologic model. The underestimation of simulated flows when using the RFE data is an agreement with results from previous research on the matter. It is thus difficult to predict the floods quantitatively using current satellite based data. We can only give an indication of probability of occurrence. This suggests that remotely sensed rainfall estimates needed to be adjusted prior to use for flood prediction.

References

Aitken, A.P. (1973) Assessing Systematic Errors in Rainfall-Runoff Models. *J. Hydrol*., Vol. 20. 121-136.

Artan, G.A.; Asante, K.O.; Smith, J.L.; Pervez, S.; Entenmann, D.; Verdin, J.P.; Rowland, J. (2007b) *Users manual for the Geospatial Stream Flow Model (GeoSFM).* US Geological Survey Open-File Report 2007-1440, p.194. Reston, Virginia.

Artan, G.A.; Gadain, H.; Smith, J.L.; Asante, K.; Bandaragoda, C.J.; Verdin, J.P. (2007a) Adequacy of satellite derived rainfall data for streamflow modelling. *Nat. Hazards*, 43, 167-185.

Asante, K.O.; Artan, G.A.; Pervez, S.; Bandaragoda, C.; Verdin, J.P. (2007b) *Technical manual for the Geospatial Stream Flow Model (GeoSFM)*. US Geological Survey Open-File Report 2007–1441, p. 99. Reston, Virginia.

Asante, K.O.; Macauacua, R.D.; Artan, G.A.; Lietzow, R.W.; Verdin, J.W. (2007a) Developing a flood monitoring system from remotely sensed data for the Limpopo Basin. IEEE Trans. *Geosci. Remote Sens*. 45(6), 1709–1714.

Bhusal, J.N.; Bhattarai, K.P. (2002) Lessons from the extreme floods in south central Nepal in 1993. *International Basin of Network Organization's (INBO) General Assembly*, Quebec City.

Chalise, S.R., Shrestha, M.L., Thapa, K.B., Shrestha, K.B., Bajracharya, B. (1996) *Climatic and hydrological Atlas of Nepal*. Kathmandu: ICIMOD

Drayton, R.S.; Wilde, B.M.; Harris, J.H.K. (1992) Geographical information system approach to distributed modelling, in: Beven, K.J., Moore, I.D. (Eds.), *Terrain analysis and distributed modelling in hydrology*, John Wiley and Sons, pp. 253-368, West Sussex.

Harris, A.; Hossain, F. 2008. Investigating the optimal configuration of conceptual hydrologic models for satellite-rainfall-based flood prediction. *IEEE Geosci. Remote Sensing*, 5(3), 532-536.

Harris, A.; Rahman, S.; Hossain, F.; Yarborough, L.; Bagtzoglou, A.C.; Easson, G. (2007) Satellite-based flood modelling using TRMM-based rainfall products. *Sensors*, 7, 3416–3427.

Hong, Y.; Adler, R.F.; Negri, A.; Huffman, G.J. (2007) Flood and landslide applications of near real-time satellite rainfall estimation. *Nat. Hazards*, 43, 285–294.

Hughes, D.A. (2006) Comparison of satellite rainfall data with observations from gauging station networks. *J. Hydrol.*, 327, 399–410.

Maidment, D.R. (1993) Handbook of Hydrology. McGraw Hill, New York, San Francisco.

Moore, R.J.; Bell, V.A. (2001) Comparison of rainfall-runoff models for flood forecasting. Part 1: Literature review of models. Bristol, UK, Environment Agency, 94pp. (R&D Technical Report W241, CEH Project Number: C00260)

Nash, J.E.; Sutcliffe J.V. (1970) River flow forecasting through conceptual models: Part 1-A discussion on Principles. *J. Hydrol.*, 10, 282–290.

Nash, J.E.; Sutcliffe J.V. (1970) River flow forecasting through conceptual models: Part 1-A discussion on Principles. *J. Hydrol.*, 10, 282–290.

Sharma, C.K. (1977) *River systems of Nepal*. Sangeeta Sharma, p. 214. Kathmandu.

Shrestha, M.S., Takara, K., Kubota, T., Bajracharya, S. (2011) Verification of GSMaP rainfall estimates over the Central Himalayas. *Annual Journal of Hydraulic Engineering*, JSCE, Vol. 55 (to be published).

Shrestha, M.S.; Artan, G.A.; Bajracharya, S.R.; Sharma, R.R. (2008) Applying satellite based rainfall estimates for streamflow modelling in the Bagmati Basin, Nepal. *J. Flood Risk Management*, 1, 89–99.

Shrestha, M.S.; Bajracharya, S.R.; Mool. P. (2008) Satellite rainfall estimation in the Hindu Kush-Himalayan region. Kathmandu: ICIMOD

Weeks, W.D.; Hebbert, R.H.B. (1980) A comparison of Rainfall-Runoff Models. *Nordic Hydrology*., 11. pp 7-24.

Wilk, J.; Kniveton, D.; Andersson, L.; Layberry, R.; Todd, M.S.; Hughes, D.; Ringrose, S.; Vanderpost, C. (2006) Estimating rainfall and water balance over the Okavango River Basin for hydrological applications. *J. Hydrol.*, 331, 18–29.

Wilks, D.S. (2006) *Statistical methods in the atmospheric sciences*, 2nd ed. Elsevier Academic Press, Burlington. MA. p. 627.

Wilmott, C.J. (1982) Some comments on the evaluation of model performance. *Bull. Amer. Meteorol. Soc.*, 88, 1309–1313.

Wilmott, C.J.; Ackleson, S.G.; Davis, R.E.; Feddema, J.J.; Klink, K.M.; Legates. D.R.; O'Donnell, J.; Rowe, C.M. (1985) Statistics for the evaluation and comparison of models. *J. Geophys. Res.,* 90 (C5), 8995–9005.

Xie, P.; Arkin, P.A. (1996) Analyses of global monthly precipitation using gauge observations, satellite estimates and numerical model predictions. *J. Clim.*, 9, 840–858.

Xie, P.; Yarosh, Y.; Love, T.; Janowiak, J.; Arkin, P.A. (2002) A real-time daily precipitation analysis over South Asia. *Preprints, 16th Conf. of Hydro.*, Orlando, FL, Amer. Meteorol. Soc.

Yilmaz, K.K.; Hogue, T.S.; Hsu, K.; Sorooshian, S.; Gupta, H.V.; Wagner, T. (2005) Intercomparison of rain gauge, radar, and satellite-based precipitation estimates with emphasis on hydrologic forecasting. *J. Hydrometeorol.*, 6, 497–517.

CHAPTER 5

5 BIAS-ADJUSTMENT OF SATELLITE-BASED RAINFALL ESTIMATES

5.1 Introduction

From the previous chapter we have seen the discharge prediction in two river basins of Nepal using the satellite-based rainfall estimates (SRE). The SREs are found to detect the occurrence of rainfall and have a significantly good correlation with the gauge observed rainfall but failing to adequately capture rainfall amounts. There is significant underestimation of rainfall leading to lower predicted discharge suggesting the need for bias correction of SREs before it can be put into operational use (Shrestha *et al*., 2008). The need for bias-adjustment of the global SREs for application into water resources management and flood prediction have also been felt by Hughes (2006), Harris *et al*. (2007).

The NOAA CPCP_RFE2.0 (RFE) rainfall estimates used in the present study is a satellite-gauge merged rainfall estimate (Xie *et al*., 1996) available on a semi real time basis. Apart from the RFE currently there are no other global satellite-based rainfall products with bias-corrected rainfall estimates on a near real time basis. As explained in chapter 2 the TRMM 3B42_V6 is a research product the rainfall estimates of which are adjusted by gauge data but not in near real time. The TMPA was upgraded in early 2009 to include a climatological calibration to the post-real-time research TMPA product but was still on testing phase.

The RFE algorithm uses available rain gauge information from the WMO GTS network to remove bias from each satellite estimate component; hence the number of gauges used in each daily product is very much related to the accuracy of the final product. Currently, the WMO network of GTS gauges is relatively sparse for many of the HKH countries, thus essentially forcing the RFE algorithm to rely primarily on satellite estimates in these locations. For example, from Nepal only a few stations contribute to the GTS while none contribute from Bhutan. In mountainous areas, there is both a lack of gauge information and a tendency for satellite rainfall sensors to perform poorly, thus complicating the situation. Availability of larger number of gauge observation at a local level provides an opportunity to merge these estimates at a local level for improving the SREs.

The research problem we address in this chapter is how can SREs be adjusted for better flood prediction? Two approaches have been proposed to adjust the SREs. The first approach is a ratio based bias-adjustment using various temporal scales of adjustment; monthly, seasonal and 7-day moving average. The second approach is local tuning of SREs by ingesting the local rain gauge data into the RFE algorithm. These two approaches have been used in correcting the SREs and applied in hydrological modelling of the Narayani Basin in Nepal for the monsoon of 2003, yielding encouraging results at a daily time scale. This chapter describes the bias correction methods available in the literature, provides the procedure for bias correction developed for this study and evaluates the procedure for flood prediction.

5.2 Bias-Adjustment

As has been stressed earlier the availability of rainfall data for hydrological modeling is limited because of the sparse density of rain gauge data in various regions of the world particularly in developing countries. Satellite based rainfall estimates which provide continuous spatial variation of precipitation is one of the inputs that can drive a hydrological model however; the accuracy of the estimates so far needs to be improved. The methods available for bias correction of SREs are very few in the literature hence the methods in correcting the Regional Climate Models (RCM) were reviewed as the methods are thought to be relevant for RFE. Regional Climate Models are an important source of climate input for hydrological models. The RCM data are used in hydrological model to address the impact of climate change on the hydrological response of river basins. Though the scale of application is different from the current research the bias-adjustment of the RCM has been reviewed having precipitation as the common meteorological parameter to examine the impacts on the hydrological regime. Similar to the problem of SREs in application into hydrological modeling, the RCM data is also faced with inherent source of uncertainty coming from RCM's inability to simulate present-day climate conditions accurately. There are a number of studies that have applied bias correction to rainfall estimates derived from Global Climate Models (GCM) (Terink *et al*., 2010; Hay *et al*., 2002; Leander and Buishand, 2007; Piani *et al*., 2010). This section describes the methods for correcting rainfall using gauge observed data.

5.2.1 Gamma Transform for Bias-Adjustment

Hay *et al*. (2002) examined the use of RCM outputs for hydrologic modeling. The runoff using RCM outputs were found to have large bias compared to the observed hydrograph. Bias corrections were made on a monthly basis using a gamma transform. The Gamma transform preserves the precipitation distribution in the observed and model values. This method requires both the time series datasets of observed and model to be fit into a gamma distribution and compute the cumulative probability in the distribution. The basic assumption is that both the simulated and observed values can be approximated by using the same probability function. The probability distribution function (PDF) of the satellite-based product is adjusted to the PDF of the observed values, minimizing bias. It is assumed that the non-exceedance probability of the observed and simulated is the same. As the bias correction is a magnitude correction of the precipitation value Hay *et al*. (2002) found that the corrected precipitation did not contain the day to day variability which was present in the observed data set. Piani *et al*. (2010) applied the gamma transform method also known as the statistical bias correction to the daily precipitation in regional climate models over Europe and obtained improvement in the model results. The Gamma distribution with two parameters that is commonly used for rainfall analysis is given by equation 1.

$$f\ (x) = \frac{\beta^{-\alpha}\, x^{\alpha-1}}{G(\alpha)} \exp\left\{\frac{-x}{\beta}\right\}, \alpha > 0, \beta > 0, x > 0 \qquad (1)$$

where α and β are shape and scaling parameters and *x* is the precipitation field.

For the current study this method was not adopted as only five years of overlap data between the RFE and gauge observation was available which is not adequate to fit a gamma distribution for obtaining bias corrections.

5.2.2 Power Transform for Bias-Adjustment

Leander and Buishand (2007) used a power transformation, which converts CV as well as the mean of the rainfall estimates. This method of bias correction has been applied by Tirren *et al.*

(2010) in bias correcting RCM in the Rhine Basin. This is a non-linear correction of daily precipitation and is given by equation 2.

$$P^{*} = \mathrm{a}\ P^{b} \qquad (2)$$

where *P* is the precipitation amount and *a* and *b* are coefficients.

Parameters a and b were determined for every five day period of the year. As a first step parameter b was determined keeping the coefficient of variation (*cv*) of the corrected precipitation matching the *cv* of the observed precipitation.

$$CV\ (P) = f(b) \tag{3}$$

$$P^* = P^b \tag{4}$$

The parameter a is determined such that the mean of the transformed daily values correspond to the observed values.

Applying this technique to the Rhine River Terink *et al*. (2010) found that the bias-adjusted precipitation improved however, the RMSE of the daily precipitation differences between RMC output and observed precipitation was not smaller for the corrected precipitation values. This method was not adopted given the limitation of the number of years of data overlap available for such a correction to be meaningful.

5.2.3 Ratio Based Bias-Adjustment

Ines and Hansen (2006) applied a simple concept of bias-adjustment by applying a multiplicative shift to correct the bias of the mean monthly GCM rainfall. The concept is similar to the one proposed in this research where a correction factor for various time periods is derived by comparing the daily SREs with the gauge observed values. Though this procedure is said to adjust only rainfall intensity to reproduce the long-term mean observed monthly rainfall, it is seen to be adequate for flood prediction for capturing the peak discharges. The section below describes the three ratio based bias-adjustments derived for this research.

As the RFE are available for the South Asia domain from 2002 and the gauge observed rainfall data till 2006 there is an overlap of five years between the two data sets. Ideally for obtaining bias correction a longer data series is required preferably more than 10 years. However, with the five years of data from 2002 to 2006; the seasonal and monthly bias-adjustments were derived comparing the RFE and gridded gauge observed rainfall data at grids with one or more gauges. The bias-adjustment was derived using a two step procedure. Firstly, the daily datasets were accumulated to monthly totals to obtain the ratio of the gridded gauge observed rainfall to the RFE estimates at each grid with one or more rainfall stations. Then the monthly values of ratio were averaged over all grids with one or more station. Similarly for a

seasonal value the accumulated period was for JJAS instead of each month. The bias-adjustment "Z" is given by equation 5.

$$Z = \frac{1}{m}\sum_{i=1}^{m}\left[\frac{1}{n}\sum_{i=1}^{n}\frac{O_i}{P_i}\right] \quad (5)$$

where n is the number of grids with one or more rain gauges, O_i is the gauge observed rainfall, P_i is the satellite-based rainfall and m is the number of years.

The bias corrections were derived on a seasonal, monthly and a 7 day moving average basis. The method of bias-adjustment is schematically shown in Figure 5.1.

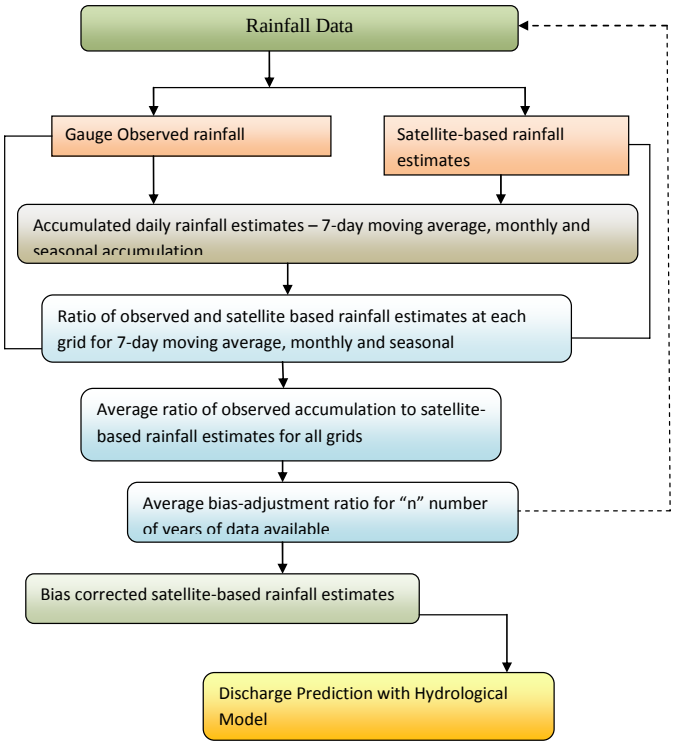

Figure 5.1 Methodology for bias correction

5.2.4 Improved Gauge-Satellite Merged Rainfall Estimates for Bias-Adjustment

The RFE is a daily satellite-gauge merged product which uses 3 SREs merged with GTS rain gauge data. The satellite data sources are of data; AMSU-B; SSM/I and GPI cloud-top IR temperature precipitation estimates. The three satellite estimates are first combined linearly using daily, predetermined weighting coefficients, then are merged with station data to determine the final rainfall. Although the RFE algorithm incorporates the available GTS data, much of the time, data are not reported from the stations in near real time for various reasons. The number of

GTS stations that report on a timely and regular basis is limited affecting the accuracy of the rainfall estimates. Therefore, at a country level, it is possible to access data from more gauges than that available from the GTS. To increase the accuracy of temporal and spatial variability of precipitation data, local rain gauge data may be added to the NOAA RFE algorithm and obtain improved satellite-gauge merged rainfall products. The increase in accuracy of the rainfall estimates depends upon the number of local rain gauges that can be added.

The RFE data can be downloaded from the ftp server using the NOAA algorithm available in FORTRAN which runs in a windows version (NOAA 2009). For use with the Windows RFE version, GTS, GPI, SSMI and AMSUB input files are available via anonymous ftp on a daily basis. For the current study the three satellite inputs available during 2003 to 2006 were used with modification to the GTS master file. The GTS master file was edited to incorporate the additional rain gauge stations in the study area. As data from all over the Himalayan region was available the master station file was modified to reflect additional 419 stations which include the 176 rainfall stations available from Nepal. Incorporation of a larger number of rainfall stations from the whole HKH region prevents discontinuity of rainfall estimates at national borders. Because no GTS data were found to report for the monsoon of 2003, all the quality checked available gauge observed rainfall data were added to obtain a new GTS file for ingestion into the algorithm. To de-bias satellite-based rainfall using gauge observed rainfall data, the algorithm described by Xie and Arkin (1996) was used. Using the merging algorithm developed by Xie and Arkin (1996), the SREs from SSM/I, AMSU-B, and GPI, and the new GTS datasets were merged to come up with new gauge-satellite merged estimates for the 2003 monsoon over the Narayani Basin (NOAA, 2009).

5.3 Rainfall-Runoff Simulation Using Bias-Adjusted Satellite-Based Rainfall Estimates

5.3.1 Satellite-Based Rainfall Estimates with Bias-Adjustment

Three ratio based bias-adjustment factors were derived and applied to the RFE rainfall estimates. The first bias-adjustment of 1.80 was derived for a season using a ratio between the total volumes of gauge observed and RFE from June through September (JJAS) for 2002 to 2006 period, at those grids with one or more rainfall stations, as explained in the earlier section. Daily

rainfall amounts from RFE and gauge observed rainfall were accumulated from June to September to yield seasonal totals for each year from 2002 to 2006.

The second bias-adjustment was derived for each month instead of a season by comparing the cumulative hyetographs on a monthly basis. Daily rainfall of the RFE and gauge observed rainfall estimates were accumulated to monthly rainfall and ratios derived based on the monthly accumulation for each year and averaged over a five year period from 2002 to 2006. The bias-adjustments for June, July, August, and September were calculated to be 1.99, 2.0, 1.58, and 1.82, respectively.

With the aim to further improve the rainfall estimates for flood prediction purposes, a moving bias-adjustment averaged over the previous seven-day period for the whole monsoon season were derived. The seven-day period was chosen based on inspection of tests to represent rainfall event duration. To further improve the flood prediction a new gauge-satellite merged product was developed using the gauge observed data not included in the GTS and the Xie and Arkin (1996) algorithm. Figure 5.2 provides the scatter plot of daily basin averaged SRE with and without adjustments for the monsoon period for 2003. Figure 5.2 illustrates the improvement in rainfall estimates by applying bias-adjustments compared to the unadjusted RFE. In the figure we can see the unadjusted RFE underestimating the rainfall values while the best adjustment is seen to be with improved RFE obtained from merging RFE with local rain gauge data.

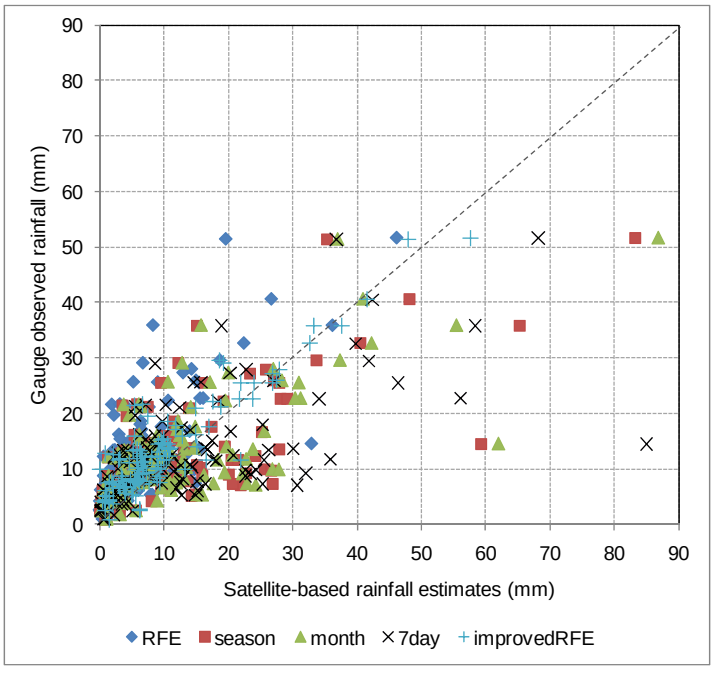

Figure 5.2 Scatter plot of daily area averaged gauge observed rainfall and SRE with and without bias-adjustment for monsoon of 2003.

5.3.2 Rainfall Simulation with Bias-Adjusted Satellite-Based Rainfall Estimates

The GeoSFM hydrologic model was used to simulate the flows with bias-adjustment. The parameters of the semi-distributed hydrological model are determined for each sub-basin derived by dividing the basin into several sub-basins using the basin threshold as was done earlier. The sub-basins were delineated from the GTOPO Hydro1K DEM using the terrain analysis module with ARCView interface as already described in the previous chapter. A total of 39 sub-basins were delineated with an average basin area of about 900 km^2.

The GeoSFM model was then run with the bias-adjusted rainfall estimates. With the seasonal bias-adjustment of the RFE, the predicted flows using GeoSFM showed considerable improvement in predicting the magnitude compared with the raw RFE simulations. There was an increase in the NSCE (from -1.23 to 0.27) and in the correlation (from 0.69 to 0.80). The RMSE decreased from 2750 to 1561, 49% of which was systematic and 51% unsystematic. The peak flow error decreased dramatically from -53% to -11% showing improvement in peak flow detection. For calculating the peak flow error a discharge threshold of 7500 m^3/sec was used corresponding to a warning level at the Devghat hydrometric station. Though the percentage of systematic error in the RMSE reduced from 81% to 49% further improvement in the performance seemed necessary. With this single bias-adjustment factor for the whole monsoon season there still remained a variation in the improvement of the simulated flows between months with amplification of false peaks (Fig.5.3). Hence finer scale bias-adjustments than a seasonal was derived and applied to assess further improvement in flood prediction.

The monthly bias-adjustments ratios were applied to the RFE estimates to obtain a new set of improved rainfall estimates for the monsoon of 2003. The improved rainfall estimates were then applied to the gauge observed calibrated GeoSFM model to assess the impact of the adjustments on flood prediction in the Narayani Basin. Figure 5.3 shows the improvement in flood prediction with applying bias-adjusted rainfall estimates. After the application of this second bias-adjustment method, the correlation and the NSCE of the predicted flows improved, compared to single seasonal bias-adjustment (Table 5.1). The NSCE increased from 0.27 to 0.38 and the

RMSE decreased from 1561 to 1471 indicating better performance with a monthly adjustment as compared to a seasonal.

A 7-day moving average bias-adjustment was also applied to the GeoSFM to assess the improvement in flood prediction. Using this bias-adjustment, no further improvement in the flood predictability of the Narayani Basin was found. Though the bias appeared small with this adjustment compared to other adjustments, the correlation decreased to 0.79 and RMSE increased to 1654 with the systematic error component increasing from 45% to 52% indicating deterioration in the model performance. Figure 5.3 and Table 5.1 present the statistics for the comparison of simulated flows using the bias-adjusted RFE with observed streamflow for the Narayani River.

Although, all three bias-adjustments showed improvement in flood predictability compared to the raw RFE, the second adjustment (monthly) was found to be the best with an 'index of agreement' (d) of 0.87 and the lowest RMSE. The streamflow predicted with the RFE adjusted with the second bias-adjustment predicted the flood peak, flow volume, and hydrograph timing more accurately. The NSCE improved from -1.23 to 0.38 and the correlation coefficient (r) from 0.75 to 0.81 using a monthly adjustment factor. The peak flow error above a threshold corresponding to the warning level at Devghat hydrological station decreased from -53% with RFE to -11% with a seasonal bias-adjustment and to -9% with monthly bias-adjustment indicating an overall improvement in the model simulation. Table 5.1 provides the error statistics with bias-adjusted rainfall estimates.

These results indicate that the SREs can be improved to better estimate the quantity of rainfall and capture the peak flow occurrence with a ratio based bias-adjustment. However, the improved rainfall estimates do not capture the day to day variability of gauge observed rainfall which may be required for other water resources applications on a daily basis. Further work is needed to identify the causes for systematic biases in the SRE and develop improved methods to remove the biases, and improve the RFE simulations of daily variability of rainfall.

Table 5.1 Error statistics of discharge with bias-adjusted CPC_RFE rainfall estimates

Dataset	NSCE	r	Bias	RMSE	RMSEs	RMSEu	d	Peal Flow Error (%)
RFE (unadjusted)	-1.23	0.75	-2458	2750	0.81	0.19	0.58	-53
RFE adjusted with a seasonal factor	0.27	0.80	-345	1561	0.49	0.51	0.87	-11
RFE adjustment with a monthly factor	0.38	0.81	-378	1471	0.45	0.55	0.87	-9
RFE adjustment with running 7 day average factor	0.22	0.79	106	1654	0.52	0.48	0.85	-17
RFE (gauge-satellite merged)	0.53	0.90	-990	1316	0.57	0.43	0.89	-7

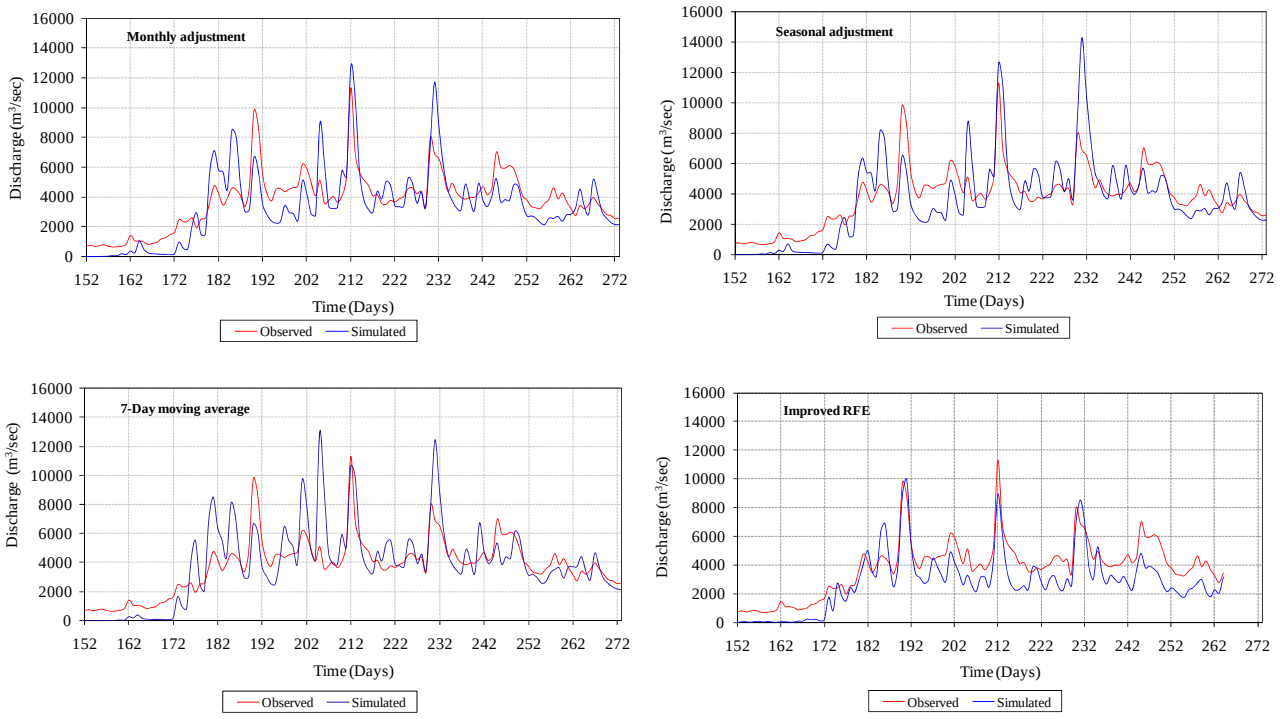

Figure 5.3 Daily observed and simulated flows using bias-adjusted CPC_RFE2.0 rainfall fields

Discharge simulation with ingestion of local rain gauge data

The new gauge-satellite merged rainfall estimates obtained from ingestion of local rain gauge data into the RFE algorithm heron referred to as “improved RFE” were used to simulate discharge at the Devghat hydrometric station. The GeoSFM model with parameters determined using gauge observed data were used to simulate runoff using the “improved RFE” estimates. With the “improved RFE” estimates the GeoSFM showed a marked improvement in flood prediction (Figure 5.3). We find the flood predictions closer to the observed river discharge. The

NSCE and correlation coefficient increased from -1.23 to 0.53 and 0.75 to 0.90 with a 'degree of agreement' (d) of 0.89 (Table 5.1). However, overall underestimation of discharge by about 25% was observed mainly during the medium flow periods. To investigate the underestimation of medium discharge with the improved RFE estimates further inspection of the rainfall over the Narayani Basin was made.

The gauge observed rainfall within the Narayani Basin was used as the 'ground truth' to verify the gauge-satellite merged analysis over grid boxes with at least one reporting station. Anywhere else, the quality of the gauge observed analysis would be compromised, especially over a region like the Narayani Basin where orographic effects work on small scales. Figure 5.4 shows good agreement between the gauge observed and estimated rainfall. The bias reduced from -33.7 to -3.4 mm and the correlation coefficient from 0.60 to 0.91 using the "improved RFE" rainfall for 9 July 2003.

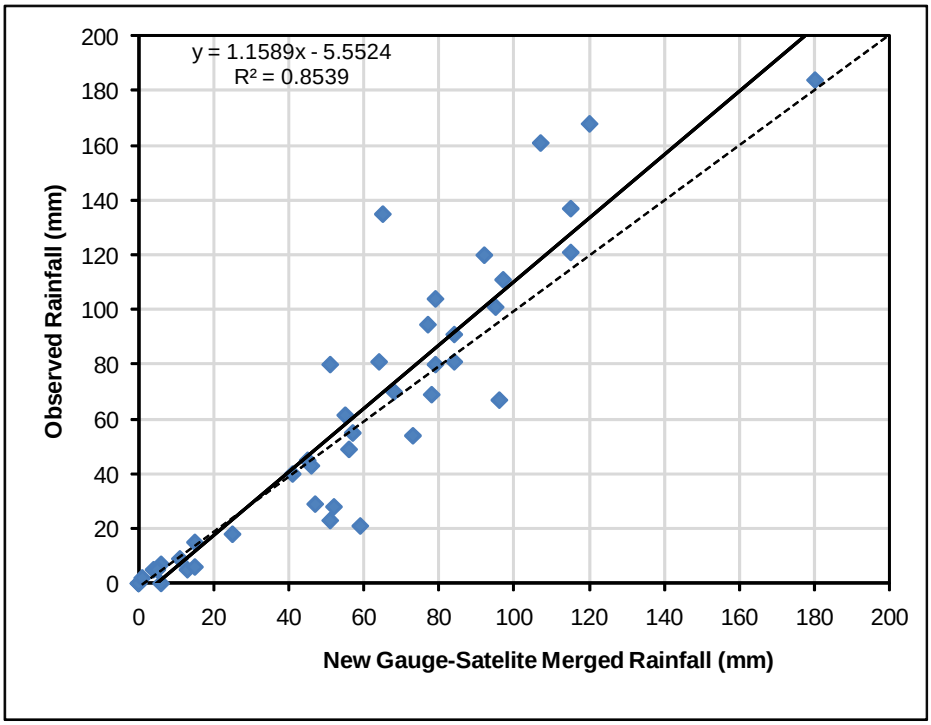

Figure 5.4. Comparison of new gauge-satellite merged and gauge observed rainfall over grid boxes where there is at least one reporting station for 9 July 2003

Visual and statistical examinations of the basin averaged rainfall estimates indicate significant improvement in the rainfall estimates with ingestion of local rain gauge data. Figure 5.5 shows comparison of basin averaged observed rainfall using RFE with and without improvement for JJAS of 2003. The comparison of basin averaged gauge observed rainfall and

new gauge-satellite merged rainfall estimates for the four months of the 2003 monsoon shows improvement in the overall estimation of rainfall but with a slight underestimation of medium rainfall (Figure 5.5). The correlation coefficient increased from 0.02 to 0.92 and RMSE decreased from 15.5 to 5.2 mm/day with the new gauge-satellite merged product compared with unadjusted RFE rainfall estimates. Figure 5.6 shows the comparison of scatter plots of observed and RFE rainfall estimates (without adjustment and with ingestion of local rain gauge) averaged over the Narayani Basin.

There is however a negative percentage error of about 25% with underestimation of medium rainfall in some days. The reason for this difference between the RFE and the gauge observed rainfall may be attributed to the inherent systematic and random errors characteristic of SRE (Xie *et al*., 2003; Hossain and Anagnostou, 2006). The underestimation of rainfall in some days may be the reason for the difference in discharge simulation between observed and simulated using the new gauge-satellite merged product where the overall underestimation of discharge was also 25%. Despite the difference in medium flows, with the new gauge-satellite merged product the accuracy of prediction of daily peak flows is high. The average error above the threshold discharge corresponding to the warning level is -7 % compared to -61% with unadjusted RFE.

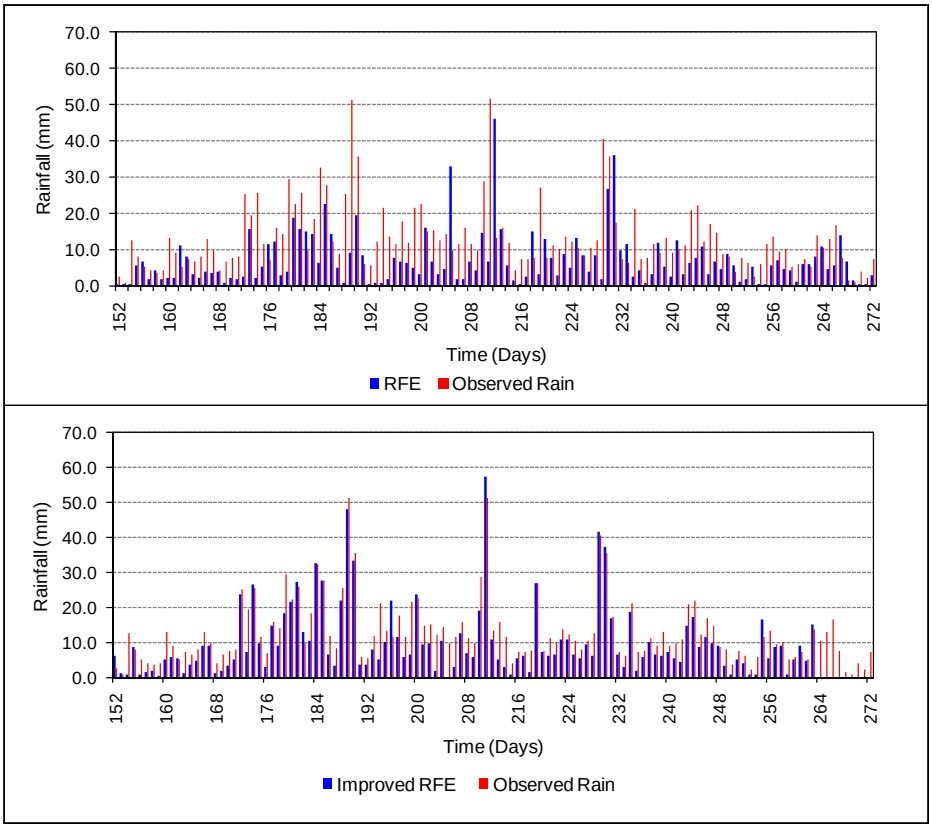

Figure 5.5. Comparison of daily basin averaged gauge observed rainfall with CPC_RFE2.0 and adjusted CPC_RFE2.0 for JJAS of 2003 in the Narayani Basin

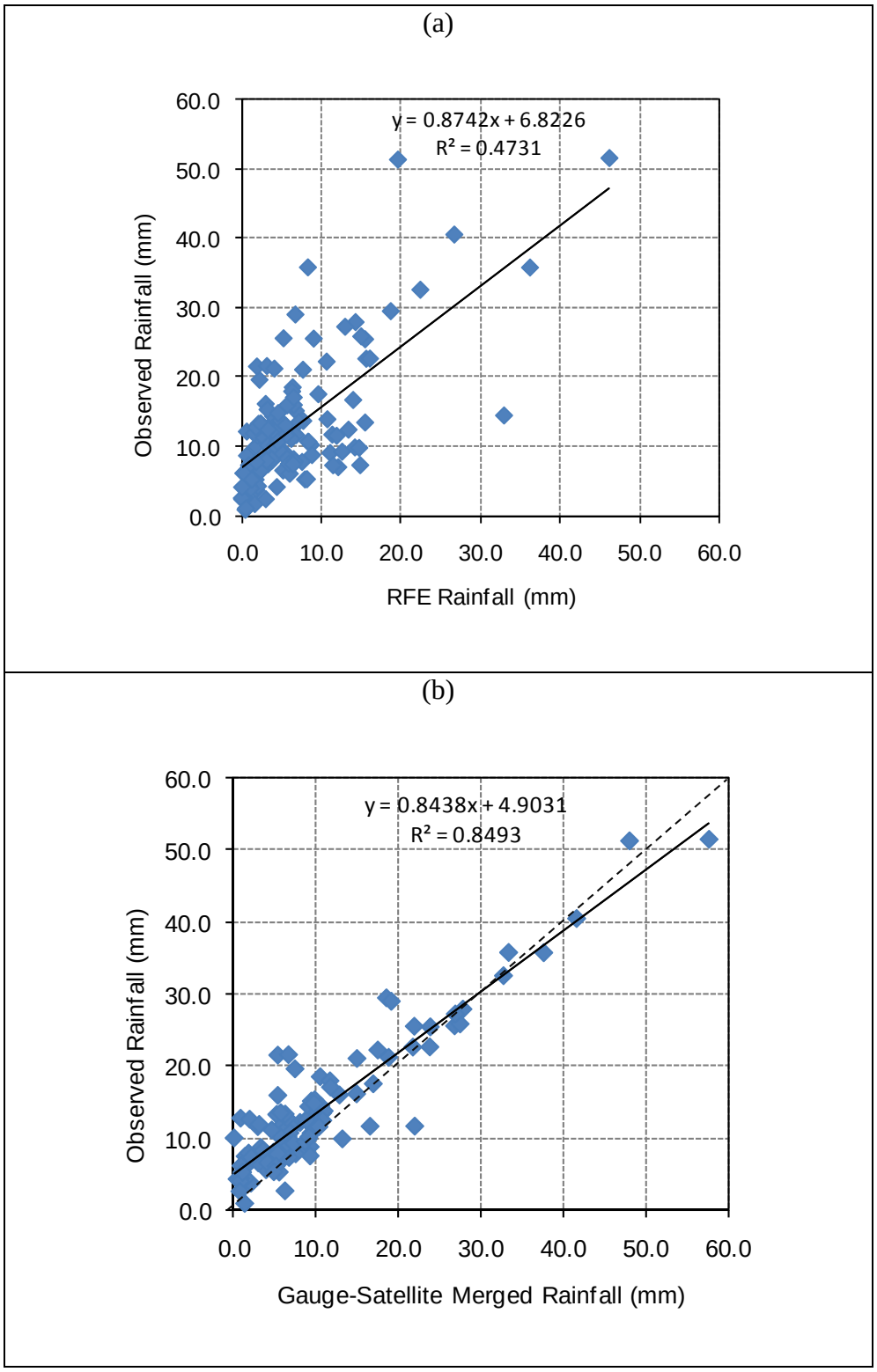

Figure 5.6. Scatter plots of observed and CPC_RFE2.0 rainfall estimates a) without adjustment and b)with ingestion of local rain gauge averaged over the Narayani Basin

To further test the improvement in performance with the improved RFE estimates the GeoSFM model was calibrated using the improved RFE estimates instead of using the gauge calibrated parameters. An improvement in the model performance was observed with the RMSE decreasing from 1316 to 900, the normalized bias decreasing from -29% to -7% and a slight increase in coefficient of correlation 0.90 to 0.92. Table 5.2 presents the statistical summary comparing the simulated and gauge observed streamflow for JJAS of 2003 with the model calibrated with gauge observed data and the improved RFE. Artan *et al.* (2008) and Hughes (2006) had also indicated the need to recalibrate a hydrologic model when SRE are used as rainfall inputs. From the current result it can be said that recalibration of the model is required not only while running the model with SREs but also for new gauge-satellite merged rainfall estimates. From this marked improvement in accuracy for flood prediction, we can infer that the "improved RFE" are good for flood prediction in the Narayani Basin but has to be recalibrated with the gauge-satellite merged rainfall estimates. The larger the number of ingested local gauges, the better will be the flood prediction.

Table 5.2 Statistical summary of the comparison between simulated and observed streamflow for JJAS of 2003with RFE, gauge-satellite merged model calibrated with gauge observed data and gauge satellite merged calibrated model.

	RMSE (m^3/sec)	RMSE (%)		Correlation Coefficient	Normalized Bias (%)
		Unsystematic	Systematic		
RFE	2750	19	81	0.73	-79
Gauge-satellite merged model calibrated with gauge observed data	1316	43	57	0.90	-29
Gauge-satellite merged calibration model	900	70	30	0.92	-7

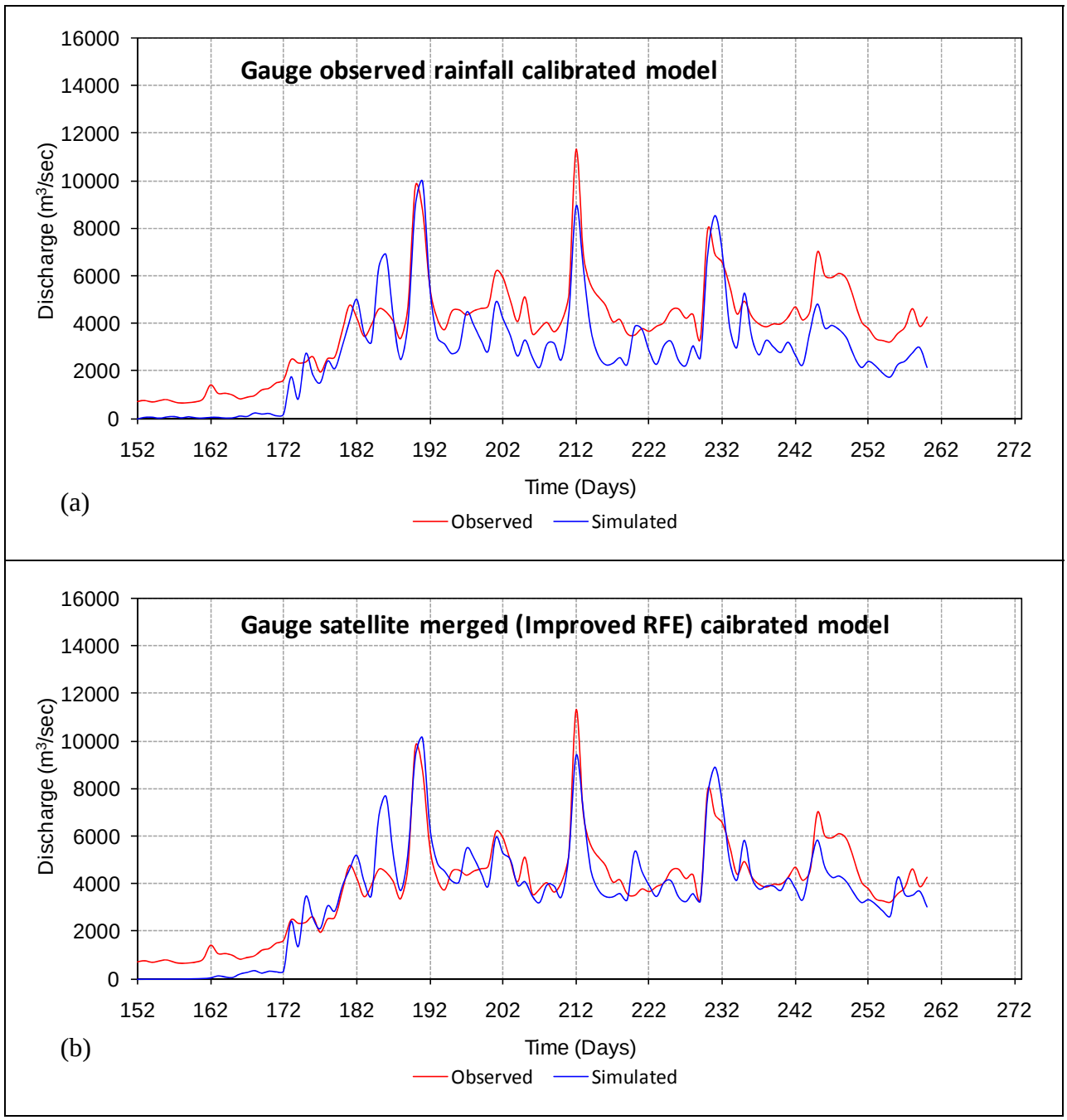

Figure 5.7 Observed and simulated hydrographs obtained when the model was calibrated with a) gauge observed rainfall and b) new gauge-satellite rainfall estimates.

5.4 Summary

In this chapter two approaches of bias-adjustment have been presented. The first set of bias-adjustment is based on ratios derived from comparing the accumulated gauge observed rainfall with RFE for the corresponding periods. Three bias-adjustments seasonal, monthly and a 7 day

moving average were derived. These bias-adjustments were applied to the RFE to obtain a new set of improved RFE rainfall estimates. These improved RFE rainfall were applied to the GeoSFM model which indicate improvement in flood prediction. The second approach is the improvement in the rainfall estimates by ingesting additional local rain gauge data into the RFE algorithm by expanding the GTS data input. When the model calibrated with the gauge observation was run with the improved rainfall estimates considerable improvement in flood prediction was achieved. However, there seemed to be some discrepancy in the medium flow estimation. Therefore keeping in mind the inherent errors in the SREs the model was recalibrated with improved RFE. The recalibrated model with new gauge-satellite merged rainfall estimates showed further improvement in the simulation of flows. Overall, findings from this study indicate that the accuracy SRE can be improved by applying a bias-adjustment. Prediction of discharge using bias-adjusted rainfall estimates can improve the accuracy discharge prediction with considerable increase in the predictive capability of flood prediction for which the hydrological model needs to be recalibrated.

References

Artan, G.A., Gadain, H., Smith, J.L., Asante, K., Bandaragoda, C.J., Verdin, J.P. (2007a) Adequacy of satellite derived rainfall data for streamflow modelling. *Nat. Hazards*, 43, 167-185.

Hay, L.; Clark, M.; Wilby, R.; Gutowski, W.; Leavesley, G.; Pan, Z., Arritt, R.; and Takle, E.: (2002) Use of regional climate model output for hydrologic simulations, *J. Hydrometeorol*., 224:3, pp. 571–590.

Hossain, F. and Anagnostou, E.N.: (2006) Assessment of a multidimensional satellite rainfall error model for ensemble generation of satellite rainfall data. IEEE Geoscience and Remote Sensing Letters, Vol. 3, No. 3: pp. 419-423.

Hughes, D.A. (2006) Comparison of satellite rainfall data with observations from gauging station networks. *J. Hydrol.*, 327, 399–410.

Ines, A.V.M. and Hansen J.W.: (2006) Bias correction of daily GCM rainfall for crop simulation studies. *Agricultural and Forest Meteorology*. 138, pp. 44–53

National Oceanic and Atmospheric Administration (NOAA), 2009. The NOAA Climate Prediction Center *CPC RFE2* rainfall estimation software for the Hindu Kush and Mekong regions of Asia.

Piani, C.; Haerter, J.O.; and Coppola, E.: (2010) Statistical bias correction for daily precipitation in regional climate models over Europe. *Theor Appl Climatol*. 99: pp. 187-192.

Terink, W.; Hurkmans, W.L.; Torfs, P.J.J.F.; and Uijlenhoet, R.; (2010) Evaluation of a bias correction method applied to downscaled precipitation and temperature reanalysis data for the Rhine basin. *Hydrol. Earth Syst. Sci. Discuss*., 7, pp. 221–267

Terink, W.; Hurkmans, W.L.; Torfs, P.J.J.F.; and Uijlenhoet, R.; (2009) Evaluation of a bias correction method applied to downscaled precipitation and temperature reanalysis data for the Rhine basin. *Hydrol. Earth Syst. Sci*., 14, pp. 687–703.

Xie, P., Arkin, P.A., 1996. Analyses of global monthly precipitation using gauge observations, satellite estimates and numerical model predictions. J. Clim. 9, 840–858.

Xie, P.; Yarosh, Y.; Love, T. ; Janowiak, J E.; and Arkin, PA. (2002) A Real-Time Daily Precipitation Analysis Over South Asia Preprints, 16th Conference of Hydrology, Orlando, FL, American Meteorological Society 12-17 January 2002.

CHAPTER 6

6 CONCLUSIONS AND RECOMMENDATIONS

The verification of satellite based rainfall estimates, bias-adjustment and application of the rainfall estimates into hydrological modeling for flood prediction are the main aspects of this research. SRE is a new technology for Nepal and prior to this research there has been very little application of SRE into hydrological modeling. This research is the first to conduct a detailed verification of the SRE over Nepal to understand the strengths and weakness of the now more easily available global satellite-based rainfall products. As there is no operational flood forecasting and warning system in place in Nepal this study has provided an opportunity to explore the application of remotely sensed data for streamflow estimation and flood forecasting.

Accurate rainfall estimations are essential for timely flood forecasting and warning. In many regions operational flood forecasting has traditionally been relied upon by a dense network of rain gauges or ground-based rainfall measuring radars that report in real time. In Nepal, like many other developing countries, the hydrometeorological station networks are sparse and rainfall data are available only after a significant delay. Due to the limited spatial coverage of ground based gauges, unavailability of real-time rainfall data, and constraint in technical and financial resources, operational flood forecasting is yet to be initiated. Thus, SRE is considered as an appropriate approach for Nepal to predict and forecast rainfall-induced runoff that may produce flooding. Two high resolution SREs were selected for verification in this research. The NOAA CPC_RFE2.0 (RFE) mutli-satellite gauge merged rainfall estimates and the JAXA GSMaP_MVK+ (GSMaP) global rainfall estimates both available at a 0.1 degree x 0.1degree spatial resolution on a daily basis. The RFE uses merging technique which increases the accuracy of the rainfall estimates by reducing significant bias and random error compared to individual precipitation data sources thereby adding value to rain gauge interpolations GSMaP includes a Kalman filtering technique. The RFE provides near real time rainfall estimates over South Asia and the GSMaP has a near real time product with a 4 hr latency which makes it attractive for flood forecasting in Nepal. In the research the RFE estimates from 2002 to 2006 and GSMaP from 2003 to 2006 have been used for verification. Gauge observed rainfall data from 176 stations made available from the DHM of the Government of Nepal were used to

conduct the validation over Nepal considering various levels of validation, whole country as a homogeneous region, various physiographic regions and in river basins. The quality of the estimates in terms of spatial distribution and amount was assessed by using the standard statistical verification technique by comparing bias, RMSE, correlation coefficient, multiplicative bias, percentage error, POD and FAR values for each set of validation data. As Nepal has a complex topography with elevation ranging from 60 m to 8848m within a short horizontal distance of less than 200 km the verification of SREs were made in various physiographic regions to better understand the performance of the rainfall estimates in such complex topography. As the final objective of this research is to assess the applicability of SREs into hydrological modeling for flood prediction rainfall verifications were also conducted at a basin level considering different basin sizes.

The USGS GeoSFM was used to simulate the rainfall-runoff processes in two river basins Bagmati and Narayani using the gauge observed and RFE. The GeoSFM model was calibrated and validated using the gauge observed data. RFE estimates were applied to simulate the discharge. Comparison of the observed and simulated discharge using the gauge observed data was very good indicating the suitability of GeoSFM into flood forecasting. However when the model was run with RFE the performance of the model deteriorated sharply indicating the need for correcting the rainfall estimates prior to further application.

As the SREs were found to underestimate bias-adjustment of the estimates were made. Two approaches of bias-adjustment, ratio based bias-adjustment at various temporal accumulations seasonal, monthly and 7-day moving average and gauge-satellite merged rainfall estimates were developed and assessed. The application of bias-adjusted rainfall estimates into the GeoSFM model showed marked improvement in flood predictability with all three ratio based bias-adjustment. However, the monthly bias-adjustment seemed to perform slightly better than the other two with better flood predictions showing a low peak flow error. As a second approach a new set of rainfall estimates were produced by ingesting the locally available rain gauge data into the RFE algorithm which when applied to the GeoSFM showed better flood predictions. However, the current research has indicated the need to recalibrate the GeoSFM with the new sets of rainfall estimates to come up with improved flood predictions.

6.1 Satellite-Based Rainfall Estimate Validation

The country level validation results indicate the RFE and GSMaP provides reasonable rainfall estimates over the Central Himalayas of Nepal but needs to be improved before it can be implemented for operational flood forecasting. The physiographic level validation has shown that performance of the SRE was better in flatter terrain compared to mountainous areas. Due to orographic effects in the mountainous areas the performance of the RFE seems to deteriorate. In the monsoon period there was underestimation of rainfall with a high negative bias. While in the rain shadow areas there was overestimation of the rainfall indicating a positive bias. The major findings and recommendations are given below.

Findings:

- The area average annual gauge observed rainfall over whole of Nepal is 1433 mm, RFE is 1021 mm and GSMaP is 748 mm for 2003 to 2006 period with an annual bias of 421 mm with RFE and 685 mm with GSMaP.
- On an annual basis there is 29% underestimation by rainfall by RFE and 48% by GSMaP for the four years period from 2003 to 2006.
- There is a negative bias of 1.1 mm day^{-1} with RFE and 1.9 mm day^{-1} with GSMaP.
- Both the SREs have significant correlation. There is higher correlation with GSMaP (0.75) than RFE (0.71).
- There is higher negative bias in averaged monsoon (JJAS) rainfall over whole of Nepal with RFE and GSMaP. With RFE there is -2.9 mm day^{-1} and with GSMaP -5.0 mm day^{-1} with the correlation of 0.72 and 0.79 respectively.
- In high intensity rainfall areas example in Pokhara valley there is underestimation of as much as 2000 mm while in rainshadow areas of Mustang there is over a positive bias with overestimation. The positive bias with RFE is larger as compared to with GSMaP.
- The performance of SREs is better in the flatter terrain and deteriorates with increase in elevation.
- The limitation of RFE is that at present it cannot register more than a certain amount of rainfall in 24 hours, which is not enough in the case of monsoon depression and

monsoon trough in Nepal. RFE does not account for orographic aspects of rainfall. GSMaP also does not have orographic corrections.

- Three ratio bias-adjustments seasonal, monthly and a 7-day moving average have been derived and applied to develop corrected rainfall estimates. The correction ratios obtained for the monsoon season is 1.82 and monthly for June, July, August and September are 1.99, 2.0, 1.58, and 1.82.

6.2 Hydrological Modelling Using Satellite-Based Rainfall Estimates

The GeoSFM hydrological model using gauge observed rainfall data and globally available soil and land cover datasets—the Digital Soil Map of the World by FAO and the USGS Global Land Cover resulted in accurate discharge prediction in the Bagmati and Narayani Basins. The GeoSFM predicted the flows accurately when observed rain gauge data have been applied and calibrated indicating reliable application to flood forecasting with good quality of rainfall estimates. However, when the RFE was used in the GeoSFM model as the rainfall input the performance of the model deteriorated with significant underestimation of flows. Although the satellite based rainfall products are capable of detecting a particular rainfall event within the magnitude of the computed discharge is much lower in the RFE driven model compared to the model with gauged observed rainfall. The NSCE was very low however the correlation was still over 0.75 indicating the applicability of improvement with a bias-adjustment.

Bias-adjustments based on ratios comparing the accumulated gauge observed rainfall with RFE for the corresponding periods were derived on a seasonal, monthly and a 7 day moving average basis. These bias-adjustments were applied to the RFE to obtain a new set of improved RFE rainfall estimates. These improved RFE rainfall were applied to the GeoSFM model which indicate improvement in flood prediction. The second approach is the improvement in the rainfall estimates by ingesting additional local rain gauge data into the RFE algorithm by expanding the GTS data input. When the model calibrated with the gauge observation was run with the improved rainfall estimates considerable improvement in flood prediction was achieved. However, there seemed to be some discrepancy in the medium flow estimation. Therefore, keeping in mind the inherent errors in the SREs the model was recalibrated with improved RFE. The recalibrated model with new gauge-satellite merged rainfall estimates showed further improvement in the simulation of flows.

The major findings are given below.

- SREs highly under predicts peak discharge.
- The accuracy flood prediction can be improved by applying a bias-adjustment.
- The bias-adjustment derived on a monthly basis yielded better improvement in the flood predictability compared to other adjustments.
- The application of improved RFE obtained by merging local rain gauge data with SREs in the model yielded the best result of flood prediction for which the hydrological model needs to be recalibrated.

6.3 Recommendations and Future Perspectives

This research reveals that the satellite estimates need to be improved over the Himalayas particularly in areas of orographic influence. This improvement may be made by correction in the algorithm by incorporating the orographic effects into the rainfall estimation. One way of doing this may be by adjusting the GOES Precipitation Index (GPI) for the Geo-stationary input data so as to incorporate a variable brightness temperature to rain rate conversion in the HKH region. Passive microwave measurements depend strongly on the relations between the hydrometeor size distribution, types and the rain intensity. Therefore, it is essential to obtain information about the hydrometeor sizes for achieving reasonable accuracy of the precipitation intensities.

The basic algorithms, for example in the RFE ignores the GTS data when it reports more than 200 mm, should be modified and included in the heavy rainfall event. There are many events in a year when rainfall exceed 200 mm per day in Nepal. Another example is the GSMaP algorithm where a statistical database of precipitation vertical profiles classified into 10 types are used, but currently does not reflect profiles of localized precipitation systems. The profiles of heavy orographic rainfall in the Himalayas are unique and largely different from those in the database, which could be considered to be improved for better rainfall estimation.

The current verification has been conducted using limited data. Further verification may be conducted with additional data and products and using finer temporal and spatial scales for the utility of SRE in flood forecasting. The bias-adjustment technique could be further explored as additional data becomes available. Longer sets of concurrent data between the SRE and gauge

observation may provide a better estimate of bias correction which could be applied for improved flood forecasting.

Finally, bias-adjusted SREs appear to be an effective and viable means to achieve an estimate of precipitation over Nepal. The GeoSFM model with the bias-adjustments derived from this study will be evaluated in the coming monsoon season in near real time for the Narayani Basin for flood prediction.

Annex A

Loss from Floods, landslides and avalanches in Nepal (1983-2005)

Year	Death (No)	Injured (No)	Livestock lost (No)	Houses destroyed (No)	Family Affected (No)	Land Affected (ha)	Infrastructure damaged (No)	Estimated loss (NRs)
1983	293	na	248	na	na	na	na	240.00
1984	363	na	3114	7566	na	1242.00	869	37.00
1985	420	na	3058	4620	na	1355.00	173	58.10
1986	315	na	1886	3035	na	1315.00	436	15.85
1987	391	162	1434	33721	96151	18858.00	421	2000.00
1988	342	197	873	2481	4197	na	na	1087.00
1989	700	4	2979	6203	na	na	na	2528.61
1990	307	26	314	3060	5165	1132.00	na	44.00
1991	93	12	36	817	1621	283.00	25	21.20
1992	71	17	179	88	545	135.00	44	10.78
1993	1336	163	25425	17113	85254	5584.00	na	4904.00
1994	49	34	284	569	3697	392.00	na	59.00
1995	246	58	1535	5162	1E+05	41867.28	na	1419.00
1996	262	73	1548	28432	37096	6063.40	na	1186.00
1997	87	69	317	1814	5833	na	na	102.00
1998	273	80	982	13990	33549	326.89	na	969.00
1999	214	92	331	2543	9769	182.40	na	365.00
2000	173	100	822	5417	15617	888.90	na	932.00
2001	196	88	377	3934	7901	na	na	251.10
2002	441	265	2024	18181	39309	10077.50	na	418.91
2003	232	76	865	3017	7167	na	na	234.78
2004	131	24	495	3684	14238	321.82	na	219.28
2005	162	34	588	1103	2130	na	na	137.81
Average	309	83	2161	7570	27654	5626.51	328	749.58

Source: Compiled from *Annual Disaster Review*, different series published by Department of Water Induced Disaster Prevention (DWIDP)

ANNEX 2

List of Rainfall Stations used for the research

S.No	Longitude	Latitude	Station Name
1	80.58	29.30	Dadeldhura
2	80.60	28.68	Dhangadhi
3	82.17	29.28	Jumla
4	84.00	28.22	Pokhara Airport
5	83.43	27.52	Bhairhawa Airpo
6	84.98	27.17	Simara Airport
7	85.37	27.70	Kathmandu Airpo
8	86.50	27.32	Okhal Dhunga
9	87.67	27.35	Taplejung
10	87.35	26.98	Chandpur
11	87.27	26.48	Biratnagar Airp
12	80.50	29.65	Kakerpakha
13	80.42	29.55	Baitadi
14	80.35	28.68	Belauri
15	80.47	29.53	Satbanj
16	80.87	29.62	Pipalkot
17	81.32	29.38	Bajura
18	81.13	29.00	Katai
19	81.45	28.95	Asara
20	80.92	28.75	Sandepani
21	81.12	28.97	Bangga
22	81.20	29.38	Khaptad
23	80.82	28.57	Sitapur
24	80.68	29.12	Kola Gaon
25	81.28	29.15	Mangalsen
26	81.77	29.32	Thirpu
27	82.32	29.28	Guthi
28	81.60	29.13	Sheri Ghat
29	82.15	29.55	Gam Shree
30	81.90	29.20	Magma

31	81.63	29.23	Bijayapur
32	81.33	28.78	Jamu
33	82.20	28.70	Jajarkot
34	82.12	28.02	Kusum
35	81.35	28.17	Gulariya
36	81.58	28.78	Bale
37	81.10	28.43	Rajapur
38	81.72	28.27	Naubasta
39	81.70	28.35	Shyano Shree
40	81.90	28.05	Baijapur
41	81.35	28.43	Bargadaha
42	82.28	28.98	Maina Gaon
43	82.63	28.60	Rukumkot
44	82.63	28.30	Libang
45	82.87	28.10	Bijuwar Tar
46	82.12	28.22	Nayabasti
47	82.50	28.05	Ghorahi
48	82.53	27.70	Koilabas
49	82.28	28.30	Luwamjula
50	83.65	28.48	Tatopani
51	83.88	28.82	Ranipauwa
52	83.88	29.05	Ghami
53	83.97	29.18	Mustang
54	83.75	28.18	Karki Neta
55	83.10	28.40	Bobang
56	83.22	28.60	Gurja
57	83.73	28.40	Ghorapani
58	83.65	28.03	Tribeni
59	83.40	28.38	Darbang
60	83.57	28.15	Rangkhami
61	83.78	28.97	Samar
62	83.68	28.90	Samoa
63	83.60	28.47	Bega
64	83.48	28.38	Kuhun

65	83.38	28.57	Baghara
66	83.62	28.13	Sirkon
67	83.43	27.95	Ridi Bazar
68	84.05	27.68	Beluwa
69	83.67	27.53	Parasi
70	83.87	27.58	Dhumkibas
71	83.05	27.77	Pattharkot
72	83.27	28.17	Musikot
73	82.80	27.68	Bhagwanpur
74	83.80	27.87	Garakot
75	83.28	27.47	Lumini
76	84.90	28.37	Jagat
77	84.62	28.67	Larke Samdo
78	84.35	28.13	Kunchha
79	84.42	27.93	Bandipur
80	83.82	28.27	Bhadaure
81	84.28	27.97	Damauli
82	83.97	28.27	Lamachaur
83	84.02	28.67	Manang
84	83.80	28.38	Ghandruk
85	84.62	28.20	Gharedhunga
86	84.10	28.37	Siklesh
87	83.77	27.98	Walling
88	84.13	27.87	Rumjakot
89	83.75	28.27	Sallyan
90	83.78	28.27	Pamdur
91	84.53	27.58	Jhawani
92	85.13	27.55	Chisapani
93	85.00	27.28	Amlekhganj
94	85.17	27.18	Nijgadh
95	85.38	27.02	Ramoli
96	85.15	27.62	Markhu
97	84.87	27.00	Birganj
98	85.17	27.42	Makwanpur
99	84.82	27.55	Beluwa

100	85.00	27.03	Kalaiya
101	85.02	26.92	Kolbhi
102	85.13	26.95	Chuntaha
103	84.98	27.43	Rajaiya
104	85.38	28.28	Timure
105	84.82	28.05	Aru Ghat
106	84.93	27.87	Dhading
107	85.87	27.87	Gumthang
108	85.62	27.80	Nawalpur
109	85.72	27.78	Chautara
110	85.20	27.68	Thankot
111	85.60	27.95	Sarmathang
112	85.57	27.87	Dubachaur
113	85.57	27.78	Baunepati
114	85.65	27.70	Mandan
115	85.72	27.63	Dolal Ghat
116	85.63	27.92	Dhap
117	85.90	27.78	Barabhise
118	85.75	27.57	Pachuwar Ghat
119	85.48	27.75	Sankhu
120	85.52	27.58	Khopasi (Panauti)
121	85.42	27.67	Bhaktapur
122	85.32	28.17	Thamchit
123	85.55	28.00	Tarkhe Ghyang
124	85.42	27.70	Changu Narayan
125	85.33	27.60	Chapa Gaon
126	85.72	27.70	Sanga chowk
127	85.78	27.70	Thokarpa
128	85.42	27.77	Sundarijal
129	85.28	27.58	Lele
130	85.25	27.68	Naikap
131	85.42	27.75	Sundarijal
132	85.63	27.90	Dhap
133	85.25	27.75	Nararjun

134	86.10	27.68	Nagdanda
135	86.05	27.67	Charikot
136	86.05	27.52	Melung
137	86.17	27.18	Bahun Tilpung
138	85.67	27.08	Pattharkot (east)
139	85.92	27.03	Tulsi
140	86.17	26.92	Chisapani Bazar
141	85.82	27.45	Nepalithok
142	85.50	27.33	Hariharpur Ghad
143	85.78	26.88	Gausala
144	85.57	26.87	Malangwa
145	86.08	27.47	Manthali
146	86.72	27.70	Chaurikhark
147	86.57	27.43	Pakarnas
148	86.75	27.35	Aisealukhark
149	86.42	27.48	Mane Bhanjyang
150	86.43	27.13	Kurule Ghat
151	86.83	27.03	Khotang Bazar
152	86.22	26.65	Siraha
153	86.58	27.50	Salleri
154	86.80	27.22	Diktel
155	86.38	27.55	Sirwa
156	86.90	26.60	Barmajhiya
157	87.28	27.55	Num
158	87.28	27.13	Leguwa Ghat
159	87.23	27.03	Munga
160	87.33	26.93	Mul Ghat
161	87.15	26.93	Tribeni
162	87.38	26.62	Haraincha
163	87.17	26.82	Chatara
164	87.42	27.77	Chepuwa
165	87.22	27.28	Tumlingtar
166	87.17	26.97	Machuwaghat
167	87.15	27.37	Dingla
168	87.78	27.55	Lungthung

169	87.78	27.48	Taplethok
170	87.93	27.20	Memeng Jagat
171	87.70	26.67	Damak
172	87.98	26.63	Anarmani Birta
173	88.03	26.88	Himali Gaon
174	88.05	26.57	Chandra Gadhi
175	87.97	26.68	Sanishare
176	87.60	27.35	Dovam